



Programme Area: Carbon Capture and Storage

Project: High Hydrogen

Title: Interim Project Report: Experimental results and detailed analysis

Abstract:

This is the last interim report for the High Hydrogen project. It describes and discusses the work performed to date at Buxton, the process used to design commission and operate the circular duct test rig for exploring the operational capability of plant using hydrogen-based fuels with heat recovery systems on their exhaust systems. There will be one further deliverable from this project which will provide results for the HRSG model tests and draw the full programme of works together from the literature review, through the laboratory experiments and the two scale experimental rigs. The executive summary on page 9 provides a good insight into the report and its objectives. The key insights from Prof Hans Michels, whilst on a limited number of tests, provide some key information that begins to link the project phases (page 81).

Context:

Hydrogen is likely to be an increasingly important fuel component in the future. This £3.5m project was designed to advance the safe design and operation of gas turbines, reciprocating engines and combined heat and power systems using hydrogen-based fuels. Through new modelling and large-scale experimental work the project sought to identify the bounds of safe design and operation of high efficiency combined cycle gas turbine and combined heat and power systems operating on a range of fuels with high and variable concentrations of hydrogen. The goal of the project was to increase the range of fuels that can be safely used in power and heat generating plant. The project involved the Health and Safety Laboratory, an agency of the Health and Safety Executive, in collaboration with Imperial Consultants, the consulting arm of Imperial College London.

Disclaimer:

The Energy Technologies Institute is making this document available to use under the Energy Technologies Institute Open Licence for Materials. Please refer to the Energy Technologies Institute website for the terms and conditions of this licence. The Information is licensed 'as is' and the Energy Technologies Institute excludes all representations, warranties, obligations and liabilities in relation to the Information to the maximum extent permitted by law. The Energy Technologies Institute is not liable for any errors or omissions in the Information and shall not be liable for any loss, injury or damage of any kind caused by its use. This exclusion of liability includes, but is not limited to, any direct, indirect, special, incidental, consequential, punitive, or exemplary damages in each case such as loss of revenue, data, anticipated profits, and lost business. The Energy Technologies Institute does not guarantee the continued supply of the Information. Notwithstanding any statement to the contrary contained on the face of this document, the Energy Technologies Institute confirms that the authors of the document have consented to its publication by the Energy Technologies Institute.

Harpur Hill, Buxton
 Derbyshire, SK17 9JN
 T: +44 (0)1298 218000
 F: +44 (0)1298 218986
 W: www.hsl.gov.uk



**ETI WP2, Task 2. Interim Project Report:
 Experimental results and detailed analysis.**

MHU/15/138

Report Approved for Issue By:	J.T. Allen PhD
Date of Issue:	06/10/2015
Lead Author:	K. Moodie MSc.
Lead Author Section 10 & Appendices B-F:	Hans. J. Michels Drs, Phd, DIC, CEng, CPhys, FInstP, Professor of Safety Engineering IC.
Contributing Author(s):	B.C.R Ewan PhD. W. Rattigan BSc. L. O'Sullivan BSc. S. Hawksworth PhD.
Technical Reviewer(s):	S. Hawksworth PhD.
Editorial Reviewer:	J.T. Allen PhD
HSL Project Number:	PE02162

This report and the work it describes were undertaken by the Health and Safety Laboratory under contract to the Energy Technology Institute. Its contents, including any opinions and/or conclusion expressed or recommendations made, do not necessarily reflect policy or views of the Health and Safety Executive.

DISTRIBUTION

Paul Winstanley ETI
Andrzej Pekalski Shell
Hans Michels Imperial London
Bruce Ewan

John Gummer HSL
Keith Moodie HSL
Wayne Rattigan HSL
Louise O'Sullivan HSL
Stuart Hawkesworth HSL
Rosemary Gibson HSL

ACKNOWLEDGEMENTS

The authors wish to thank Paul Winstanley of the Energy Technologies Institute (ETI) together with their sponsors, in particular Colin Etheridge, also Prof. H. Michels and Dr. A Pekalski for all the worthwhile contributions they made in both formulating the test programme and in contributing to the many technical discussion sessions held throughout its duration.

ACRONYMS

ETI – Energy Technology Institute
HSL – Health and Safety Laboratory
IC – Imperial College
CCGT – Combined Cycle Gas Turbine
CCGE – Combined Cycle Gas Engine
WP – Work Package
CHP – Combined Heat and Power
DDT – Deflagration to Detonation Transition
BoD – Basis of Design
FSD – Full Scale Deflection
FSO – Full Scale Output
ESTOPS – Emergency Stop Devices / Software
RPM – Revolutions per minute
CFD – Computational Fluid Dynamics
HRSG – Heat Recovery Steam Generator
P&ID – Pipe and Instrumentation Diagram
PID – Proportional Integral Derivative (Controller)
HAZOP – Hazard and Operability Study
EQR – Equivalence Ratio
TDMS – LabVIEW Test Data Exchange Stream
CSV – Comma Separated Values file

CONTENTS

EXECUTIVE SUMMARY (HSL)		VII
1 INTRODUCTION		1
1.1 Contractual requirements.....		1
1.2 Background.....		1
1.3 Expectations		3
2 PROJECT OBJECTIVES		4
2.1 Overall Objectives.....		4
2.2 Contractual Obligations		4
2.3 Specific Objectives		5
2.4 Deliverables		5
2.5 Acceptance criteria		5
3 BASIS OF DESIGN (BOD)		7
3.1 Design Philosophy		7
3.2 Design specification.....		7
4 DESCRIPTION OF THE TEST RIG		11
4.1 Basic layout of the engine and duct.....		13
4.2 Diverter section.....		16
4.3 Transition section.....		17
4.4 Fuel and oxygen supply system.....		20
4.5 Housing for the rig		22
4.6 Engine control system		23
4.8 RIG DATA COLLECTION		26
5 COMMISSIONING		27
5.1 Introduction		27
5.2 Major rig components		27
6 INSTRUMENTATION		33
6.1 Sensor types and locations.....		33
6.2 Flame ionisation (IP) Sensors.....		34
6.3 Optical flame (OP) sensors.....		36
6.4 Pressure sensors.....		40
6.5 Velocity measurements		41
6.6 Temperature measurements.....		42
6.7 Ignition system.....		43
6.8 Data synchronisation		43
7 RIG OPERATING PROCEDURES		45
7.1 Safety procedures.....		45
7.2 Calibration procedures.....		46
7.3 Operating procedures		49

7.4	Safety record during testing.....	52
8	RESULTS.....	54
8.1	Introduction.....	54
8.2	Presentation of results.....	54
8.3	Combustion test summary data.....	55
9	DISCUSSION OF RESULTS.....	61
9.1	Validity of Pressure sensor data.....	61
9.2	Observations regarding the use of flame sensors.....	65
9.3	Consistency of data.....	65
9.4	High Speed Video Data.....	68
9.5	conclusions relating to the overall performance of the test rig.....	69
10	DETAILED ANALYSIS.....	71
10.1	The safe operating modes for H ₂ /CH ₄ /CO model fuel mixtures.....	71
10.2	The influence of heat exchanger model obstructions on the character of combusting flow.....	79
10.3	Detailed Analysis of Task 2 Experimental Data.....	82
10.4	Results: Construction of distance versus time diagrams.....	82
10.5	Evaluation of Results.....	83
10.6	Further Suggested Work.....	86
11	REFERENCES.....	88
	APPENDIX A: RIG DETAILS AND RESULTS.....	89
11.1	Contractual requirements.....	89
11.2	Kulite pressure sensor data sheet.....	91
11.3	Format used to summarise the test results.....	93
11.4	Combustion tests summary of data.....	94
11.5	Flame speed, temperature and pressure highlights.....	114
	APPENDIX B: DETAILED ANALYSIS FOR TEST 27.....	132
	APPENDIX C: DETAILED ANALYSIS FOR TEST 10.....	140
	APPENDIX D: DETAILED ANALYSIS FOR TEST 24.....	142
	APPENDIX E: DETAILED ANALYSIS FOR TEST 29.....	144
	APPENDIX F: DETAILED ANALYSIS FOR TEST 25.....	146

EXECUTIVE SUMMARY (HSL)

The report describes the design, construction and operation of a 0.6 metre diameter by 12 metre long cylindrical test rig. The purpose of the facility is to measure the consequences of ignitions in binary flammable gas mixtures, hydrogen/methane or hydrogen/carbon monoxide, when they are injected into the hot exhaust stream from a Rolls-Royce Viper gas turbine. Such tests have been performed and, in addition a small number of tests were also undertaken using a flammable gas of ternary mixtures of all three binary components.

The objectives of the tests were to model at reduced scale, the consequences of a flameout in a full-size combined cycle gas turbine (CCGT) when running on high hydrogen fuel mixtures. The test parameters varied were the fuel mixture composition, the equivalence ratio and the exhaust gas temperature. The heat recovery steam generator (HRSG) was modelled by a series of tubes giving a blockage ratio of 40% per tube row. The numbers of tube rows tested were 0, 8 and 15.

This report presents the results obtained without analysis, (see Section 11.4 Combustion tests summary of data), it does however comment upon the consistency of the data sets (Section 9.3), in respect of the parameters tested. The expected trends in the data were observed, namely that increasing Equivalence Ratio (EQR) and increasing the number of tube rows in the HRSG model, resulted in increasing overpressures for a given gas mixture. It was also noted that in some instances detonation occurred.

The accuracy of the various types of sensors used was also examined in particular the performance of the two types of pressure transducers used throughout the test programme. Detection of the flame by means of flame ionisation and optical emission techniques have provided complementary measurements in that the optical sensors observed a line of sight across the diameter, whilst the ionisation sensors were point measurement devices located on the side walls and would only detect when a flame was locally present. Generally the optical sensors captured the flame passage under most conditions, whilst the ionisation sensors were more intermittent in their detection, with weak flame events often being unrecorded, either due to their inherent weakness or their absence in the wall region. A number of high speed photography tests have confirmed the variability in flame behaviour under different conditions of mixture and equivalence ratio. The pressure detection often showed complex behaviour arising from the different sensor locations and the changing flame speed behaviour within the duct due to the distribution of obstacles. In many cases the peak pressure was of short duration and followed by longer duration, lower pressure components. This may have implications for the real impact of pressure pulses on the containing structures.

In general the instrument locations have been considered satisfactory and have remained unchanged for the majority of tests.

The work formed part of a test programme at increased scale and demonstrated the utility of the rig and its ability to provide the necessary data. As a consequence it is recommended that the third part of the test programme proceeds forthwith.

Section 10 of the Report provides a detailed analysis and discussion of the first set of results from Work Package 2, Task 2 of the ETI contract PE0202 “High-Hydrogen (HyH) Project” obtained at the HSL, Harpur Hill Buxton, between autumn 2014 and summer 2015. Full details of the facilities used and tests carried out can be found in the earlier sections of this report.

The results database of the full set of 61 tests on the three component H₂/CH₄/CO fuel system are used to establish the lowest hazardous and highest safe fuel-air mixture concentrations for turbine exhaust streams passing through model heat exchanger type obstructions (See Section 10.1)

Section 10.2 considers the primary evidence from the 61 tests on the impact the presence of heat exchangers models has on the character of the combustion process and identifies a selection of mixtures most suitable for more detailed analysis. Limitations to this investigation as result of the technical challenges associated with large scale facility and known limitations of the instrumentation are listed. Details and required scope of a review of the data presented to date are discussed.

An outline the procedure to extract relevant information from the available results is presented in section 10.3. Appendices B-F give greater detail on these procedures, providing a step by step process and is illustrated with a detailed account of the analysis of one of the primary test results from the experimental WP2.2 programme

Section 10.4 presents the results of such analysis of 5 core tests for the delivery of the intermediate objectives of the programme which has culminated in distance vs time diagrams as a base for further forthcoming work in both WP2.2 and WP2.3.

Section 10.5 evaluates the meaning of the findings, emphasising both more fundamental confirmation of the general lessons from the work of Section 10.1 and important advice for the WP2.3 programme.

Section 10.6 identifies potential further analysis that is recommended to ensure the maximum information is obtained from WP2.2.

1 INTRODUCTION

1.1 CONTRACTUAL REQUIREMENTS

The report describes the experimental work undertaken as well as presenting the results obtained using the circular duct test rig forming Work Package 2, Task 2 (WP 2.2) of the ETI sponsored high hydrogen project. The work was done as part of the requirements under the terms and conditions of the ETI Contract Number PE02162. Section 6, Task 2: Experimental investigation at increased scale using a circular tube. See Appendix Section 12.1 for the full contractual requirements.

1.1.1 Project value objectives

The overall project value objectives are to provide a more detailed evidence base for, and advance the state-of-the-art in, the safe and efficient operation of high hydrogen gas mixtures for energy production in order to enable in respect of WP 2.2 the following outcomes:

- Identify the bounds of safe design and operation of proposed high hydrogen systems to avoid unpredicted hazardous outcomes (limits of flammability, ignition and significant overpressure potential [including DDT] in exhaust systems for a range of CHP/CCGT applications);
- Operate existing systems with more confidence within their bounds of safety in order to increase energy production and avoid unnecessary trips (for example, enabling gas engines to run at higher fuel/air mixes, or operating CCGT systems with higher trip set-points); and
- Outline the applicability of the results by extrapolation to larger duct dimensions and geometries, identifying specific limitations on validity, plus any further work required to increase confidence in the extrapolation process.

1.2 BACKGROUND

The project required the design, manufacture, commissioning and operation of a test rig comprising a Rolls-Royce Viper jet engine, and a nominal 600 mm diameter tube that was some 12 metres long. The engine exhaust provided a hot vitiated air flow that travelled along the tube and into which flammable high hydrogen gas mixtures were added and ignited. The rig's design, manufacture, installation, commissioning and operating procedures are covered in separate reports; see (1, 2 and 3).

The rig provided an experimental facility for investigating the flameout of CCGT/CCGE systems and the consequences of unburnt fuel passing through the turbine (in the CCGT case) and into the exhaust system and igniting. In such circumstances the maximum hydrogen concentration in the downstream mixture is not expected to exceed 10-12% v/v hydrogen (when fuelled with pure hydrogen). Measured duct flow temperatures at the normal engine running condition of 12,200 rpm were in the range 400 - 500 °C following fuel and oxygen injection, with the higher value corresponding to the upstream region of

the duct (TC0 at 1250 mm) and the lower value to the exit region (TC15 at 10250 mm). For lower engine running speeds and different degrees of compression, lower duct temperatures could be achieved and were utilised for a small number of the test cases. These temperatures are within the specification range of 350 - 600 °C as detailed in Section 3.2. It is noted that duct temperatures prior to fuel and oxygen injection are 50 °C higher based on observations on extended data acquisition tests. For CCGE applications the hydrogen concentration may be higher by up to a factor of two. If re-ignition in the exhaust system is assumed to occur, the project seeks to assess the potential consequences, particularly in respect of the flame acceleration and the detonation propensity of the combusting air/fuel mixtures.

The rig provided a reduced-scale model of an actual turbine exhaust system such that the appropriate scaling criteria could be identified to enable predictions to be made of the hazards at full scale. The rig could also contain a simulated heat exchanger to examine its effect on initiating detonations as a precursor to the definitive heat exchanger tests proposed for the WP2.3 test rig, which use an actual heat exchanger but scaled down to a representative size. The tests quantified the combustion behaviour, as measured by the flame speeds and over-pressures observed for the fuel mixtures being tested. The data gathered was used to assess the influence of the heat exchanger on combustion intensity, as measured by generated pressures and flame speeds, which could lead to a better understanding of the propensity of the mixtures to detonate as they passed through the model heat exchanger, thus allowing safe concentration limits to be identified for the mixtures being tested, in a similar way to those presented in a separate report from Imperial College by H. Michels (4).

The rationale for using the size of rig employed was based on the consistent experimental and theoretical evidence for hydrogen mixture compositions with marginal detonation behaviour. In such cases the detonation cell size is characteristically several times that of a stoichiometric fuel mixture and rises asymptotically towards the detonation limit within a few per cent for further mixture dilution. With an established detonation cell width for stoichiometric hydrogen-air of approximately 10 mm at near ambient conditions and a critical channel width for detonation propagation of no more than this, it is feasible to accommodate, close to the detonation composition limits, a potential hydrogen detonation with multiple cells across the width of the 600 mm duct.

The experiments have built on the findings from WP 1 and WP 2.1, using a hot vitiated airflow at several, but constant, flow rates. These have enabled validation to be controlled in a systematic manner for the modelling, test results and the scaling parameters obtained from WP 2.1.

The facility has also provided a better appreciation of the technology required to safely control and operate gas turbine engines running with hydrogen-enriched fuels, in particular where and when a combustible gas mixture exists in the exhaust gas stream immediately downstream of the turbine.

1.3 EXPECTATIONS

The test programme comprised some sixty ignition tests, carried out on releases of flammable gas mixtures made up of various combinations of hydrogen, methane and carbon monoxide. The information generated by these tests, which comprised over-pressure, flame and wave speed measurements, is documented in this report and was used subsequently by Imperial College staff to analyse the results including the detonation propensity of the various mixtures tested. The primary objective being to understand how such mixtures would behave in full-size industrial CCGT systems. There is also a requirement to provide data that can be used to validate CFD models of CCGT systems.

It is expected that the information generated from the analysis will be used to help define the safe working envelope for industrial systems in the event of accidental releases and ignition of flammable gas mixtures as a consequence of a flame-out in the gas turbine or gas engine.

2 PROJECT OBJECTIVES

2.1 OVERALL OBJECTIVES

The overall objective of this part of the programme of work (WP 2.2) was to design and manufacture an experimental test rig, comprising a Rolls-Royce Viper gas turbine whose exhaust flowed through a 600 mm diameter duct into which flammable gas mixtures could be added in a controlled manner. The test rig was designed to reproduce at a reduced scale the conditions likely to occur in the event of a flame out in an industrial CCGT in which high hydrogen flammable gas mixtures enter the turbine exhaust and ignite subsequently. As a consequence the combusting gas mixture may produce unacceptably high over pressures in the exhaust system, especially as the flame front passes through the heat exchanger where the high turbulence levels increase the risk of a detonation occurring.

The supporting experimental programme therefore sought to quantify the flame speeds and over-pressures that occurred for a range of representative high hydrogen gas mixtures. The design of the test programme drew upon the literature review and the laboratory work already completed the latter as WP 2.1. The initial experimental plan involved testing on an open duct, but early commissioning work (2) and discussion within the consortium indicated that the real value for subsequent scaled-up tests would lie in an experimental plan that more closely reproduced the conditions within a real HRSG geometry. As a result, the bulk of the testing programme involved the use of banks of pipe-type obstacles to simulate heat recovery tubes.

The experimental programme also acted as a test bed for the essential configurations and diverse situations that will be encountered with the WP 2.3 test rig in which a replicate heat exchanger will be present, such that its influence on the combustion intensity can be fully examined with a view to identifying the operational limits necessary to avoid any detonation propensity.

2.2 CONTRACTURAL OBLIGATIONS

The contractual obligations in respect of WP 2.2 are as follows:

- To investigate in a 600 mm diameter duct the effect of its confinement on the results of the small scale study of Task 1 into the ignition, limits of flammability, and DDT potential for the selected systems of high hydrogen fuels;
- To assess the risk of ignition of non-combusted hot exhaust gases on hot surfaces for a specified flow rate and exhaust gas temperature; and
- To re-examine and validate the scaling criteria applied to the conditions and results of Task 1 to ensure that they may confidently be applied for scale-up to the Task 2 test rig.

2.3 SPECIFIC OBJECTIVES

The specific objectives of this part of the project were as follows:

- Provide details of the design basis for the test rig together with its operational procedures;
- Define the operational envelope for the test rig through a comprehensive commissioning programme;
- Ensure that this envelope covered all of the test programme requirements as defined in the agreed test programme and the subsequent variations to the programme;
- Undertake a series of ignition tests for a range of high hydrogen gas mixtures in which initially no heat exchanger was present (open tube), secondly with an eight row heat exchanger present and finally with a fifteen row heat exchanger present;
- Complete a test programme comprising twenty-nine tests initially, to be followed by a further test series comprising thirty-five additional tests. It is noted that five tests involving the use of carbon monoxide were initially unsuccessful due to pre-ignition and were scheduled for later in the programme using a change in the methodology; and
- Report the results from both series of tests together with all the relevant information arising from the previous bullet points. (NB: The analysis of the results is contained on a separate report (4)).

2.4 DELIVERABLES

In respect of reporting this part of the overall project, a comprehensive report is to be provided describing the test facility, its means of operation and the results obtained during the test programme. A comprehensive photographic record of the test rig and the tests results will also be provided as part of the report. The results detailed will also provide an opportunity to comment on the suitability of the instruments used and whether these provide an acceptable suite of sensors for use in the future larger HRSG tests. Consideration will also be given here as to the effectiveness of these under weak flame conditions, which may be more prevalent in the future tests.

A second report from Imperial College will be provided that will include details of the scaling criteria used and a detailed analysis of the test results as a means of validating the chosen scaling criteria. This report will also include a comparison of the results for the flammability limits, hot surface ignition and DDT potential for the selected fuel mixtures with those from the smaller-scale studies.

2.5 ACCEPTANCE CRITERIA

The acceptance criteria is provision of a comprehensive report of the experimental programme describing the test facility, its means of operation and the experimental results obtained during the circular test programme (minimum 20 tests). A comprehensive

photographic record of the test rig and the tests is also to be provided as part of the report, together with evidence for the use of carbon monoxide (CO) as part of the test programme.

Evidence of a technical oversight from an industrial perspective is to be provided by the Chief Industrial Technology Officer.

3 BASIS OF DESIGN (BOD)

3.1 DESIGN PHILOSOPHY

The design philosophy followed was to provide a versatile rig that would enable a wide range of test parameters to be examined together with a large range of flammable gas mixtures, representative of those expected to be used in practice. In addition, safe operation of the rig was paramount, which was implemented through the safe working pressure that the rig was designed to withstand, the use of high temperature stainless steel for the key structural elements of the rig and through a comprehensive HAZOP study of the whole rig design and its operating procedures. The latter resulted in strict operating procedures and control measures, which were intended to mitigate the consequences of the major accident scenarios.

The design, manufacture, installation and operation of the rig were in compliance with the relevant CDM, DSEAR and Pressure Systems Regulations.

3.2 DESIGN SPECIFICATION

The specification for the rig was given originally in the BoD and commissioning documents (1 and 2), however as a consequence of commissioning the rig and its subsequent operation when undertaking the test programme, several changes were made to the design specification as work progressed. The original specifications are listed below and any changes made, where relevant, are shown in italics. The latter represent the current capabilities of the rig.

1. The main component of the rig is to be a 600 mm diameter stainless steel duct. Its length is to be 12 metres and it is to comprise four 3 metre long flanged and bolted sections. The maximum operating pressure for the duct is to be 22 barg, and the maximum wall design temperature to be 400 °C.
2. A Rolls-Royce Viper, type 301, gas turbine, running on butane, is to be used to supply a vitiated exhaust stream to the duct.
3. Engine mass flow rates are to be between 18 kg/s and 5 kg/s depending on engine rpm. Measurements are to be within $\pm 2\%$ of the required value. *Two mass flow rates were chosen to represent high and low flow conditions; these were approximately 11.75 kg/s and 2.5 kg/s. The accuracy to which these were measured was defined by the resolution of the pressure transducer(s) used to measure the dynamic pressure across the duct. These were within $\pm 1\%$ FSD of all transducers used. For the low mass flow within the duct, this corresponds to an error of ± 0.3 m/s or ± 0.03 kg/s and for the high flow an error of ± 2 m/s or ± 0.2 kg/s.*
4. The mass flow rate is to be controlled by orifice plates in combination with an exhaust diverter that allows some of the flow to be exhausted to atmosphere before entry into the duct. Control of the mass flow through the diverter section gives velocities along the test duct of between 20 to 90 m/s. Measurements to be within $\pm 2\%$ of the required FSD value. *See item 3 above.*
5. Test gas mixtures and make-up oxygen are to be injected into duct in the transition section just before the entrance to the duct. Three spray bars, equi-angled across

the section are to be used for injecting the test mixture and a further three for injecting make-up oxygen. The maximum injection pressure is to be 20 barg, through 26 holes in each spray bar.

6. Test gases and oxygen are to be prepared and stored in two separate 220-litre pressure vessels. Their flow rates are to be measured and controlled via Coriolis flow meters linked to flow controllers operating at a pressure of 40 barg.
7. Turbulence is to be generated in the duct by a 50 mm square grid located at the beginning of the duct.
8. A heat exchanger is to be simulated by a series of eight or fifteen rows of 38 mm diameter pipes running vertically and located half way along the duct between the end of section 2 and the beginning of section 3. The blockage ratio is to be 40%. Other locations are possible.
9. Instrument ports are to be located diametrically opposed along both sides of the duct at a distance of 500 mm apart. In addition there are to be quartz viewing ports 500 mm from the start of each duct section together with a further instrument port on the top of each section at a distance of 250 mm from the section start.
10. Instrumentation is to comprise fast response pressure transducers, ionisation probes, optical probes and thermocouples. A pitot static probe is also to be used to obtain the velocity profile across the duct at the start of each test run, located 250 mm from the beginning of the second duct section. A gas analyser is to be used to measure the oxygen concentration in the exhaust stream at the exit from the duct.
11. Operating temperatures in the duct (after addition of fuel and oxygen) are to be within the range 350 to 600 °C. Measurements to be within $\pm 1\%$ of the required values. *Temperatures measured using 'K' type thermocouples manufacturer specified accuracy of ± 2 °C at 600 °C. (Note Section 1.2 above confirms the temperature range actually achieved).*
12. Provide the capability for injecting oxygen sufficient to restore levels to 21% in the exhaust stream when operating at 15 kg/s. This is equivalent to a maximum oxygen mass flow rate of 1.12 kg/s. Measurements to be within $\pm 2\%$ of the required full scale output (FSO) range of the device. *Maximum oxygen flow rate required was reduced to 0.88 kg/s. Emerson Coriolis flow meters used, types F050S & F100S, accurate to better than $\pm 0.2\%$ FSD, which in this case was ± 0.003 kg/s.*
13. Provide capability for injecting fuel mixtures up to 15% by volume of the total flow at the highest operational mass flow rate used. Measurements to be within $\pm 2\%$ of the FSO values for the respective gases. *Maximum fuel quantity to be injected was reduced to 12% by volume. Mass flow rates were measured using Emerson Coriolis flow meters, types F050S and F100S, accurate to better than $\pm 0.2\%$ FSD, which in this case was ± 0.02 kg/s.*
14. The fuel mixtures are to comprise mixtures of hydrogen, methane and carbon monoxide, or each gas individually up to maximum mass flow rates of 0.2 kg/s, 1.57 kg/s and 2.74 kg/s respectively. *The maximum mass flow rates required were reduced to 0.11 kg/s, 0.82 kg/s and 1.43 kg/s. The revised values were those required to give 15% of the total flow when operating at the revised maximum flow rate of about 11.75 kg/s. Note that higher percentages were possible for the lower flow rate condition.*
15. Analysis is to be made of exhaust gas mixtures for levels of NO_x (~500 ppm), oxygen, carbon monoxide, and carbon dioxide. Measurements to be to the specified accuracy of the instrument after calibration. *The gas analysis was carried out using a MultiRAE PGM-50/4P gas analyser and a MiniRAE PGM-50/5P oxygen analyser.. Oxygen concentrations during the test programme will be measured using a Servomex gas analyser, accurate to $\pm 1\%$ of FSD.*

16. Measurements to be made of the degree of “mixedness” achieved within the first three metres of the duct entrance, to a level of no more than $\pm 5\%$ of the measured concentration from the mean, both temporal and spatial. Accuracy within the limits specified by ‘Cambustion’ for the HFR500 instrument being used. *The ‘Cambustion’ HFR 500 instrument measured to an accuracy ± 5 ppm, with an estimated response time of about 8 msec. Measurements were made approximately 500 mm downstream from the beginning of the second section of duct for both the high and low velocities specified. Traverses were made across the duct whilst injecting representative gas mixtures. The gas mixtures contained approximately 3000 ppm of methane when fully mixed; variations from the mean were examined as well as variations across the duct.*
17. Measurements to be made of the temperature and velocity profiles across the duct, engine exhaust and inlet planes. Accuracy to be within the stated tolerances for the pressure sensors and thermocouples specified, namely $\pm 1\%$ of FSD. *The temperature profiles were measured using eight ‘K’ type thermocouples whose accuracy was given previously at item 3. The velocity profiles were measured initially using a rake comprising seven pressure sensors. The measured values did not agree with sufficient accuracy with the Laser Doppler Analysis (LDA) measurements, which were taken as the standard. Consequently the rake was replaced with a calibrated pitot-static probe, which could be traversed across the duct to obtain velocity profiles.*
18. LDA measurements to be made of the velocity and turbulence profiles within the duct. Measurements to be within the limits specified for the instrument used. *Inlet velocity profiles were measured using a Dantec LDA system with X-optics operated in back-scatter mode and a BSAF80 processor. The velocity profiles and turbulence levels (x-direction only) in the duct were measured with the HSL owned TSI manufactured LDA system. Additional low velocity measurements were made using a calibrated pitot-static probe whose accuracy was ± 2.5 Pa ($\pm 1\%$ FSD), where the FSD was 250 Pa. Higher velocities were measured to the same degree of accuracy.*
19. Measurements to be made of both the temperatures and dynamic pressures along the duct during testing. These to be measured to within the levels of accuracy specified by the manufacturers of the instruments being used, namely Kulite and PCB pressure sensors and ‘K’ type thermocouples, namely within $\pm 1\%$ of FSD. Note that both types of pressure sensors will be used to measure the dynamic pressure rises following an ignition within the duct. *The ‘K’ type thermocouples were to the same accuracy as specified previously. However, there was a noticeable lag in the measurements due to the thermal mass of the measuring rake. The pressure sensors were within the specified accuracy, being in both cases 0.1% of FSD.*
20. Ionisation probes and optical (photoconductive) sensors to measure flame front velocities. These are on/off devices as designed and manufactured by Chemtech. *These units were tested prior to installation by subjecting them to a flame front and observing the response. Since the ionisation sensors are purely conductive devices their response times are short e.g. less than 1 μ sec, whilst the quoted time response of the Hamamatsu photoconductive sensors is 2 μ sec.*
21. Ignition system comprising a 2 Joule spark (minimum) to be positioned on the centreline of the rig. *An 8-10 Joule spark was used, as this was the only unit readily available at the time. It sparked repeatedly at a rate of once every 1.5-2 seconds. It was situated for test purposes on the rig centreline, 250 mm from the entrance to the first section of duct.*

22. Data logging and processing system. Resolution to 16 bit or better, maximum sampling rates 1MHz, but typically 100 kHz. Data from the foregoing sensors, except the thermocouples, are to be sampled at a rate of 100 kHz per channel using a National Instruments logger and processor. (It was acknowledged during design discussions that the above sampling rates were acceptable for non-detonation events, which would form the main focus of the work but that the occurrence of detonating events would still be identifiable). National Instruments Diadem software to be used for data analysis. *The data logger used was a Dell x desktop computer, and the data collection system and associated software was Labview 2013.*
23. Engine and control data including thermocouples to be sampled separately at a rate of 10 Hz. The two systems to be time synchronized by incorporation into the same LabVIEW data acquisition environment (virtual instrument) and the provision of synchronisation signals on channels of different acquisition cards.

4 DESCRIPTION OF THE TEST RIG

The test rig was designed to provide the means for investigating the potential consequences associated with the ignition of mixtures of flammable gases as may occur in CCGT or CCGE installations when the prime mover fails, allowing a flammable gas mixture to enter the exhaust system and ignite. A flame front and associated pressure wave will then travel through the exhaust system and enter the HRSG where the pressures they generate may cause structural failure with potentially serious consequences. The design objective is achieved by the provision of the following elements:

- a gas turbine engine that provides hot exhaust gas into a circular duct of 600mm diameter and at a temperature comparable to the full scale installation, with its associated fuel supply;
- an engine control system that can be operated remotely;
- a means of restoring the oxygen level in the duct to the normal air level;
- a means of injecting a controlled amount of test fuel into the duct to simulate flame-out conditions;
- an ignition system for the hot flammable gases in the duct, which is linked to the data acquisition event;
- a range of sensors with both medium and fast response to enable the monitoring of the operating conditions and the capture of the flame and pressure signatures during an ignition event; and
- a facility by means of which obstacles can be incorporated into the duct to simulate the heat exchanger tube banks in a normal HRSG system.

These infrastructure components are described in more detail in subsequent sections.

The isometric drawings at Figure 1 and Figure 2 show the overall installation.

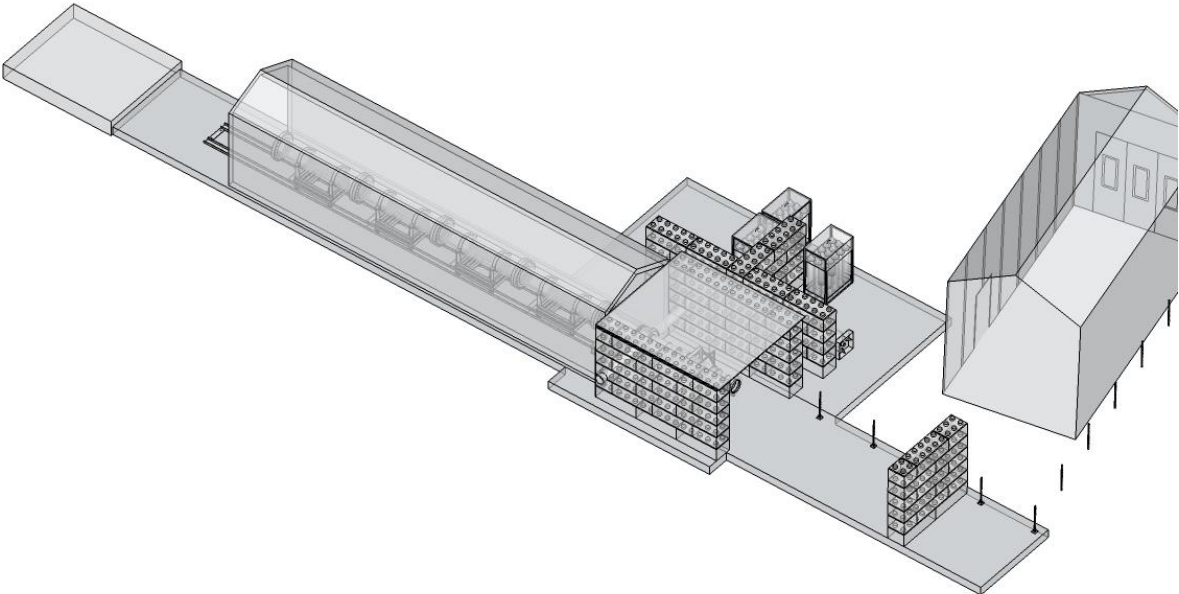


Figure 1: Isometric drawing of installation

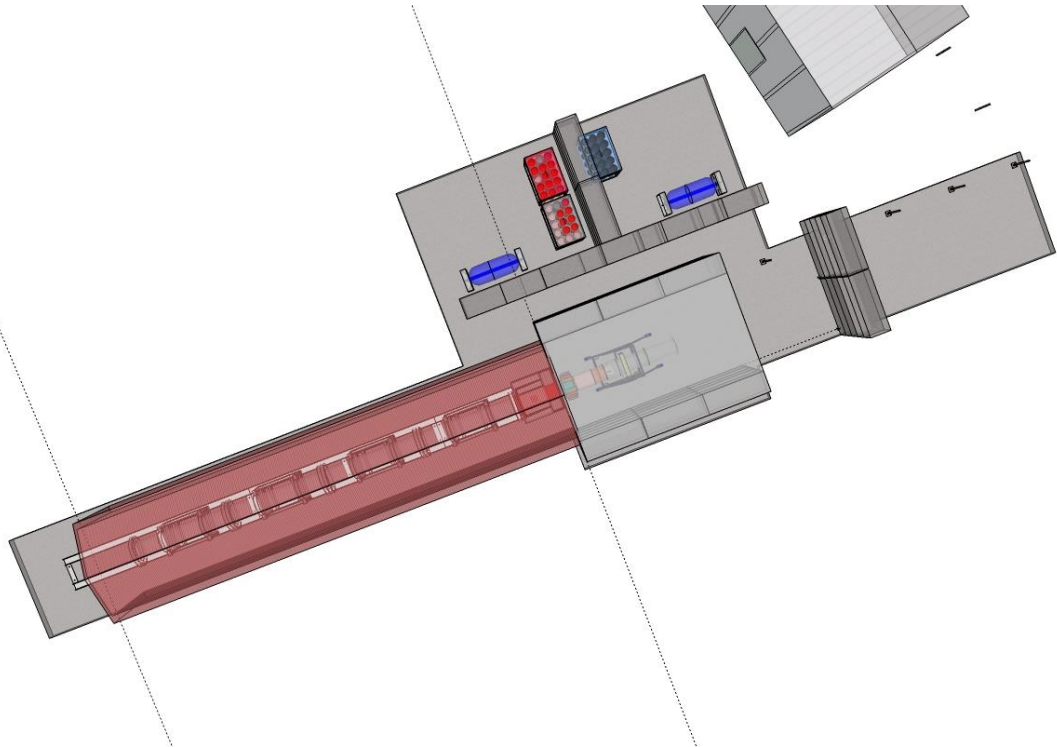


Figure 2: Isometric drawing with cut away viewed from above

4.1 BASIC LAYOUT OF THE ENGINE AND DUCT

The test rig is comprised of a Rolls-Royce Viper, type 301 gas turbine, and a circular duct, see Figure 3, the exhaust from which fed into the 0.6 m diameter circular duct, which was 12 metres in overall length and open ended. The duct comprised 4 x 3 m long insulated sections, flanged and bolted together and designed to withstand a maximum operational pressure of 22 bar, and a maximum average wall temperature of 400 °C, see Figure 4.



Figure 3: Viper engine in situ



Figure 4: Circular duct sections with insulation

The Viper gas turbine was converted to run on liquid butane. This was done in order to minimise the possibility of soot particles and other additives affecting the DDT behaviour of the gases being tested. Consequently, the design of the gas turbine rig involved modification of the engine prior to commencing the test programme as well as purchasing and installing a 9000 litre liquid butane storage tank. Modifications to the engine to run on butane involved removal of its existing fuel pump and fitting an external variable speed positive displacement pump to meter the fuel flow into the engine and therefore control its speed. To this end, expertise from another company, Reaction Engines, who have specialised technology for running a Viper engine on pure butane, was obtained so that the risks of any unforeseen technical difficulties arising from the conversion of the engine were minimised. The fuel storage and supply system are shown in the P&ID diagram given in Figure 5, and the actual fuel supply system in Figure 6.

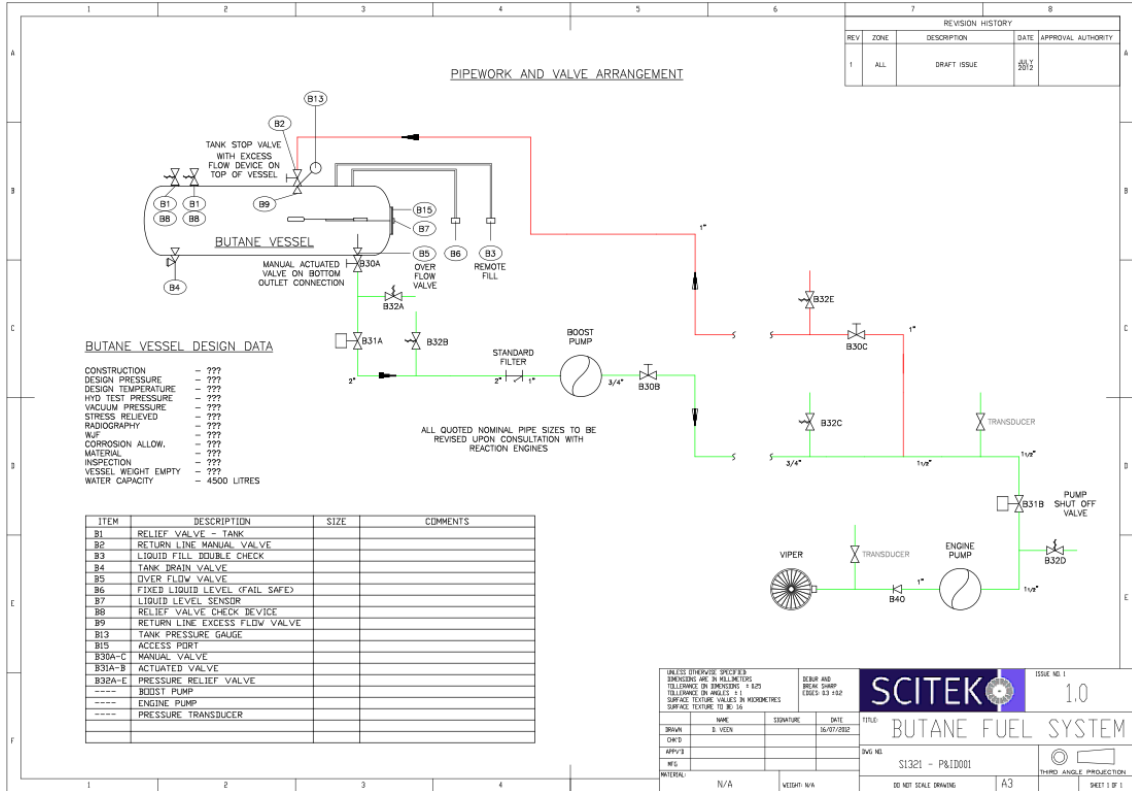


Figure 5: P&ID diagram of butane supply



Figure 6: Butane supply tank

The engine exhaust gas temperatures immediately after the turbine varied from 500 °C to 720 °C depending on the operating conditions being used. Increasing the fuel flow increased the engine speed, which increased the mass flow through the engine and the exhaust temperature as a consequence. The engine output was variable from idle conditions, when the mass flow rate was 5 kg/s, up to maximum power when the mass flow rate was 18 kg/s. Once at or above idle the exhaust temperatures remain at approximately 600 °C until almost full power output was reached. As the engine was not operated at a mass flow rate of more than 12 kg/s, temperatures above 600 °C were not reached during the test programme described herein.

4.2 DIVERTER SECTION

There was both a diverter section and a transition section incorporated between the engine's turbine and the start of the 0.6 metre diameter duct. The first of these provided a pathway from the engine turbine into the duct. It also provided a means of controlling the amount of exhaust flow that entered the test duct by enabling some of the exhaust flow to be diverted sideways to atmosphere, see Figure 7. The flow rate into the duct was controlled through the use of orifice plates in combination with the diverter; see Figure 8.



Figure 7: Gas diverter section

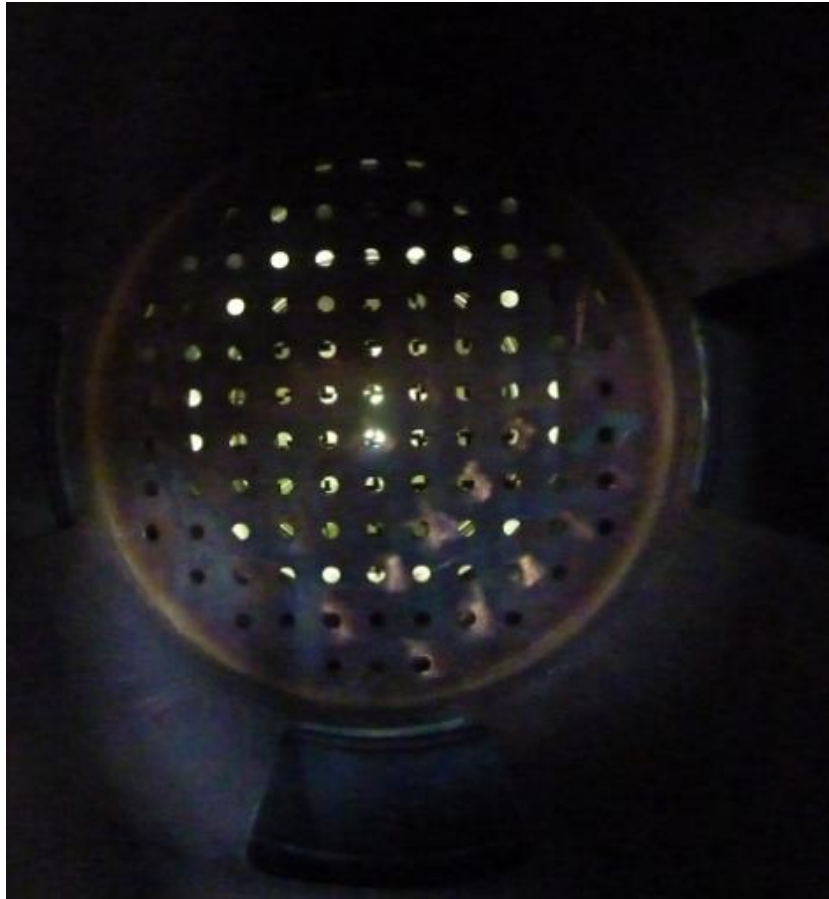


Figure 8: Orifice plate smaller holes in situ

The diverter section was also used to minimise the back pressures reaching the engine. Minimising the back pressure on the engine turbine in the event of a major deflagration/detonation in the test duct was particularly important as under the intended test conditions there was a volume of non-combusted gas mixture on either side of the ignition point. Any flame and pressure waves generated could propagate and accelerate through the gas.

4.3 TRANSITION SECTION

The transition section expanded the flow from the engine turbine into the duct (see Figure 9). Six spray bars each containing 26 holes were integrated into this section to provide a means of injecting and mixing the test gas mixtures circumferentially into the main hot gas exhaust flow from the engine; see Figure 9. These gases were injected at about ambient temperature, thus minimising the risk of ignition at this point. The first three spray bars were used to inject oxygen such that the oxygen concentration was restored to 21%, the second group of three were used to inject the gas mixtures. The transition and diverter sections were designed to the same operational parameters as the duct sections, but with maximum operating pressures of 10 bar and 5 bar respectively.

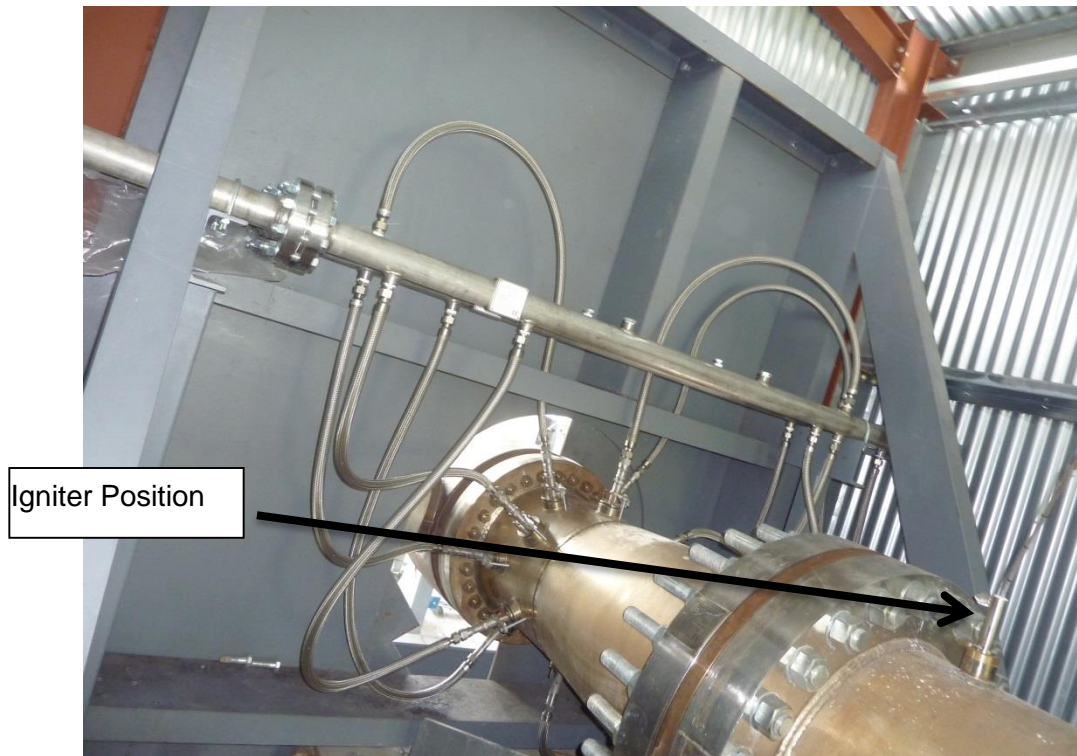


Figure 9: Transition section

The ranges of velocities achievable were typical of those found in full size CCGT/CCGE systems, namely achieving typical turbine exit velocities of around 90 m/s as well as achieving a lower velocity of around 20 m/s, which represented the average velocity at the entry plane of a typical HRSG.

There was a turbulence generator at the entrance to the first section of the duct; this consisted of a 50 mm by 50 mm square grid fitted with small deflector plates; see Figure 10. It was sandwiched between the end of the transition section and the beginning of the duct. There was a spark igniter a further 250 mm downstream located through the top instrument port on the first duct section; see Figure 9. The spark plug itself was positioned on the centreline of the duct. This position was chosen to give the maximum run-up distance for the developing flame front, which was also consistent with CFD simulations that showed that the injected fuel and oxygen would be fully mixed into the engine exhaust stream by this point. Alternative downstream locations for the igniter were available.

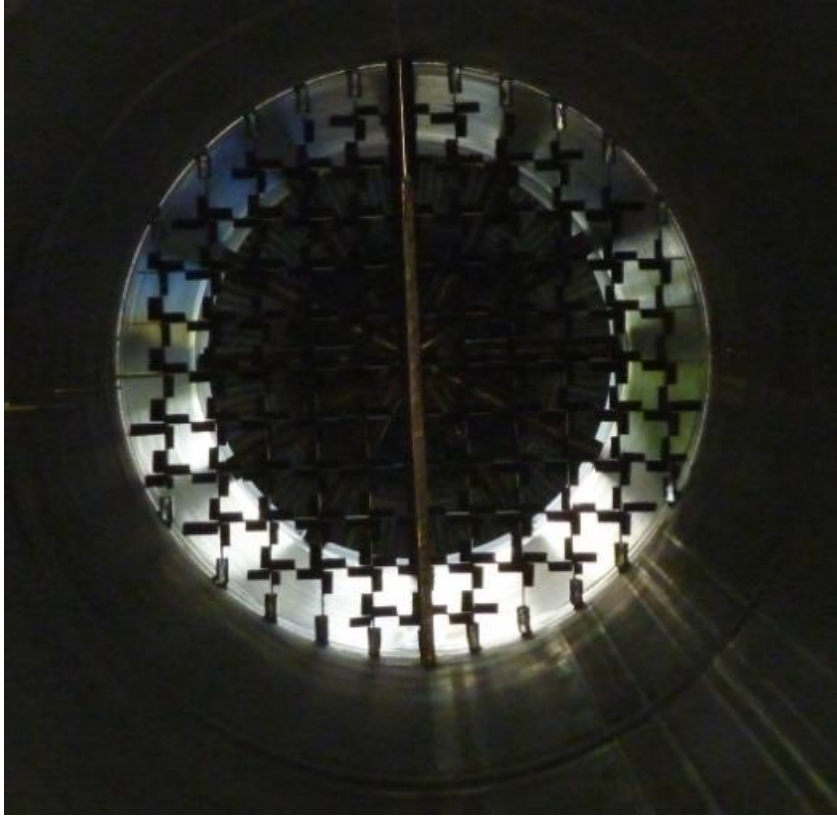


Figure 10: Turbulence generator

A pitot-static probe that traversed the duct passed through the optical viewing port on the second section of duct. This was used to obtain velocity profiles across at least half of the duct, and from which the mass flow rates through the duct were calculated for any flow condition. It was driven across the duct electrically with a stepper motor and its position recorded using a linear transducer, see Figure 11. These measurements could be made through any of the four optical ports on the side of the duct.

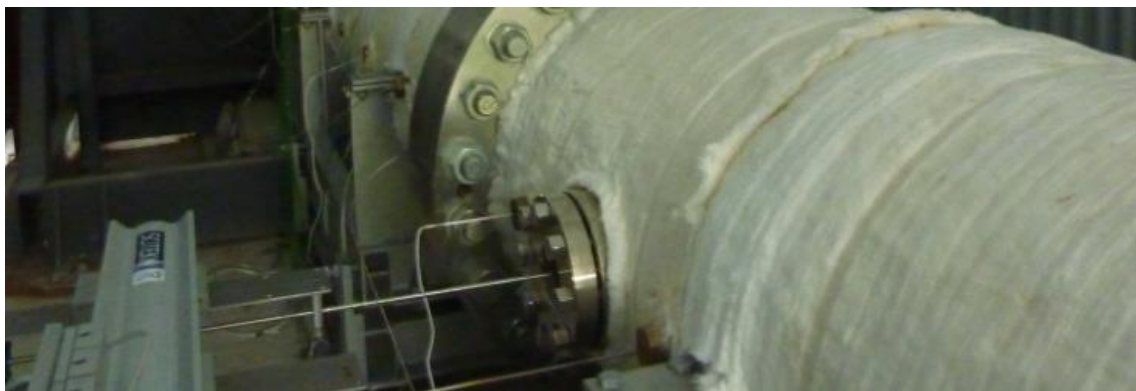


Figure 11: Pitot-static probe in situ

An HRSG was simulated in the duct by a series of removable 38 mm diameter tubes, on a pitch of 95 mm, running vertically and held in place by two parallel plates; see Figure 12.

The tubes were in either eight or sixteen rows and the blockage ratio per row was 40%. During the WP 2.2 test programme the tube bundle was sandwiched between the end of the second duct section and the beginning of the third. It could be positioned between any two duct sections.



Figure 12: Tube bundle

The reasoning for this location was to allow some distance after the igniter for flame development in order that a more uniformly distributed flame front impinged on the blockage and also to allow some distance beyond the blockage for flame and pressure monitoring before the flame exited the duct.

4.4 FUEL AND OXYGEN SUPPLY SYSTEM

The gas mixture and oxygen supply systems were positioned to the side of the main building housing the duct and engine; see Figure 13. The installation is shown in the P&ID in Figure 14.



Figure 13: Gas delivery system

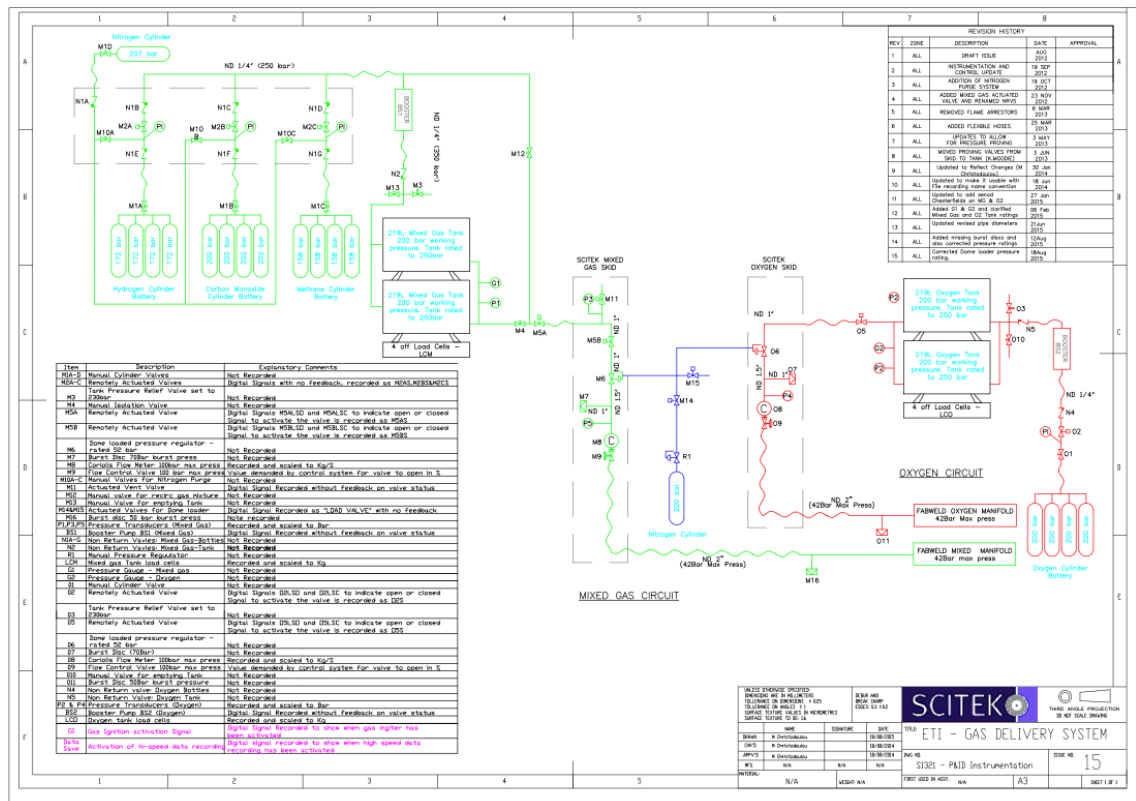


Figure 14: P&ID fuel gas and oxygen delivery systems

The system of gas mixture and oxygen supply consisted of two stainless steel pressure vessels with a maximum capacity of 225 litres and a MWP of 300 barg. One vessel contained oxygen, the other the fuel mixture. The latter comprised mixtures of hydrogen/methane/carbon monoxide and nitrogen as required. Specific gas mixtures were prepared from individual gas cylinder packs using a Haskel booster pump. Mixtures were quantified using partial pressures. Mixtures and individual gases up to 100% concentration

could be prepared in this way. During commissioning both pressure vessels were mounted on load cells, three per vessel, to enable the mass flow rates from the vessels to be measured independently.

The means of injecting the gas mixtures was a flow-through system, injecting directly into the exhaust stream and relying on the injection process to ensure that the gases were fully mixed with the exhaust stream. This avoided waste and reduced the risk of a flashback. The mass flow rates of the injected gases were measured using individual Coriolis mass flow meters and controlled using mass flow controllers. The supply line pressures were regulated using pressure regulators (55 bar maximum, but typically 40 bar). This method of flow control and monitoring provided a more accurate control system with better resolution and variability than would have been obtained by direct injection through fixed diameter orifices. The need to do so arose from an assessment of the test data obtained from WP 2.1, which showed the importance of even small variations in the mixture compositions. Hence the need to have precise control over the mixture concentrations injected, together with a wide range of mass flow rates to match the exhaust mass flows. The same method of flow control was used for the addition of oxygen.

The gas supply system was located in a well-ventilated area and piped to the rig. For safety reasons it was separated from the actual rig by a double concrete block wall located to the side of it. The pipe work with its associated pressure regulators and flow controllers was designed and installed to accord with the Pressure Systems Regulations, incorporating non-return valves and flame arrestors, where appropriate.

4.5 HOUSING FOR THE RIG

The complete test facility comprising the jet engine and the duct, with its associated components, was housed in an approximately 15 metre long by 3.0 x 3.5 metre cross-section ventilated agricultural style building. The test duct was attached directly to a substantial concrete pad, which could withstand the resulting dynamic reaction loads should a hydrogen detonation occur within it. The duct was fixed at one point only, through an anchor plate attached at the entrance area of the duct. The rest of the duct was simply supported on bogies in order to allow for thermal expansion. The Rolls-Royce viper engine was mounted independently with a variable length connection between the exit from the turbine and the beginning of the diverter section, which controlled the amount of engine exhaust flow that was spilled and also allowed for thermal expansion.

The engine itself was isolated from the test section by a steel blast wall designed to prevent any fragments from a failed engine reaching the test area. The engine was also housed within a semi open rectangular building, which was made from concrete blocks with a steel roof; see Figure 15. This building was open at one end and was designed to contain any fragments resulting from overpressures that may occur should there be an accidental release of flammable butane from the engine fuel system that subsequently ignites. The building was also designed to contain any fragments that may result from a failed engine. One engine was lost in the test programme due to a bearing failure. There were two openings in each side of the concrete block walls through which protruded the two

horizontal exhaust pipes. These ducted the excess exhaust flow from the engine away from the test area when it was operating in a low flow mode.



Figure 15: Engine enclosure

4.6 ENGINE CONTROL SYSTEM

The control system for the engine was an adaptation of the established control system used when running the Viper engine in its normal mode on kerosene. A dedicated PLC system was programmed to control the engine and ensure the prescribed safe operation of the engine, rig and facility. The specialised experience of Reaction Engines was used again in the development of the control system, as it needed to accommodate extra safety features relating to the use of butane as fuel. The engine was started using an electrical starter to spin it to some 700 rpm; it was then ignited using the main fuel injectors. The control systems for the engine and the gas delivery comprised two PLC systems.

The first PLC system was responsible for controlling the engine and for recording all engine related parameters. It also oversaw the safe operation of the engine and therefore had built-in logic and controls that determined in what sequence valves were activated. It would also shut the engine down if any of the monitored parameters exceeded set limits. The PLC communicated with a PC located in the control room that ran the user interface and recorded on disc all monitored parameters at a rate of 10Hz. Manual ESTOPS were provided on the engine frame and in the control room which shut down

the engine in case of an emergency. The PLC monitored all ESTOPS and prevented the engine being restarted until the ESTOPS had been reset. During commissioning several updates to the software were made as the engine operation and butane supply systems had to be matched. The use of a flow diverter for the exhaust changed the engine characteristics so the software also had to be tuned to allow easier operation as a consequence.

The engine control system recorded a number of other engine and rig parameters apart from rpm. These included oil pressure, compressor pressure, exhaust temperature, vibration, intake pressure and intake mass flow rate. Software was written to communicate with a National Instruments hardware cRio/PXIe/SCXI system and to display these parameters on computer screens as well as storing them on a hard drive. The clock of the engine control system was synchronised with that of the data acquisition system so that data from other instruments could be correlated with engine parameters.

The cRio/PXIe/SCXI was located in close proximity to the engine whilst that part of the control system responsible for displaying and storing the engine parameters was in the control room. For safety reasons this was situated approximately 90 metres from the engine and test area. Engine start, speed settings and shutdowns were carried out from the control room. Failsafe hardware was installed, which in the event of a power failure, gas leakage, and engine over-speed or over-temperature would automatically shut down the engine and the rest of the system. A typical control screen for the engine system is shown in Figure 16.



Figure 16: Engine control system

4.7 GAS DELIVERY SYSTEM

The second PLC unit was responsible for controlling the gas delivery system and for recording all process parameters at a rate of 10Hz. This system also recorded the engine speed (rpm) signal (same signal that the engine control PLC was recording). This was synchronised (to within 0.1 seconds) with the recorded parameters from the gas delivery system together with the data recorded by the engine control system. The gas delivery system PLC communicated with a PC located in the control room that had a user interface and also recorded all process parameters onto disc. The gas delivery system also provided digital trigger signals for the high speed data acquisition system to initiate high speed (up to 1 MHz) recording of the rig data. During commissioning several updates were made to allow tuning of the PID parameters for the control valves so that their response times were optimised for fast response with a small amount of overshoot. Also, from the experience gained in running the oxygen and mixed gas system it was necessary to change the logic of how the software triggered the two systems to start operating and how the valves and dome loaders were operated. The key information collected from the gas mixing (injection) system was fuel and oxygen storage pressures, mass flow rates, valve responses and, during commissioning only, the weights of the gas storage cylinders.

The engine operation and the fuel/oxygen injection systems were both controlled from the control room situated approximately 90 metres from the test rig, but in line-of-site. Several updates were made to these systems in the course of commissioning. The control screen for the injection system is shown in Figure 17.

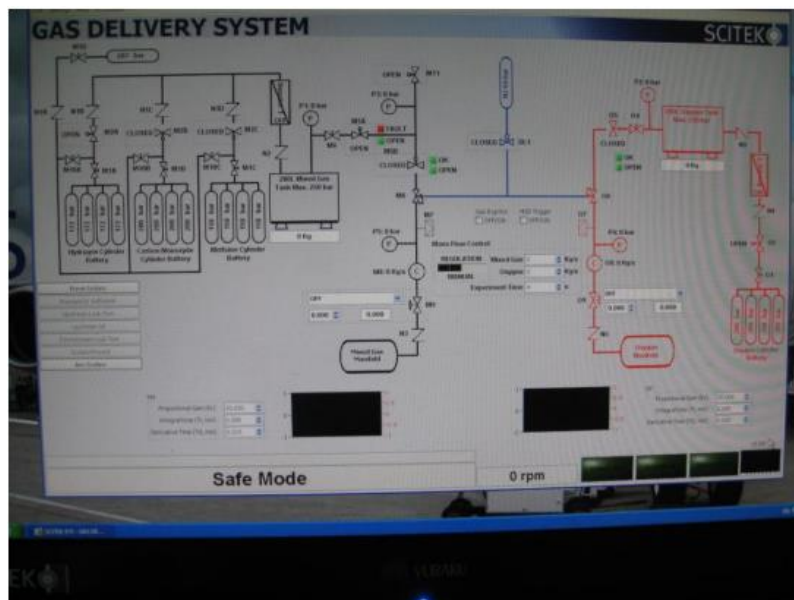


Figure 17: Gas delivery control system

4.8 RIG DATA COLLECTION

A consortium partner, SCITEK, designed and installed the data acquisition system for the rig, using hardware from National Instruments in the form of cRio/PXIe/SCXI systems which have fast data acquisition capability as well as signal conditioning capability for different types of sensors. This system was also interfaced to the engine control system, which was also a PXIe/SCXI system. The data collection software ensured that all critical data was displayed in numerical and graphical form and stored for more detailed analysis in due course. The software for data acquisition and control was written by SCITEK in LabView, which is the industry standard.

The PXI system used for the fast data logging was PC based and could record data at up to 1 MHz from the sensors on the rig during the experimental test programme. The actual data acquisition rates used were chosen appropriately for each of the sensors being sampled. Gas delivery and engine monitoring sensors were sampled at 10 Hz, engine rpm, exhaust O₂, ignitor and duct thermocouples were sampled at 5 kHz and the main ignition event sensors of pressure, flame ionisation and optical flame sensing were sampled at 100 kHz. This system was configured to record all experimental parameters using software that allowed quick processing of the data. Data processing and analysis was undertaken using the Diadem software package.

Prior to signing off the data logging and processing it was observed that there was considerable noise on several channels when logging the high-speed data channels during actual ignition tests. The noise was found to have been generated by the inverter operating the engine fuel pump. The problem was finally resolved by providing a separate earth for the inverter and screening it off from the PXI system and the rest of the data logging system, in accordance with the installation instructions for the inverter.

5 COMMISSIONING

5.1 INTRODUCTION

Commissioning took longer than anticipated, primarily because of the necessary changes required to achieve an acceptable range of operating conditions within the duct, i.e. in terms of exhaust flow velocities and temperature. However, additional time and testing proved necessary in order to improve the operation of the gas and oxygen injection systems and ensure that satisfactory operation was achieved. In practice it was necessary to accept longer injection times than originally planned because of the time delays taken by the flow control systems to reach steady-state conditions.

5.2 MAJOR RIG COMPONENTS

The test rig comprised five major components/systems as follows:

1. **Liquid butane system.** Comprising: Liquid butane storage tank and pumps for supply of liquid butane to run the engine.
2. **Gas turbine.** Comprising: Rolls-Royce Viper gas turbine. Converted to run on liquid butane.
3. **Test rig.** Comprising: Twelve metre long by 0.6 metre diameter test duct. Comprising 4 x 3 m long sections bolted together, together with transition and diverter sections, a removable turbulence generator, igniter, orifice plates and an 8 or 15 row tube bundle simulating a HRSG heat exchanger.
4. **Fuel and oxygen supply systems.** Each comprising: A reservoir, pressure regulator, Coriolis mass flow sensor, bursting disc, flow control valve and stop valves.
5. **Instrumentation.** Comprising: Sensors and the central data acquisition and control systems.

Once the foregoing items had been completed and installed according to the BoD requirements, a series of commissioning procedures/trials were undertaken. These were done in order to establish that the performance of the system was satisfactory and that the system met all the required safety standards defined through the HAZOP studies. They were completed and reported upon in (2) prior to beginning the test programme described in this report.

The salient features of the final outcomes of the commissioning process are given in the following text under the five major component/system headings. The commissioning process sought to commission each of the above five items separately prior to integrating them into the test rig and testing it in its totality. The two key aspects of this process were the following:

- a) Test integrity, including leak and pressure testing, and
- b) Test for correct functioning, i.e. system meets design specification requirements.

5.2.1 Liquid butane system

The butane supply system was installed and tested in accordance with the P&ID shown previously as Figure 5. The supply system was leak-proof and was shown to deliver liquid butane to the main engine fuel pump at a rate that met the maximum operating requirements of the engine. Due to the limited height difference between the tank and the engine it was not possible to operate the system with less than 30% butane in the supply tank, due to the butane vaporising in the fuel line. This was likely due to parameters associated with the fuel pump, i.e. suction head, which was not fully known at the time of the fuel system installation. The fuel supply was under the control of the engine management software, a typical graphical display from which is shown in Figure 16

5.2.2 Gas turbine

Modifications to the engine installation were made in order to give the required performance characteristics once the operational characteristics of the Rolls-Royce Viper type 301 gas turbine had been established. These proved to be substantially different from those of the previous engine model, upon which the test rig had been originally designed. In addition the engine was converted to run on butane instead of aviation fuel, for which appropriate performance characteristics were not available. In the event, the performance characteristics of the 301 were not as expected, and as a consequence extensive modifications were also designed into the rig and implemented as part of the operational procedures, (see following section).

5.2.3 Test rig

Based on the BoD, two velocity conditions were required in the working section of the duct. These were a high (80-90 m/s) and a low flow (18-25 m/s) velocity, with exhaust gas temperatures in a specified range of 400 - 600 °C, before the addition of the test gas mixture and the make-up oxygen. In practice these conditions were achieved by running the engine at high speed, namely at 12,200 rpm combined with a relatively high back-pressure, and in the case of the low flow condition diverting some 85% of the flow out of the duct. This amount was far more than the rig was originally designed to cope with. Consequently the original diverter design, which had contained a forward facing cone to help divert flow away from the duct entrance and into the diverter exhaust pipes, was modified by removing this cone.

In order to achieve the correct combinations of temperatures and low velocities in the duct, the diverter control section, which was originally designed to slide in and out, was also modified to open/close by being rotated through 45 degrees to make its operation more

convenient. This required four rectangular slots to be cut into its sidewalls in the appropriate positions. This is shown in Figure 7.

An analysis of the data at the time suggested that the alternative approach of using two orifice plates of suitable dimensions offered the most promising solution. An orifice plate containing 120 holes 14 mm in diameter, together with the diverter fully open, gave the required low flow operating conditions when the engine was running at some 12,200 rpm. That is to say it gave a velocity of 20-25 m/s at a temperature of around 550-600 °C in the duct, when measured 250 mm downstream from the beginning of the second duct section. The orifice plate was inserted at the entrance to the transition section immediately after the diverter. The high flow orifice plate was made from the same material, but contained a single 300 mm diameter hole. This enabled velocities of some 90 m/s to be achieved at a temperature of about 580 °C with the diverter fully open. Both plates proved satisfactory during the subsequent commissioning work; however, changing plates was not a simple task.

A third orifice plate was manufactured for meeting the low flow rate condition but at a lower temperature. This enabled a test programme to be offered with two distinct temperatures. The low flow conditions were obtained with the diverter fully open as also proved to be the case for the high flow condition. The single hole high flow rate orifice plate is shown in Figure 18.



Figure 18: High velocity orifice plate

A turbulence generator was added to the rig at the beginning of the first section of the duct. End-on it consisted of a series of 50 mm squares with flat plates attached at the exit end inclined alternately at 10 degrees. The grid produced only a minor resistance to the flow and the turbulence generated by the grid was not measured explicitly but assumed to be a component in the overall measured turbulence levels. Flow and turbulence

measurements were therefore made downstream of both injector pipes and the turbulence grid.

5.2.4 Fuel and oxygen supply systems

The oxygen and gas injection tubes were situated approximately 2.5 metres downstream of the engine turbine where the measured exhaust temperature was as high as 600 °C. In the high flow case the temperature of the exhaust flowing past these tubes was expected to be only marginally lower than at the turbine exit, namely around 600 °C. In addition, the gas velocity approached 400 m/s as it flowed through the orifice plate immediately upstream of the injection tubes. Consequently the stagnation temperature on the front of them could be an additional 40 °C. This increased the heat-up rate for the injected gases, which helped account for the observed lower than expected temperature drop in the exhaust gas flow once the injected gases had fully mixed with it.

Commissioning of the fuel and oxygen supply systems took longer than anticipated due primarily to several control valves not meeting the manufacturers' specification when originally supplied. These were eventually replaced by the manufacturers with valves that did meet the specifications. In addition, the original oxygen flow control valve and Coriolis flow meter were not suitable for oxygen service as originally supplied. These were returned to the supplier to be modified before commissioning of the oxygen injection system could be completed.

Problems were also encountered with a 3-way solenoid valve that controlled the pressure being applied to the domes of the two Hale - Hamilton pressure regulators. This valve would not operate consistently at the operating pressures required to achieve high gas injection rates. An alternative valve was not available immediately from the suppliers; consequently, an alternative means of controlling the dome pressures was devised using two 2-way valves.

In developing a satisfactory means of operating the gas and oxygen injection systems, three bursting discs protecting the injection components downstream of the Hale-Hamilton pressure regulators failed and had to be replaced. This was not expected but occurred as a result of the slow reaction times of these two regulators when operated in a no-flow condition with their domes pressurised. A work-round was developed and incorporated into the controlling software, which required a change in the operating sequences for both the fuel and oxygen injection sequences.

Two hand-operated vent valves were added at the filling point of the two gas storage cylinders to enable them to be safely emptied in the event of the remotely operated main discharge valves failing to open when the cylinders were under pressure, as happened once during commissioning of the oxygen system.

The final layout for both the fuel and oxygen supply systems was as shown in the P&ID; Figure 14.

5.2.5 Instrumentation (Commissioning only)

Only the commissioning-specific instrumentation tests are described in this section. The instrumentation used routinely during the test programme is described in Section 6 of the report.

5.2.5.1 Velocity and turbulence measurements

Velocity and temperature profiles across the duct were measured by traversing a pitot-static probe across it with a thermocouple attached. The traversing mechanism available covered a distance of 510 mm; consequently, a full traverse was not possible in one run. The probe was not particularly flexible; therefore, to avoid it jamming as a result of the expansion of the duct when heated, the runs were done before the duct walls had reached their operating temperature. This was considered to have only a marginal influence on the gas velocity. Several traverses made across both halves of the duct showed that they were practically the same.

Velocity measurements were also obtained by traversing a TSI manufactured LDA system across the duct using the same traversing mechanism used for traversing the pitot-static probe. The optics were arranged so that the laser beams entered through the quartz glass optical viewing window situated 500 mm from the beginning of the second section of duct. The high temperature of the flow stream necessitated the use of solid particle seeding using the SCITEK LS-10 seeder. The seeding material used was titanium oxide powder with a grain size of one micron. An extensive literature database supports the use of this material and this size range for gas flow measurements. Providing aggregation is avoided by keeping the material dry, then this particle size and material is known to be able to follow the flow and turbulence fluctuations up to several kHz. The seeding was injected across the flow using a rake located just downstream of the gas injection pipes through one of the ports along the centreline of the rig. The rake was downstream of the turbulence generator screen. The LDA and seeding systems were operated remotely from the control room. Some time and effort was spent getting the seeding system to work satisfactorily and providing sufficient particles to give statistically meaningful results.

LDA measurements were made at both high and low velocities with the engine running at about 11,500 rpm. Additional single point locations were measured at the higher engine rate of 12,200 rpm for comparison. The results obtained, see (2), comprised the mean velocity, which was averaged from a few thousand particles passing through the LDA probe volume, and the turbulence intensity comprising the distribution of velocity about the mean velocity. Both measurements were calculated by the system and presented as the results. The reduced engine speed was used in order to minimise the fuel consumption as each traverse took approximately one hour due to the time required by the LDA system to acquire the data.

The turbulence levels existing in the duct were measured using the TSI LDA system, utilising an argon ion laser and a fibre optic probe with a 500 mm focal length operated in back-scatter mode. The TSI IFA-750 processor was used to process the LDA signals and

calculate mean velocity and turbulence intensity. The system used a probe volume size of around 1 mm in length and 0.1 mm in width. The LDA probe was mounted on the existing traverse mechanism and viewed the flow within the duct through the quartz window positioned 500 mm from the beginning of the second section of duct. It was traversed along a horizontal diameter of the duct. Measurements were made at the two chosen test velocities; the results are given in (2).

5.2.5.2 Mixedness measurements

The mixing, i.e. the degree of mixedness, of the injected gases with the exhaust stream from the engine was measured experimentally by injecting a mixture of nitrogen containing a small amount of methane. Simulations obtained from CFD modelling of the hydrogen injection and mixing process were used to predict when the mixing process would be completed, and these were confirmed experimentally. The potential differences in the mixing behaviour of the nitrogen/methane mixture when compared with a light gas mixture were assessed by undertaking additional experimental measurements using a low-density inert gas (helium) plus methane in order to simulate experimentally the mixing of a hydrogen/methane mixture. The mixedness testing was undertaken using a “Cambustion” fast flame ionisation detector, model 500HFR hydrocarbon detector. The unit used had an estimated response time of some 7-8 msec when installed to measure across the 600 mm diameter duct. The results from these tests are given in (2).

An unexpected problem arose at the beginning of these tests as it proved difficult to ensure that the gases were adequately mixed in the storage cylinder prior to injecting the mixture. This became apparent from the first of the mixedness tests when the results clearly showed that they were not adequately mixed. A method of mixing the two gases was therefore devised in which the lightest gas was the first one to be injected into the cylinder, followed by the heavier one. Additional pipework was also added to the system to provide a recirculation pathway. The gas mixtures were then recirculated through the cylinder and associated pipework using the Haskel boost pump, for a period of at least one hour prior to making any test measurements. This procedure was incorporated into all the fuel mixture tests.

6 INSTRUMENTATION

6.1 SENSOR types AND LOCATIONS

The permanent instrumentation attached to the rig comprised thermocouples, pressure transducers and optical sensors; both flame ionisation (IP) sensors and optical flame (OP) sensors. There were up to twenty-four flame ionisation sensors positioned along one side, the LHS when looking from the engine. These included those sensors built into the four or five rakes that were located across the duct. Each of these rakes contained three IP sensors. Along the opposite side there were up to six piezo-resistive pressure transducers manufactured by Kulite. An additional fast-response piezo-electric pressure transducer manufactured by PCB Piezotronics was also available, but only used in the later tests. There were also several 'K' type thermocouples attached to the duct for measuring both the gas and wall temperatures. The thermocouples measuring the gas temperature were inserted through the duct wall using the fixed transducer locations and protruded some 50 mm into the flow in order to be clear of the thermal boundary layer. Those thermocouples measuring the wall temperatures were bonded to the external wall surface under the layer of insulation. There was a sampling probe at the exit from the duct used for gas sampling but during testing it was connected to a Servomex oxygen gas analyser. All of the possible locations for the sensors on the duct are shown in Figure 19.

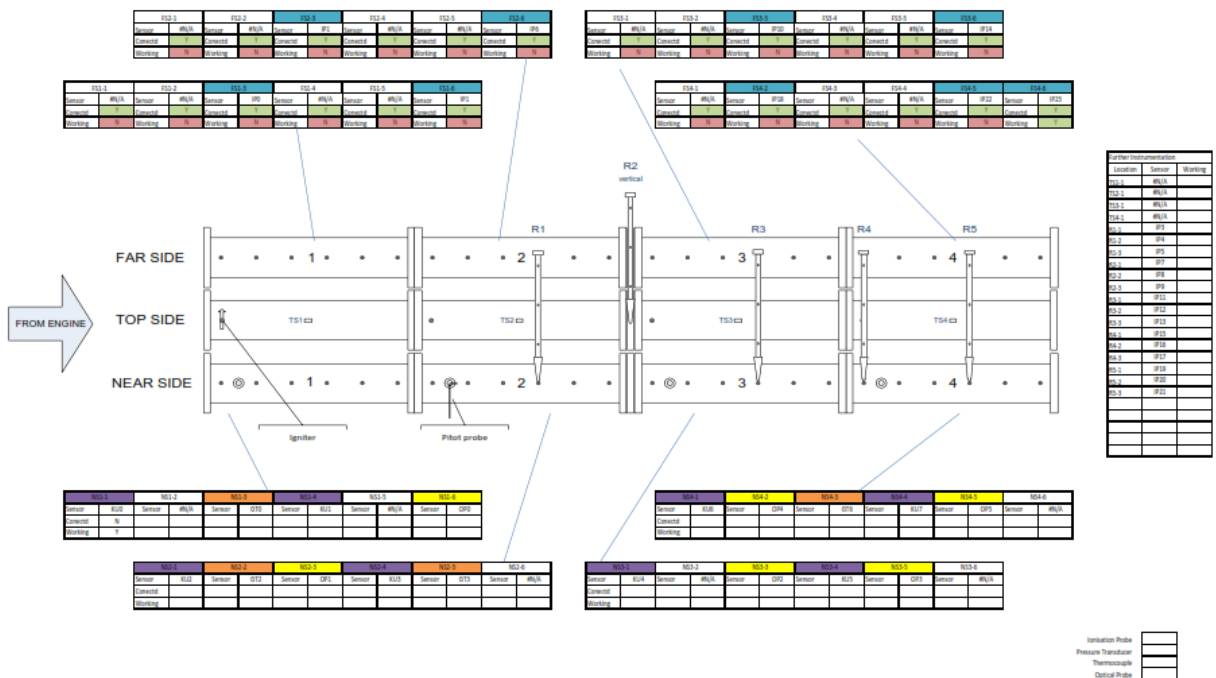


Figure 19: Example instrumentation positions; expanded figure shown in section 11.3

There were some additional pressure sensors and thermocouples situated immediately downstream of the engine turbine and in the transition section; these formed part of the engine monitoring and operation system. The igniter was located as also shown in Figure 19. Its position could be varied, but for the entire test programme it was located near the start of the first duct section.

A typical example of the data sheet format used to indicate the types and locations of the sensors used in each individual test are shown in Appendix 12.2. Sensor positions were changed depending on the test parameters used for individual tests and on the operational status of sensors. Experiments were only undertaken with a minimum of five pressure transducers and six wall ionisation probes, together with four rakes, four optical probes and ten thermocouples (wall and gas temperature combined), all working and in calibration. These were considered the minimum numbers of sensors operational in order to deliver a valid data set, accepting that no more than one sensor of each type may fail to record during a test. It is noted that initially the pressure sensors were chosen with a range of 50 bar as a result of early discussions on possible detonation pressures. These were replaced at an early stage with 7 and 10 barg transducers when the first pressure indications were very much lower. For the small number of detonation cases observed, the maximum pressures observed were around 10 barg.

6.2 FLAME IONISATION (IP) SENSORS

The flame ionisation sensors were manufactured in-house, and each of the 24 flame ionisation sensors used to detect flame arrival within the duct was based on the sensor design shown in Figure 20.

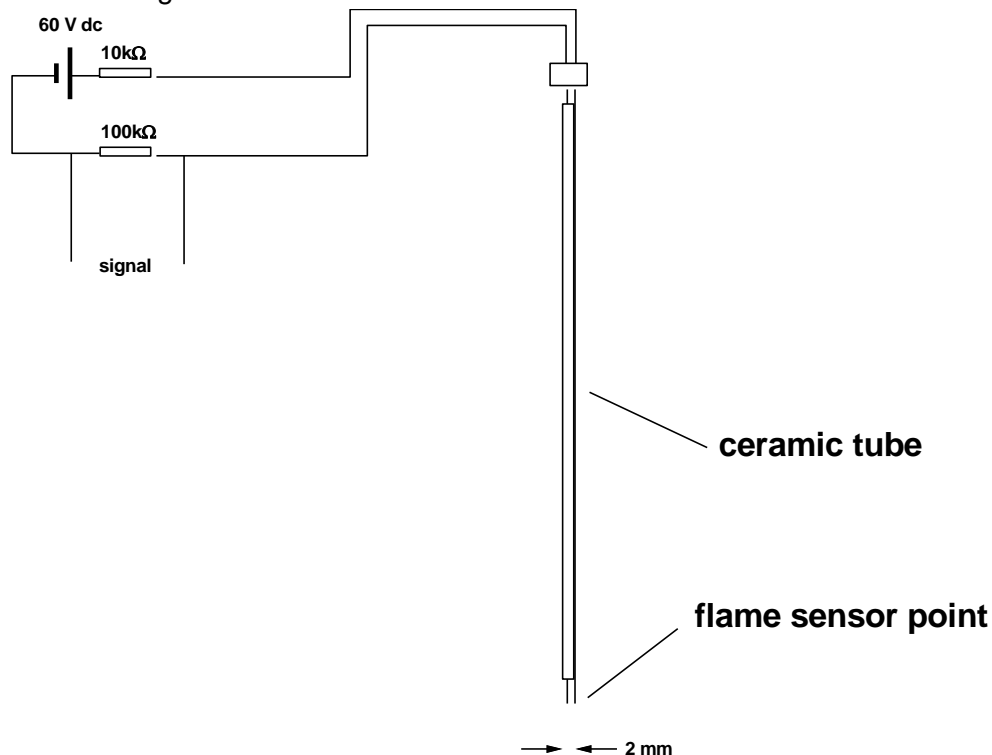


Figure 20: Flame ionisation probe design.

Currents generated from the flame front arose from the raised but small conductivity associated with the flame and were in the 5 μA range, giving rise to voltages in the 0.2 - 1 V range using the load resistor shown (100 k Ω). The devices were bench tested using a hand held propane flame. This was considered adequate for this purpose as the device is not sensitive to which particular flame ions are responsible for conduction.

Since the circuit was purely resistive, response times were fast (e.g. < 0.1 μsec) and much less than the sampling intervals used within the data collection system, which were 10 μsec for flame detection. Due to the small signal currents, the sensor body needed to be kept dry as dampness in the external environment could give rise to a leakage current and a resulting DC offset voltage, which could be several volts. This was achieved by heating each of the sensor tips at the start of each day's testing.

Examples of IP sensor signal obtained using a hand-held torch and from real rig tests are shown in Figures 21 and 22.

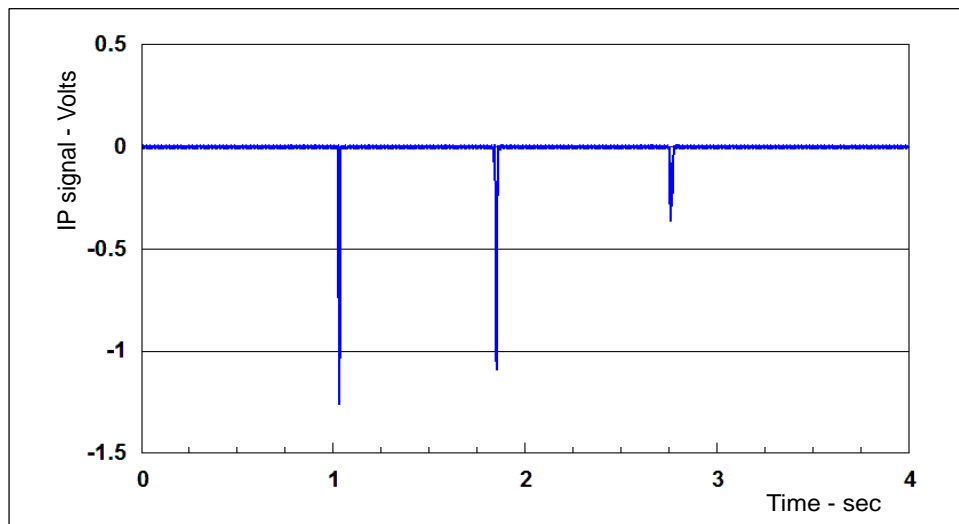


Figure 21: Example of IP sensor signal using a hand-held butane torch and 3 sweeps across the tips of the sensor.

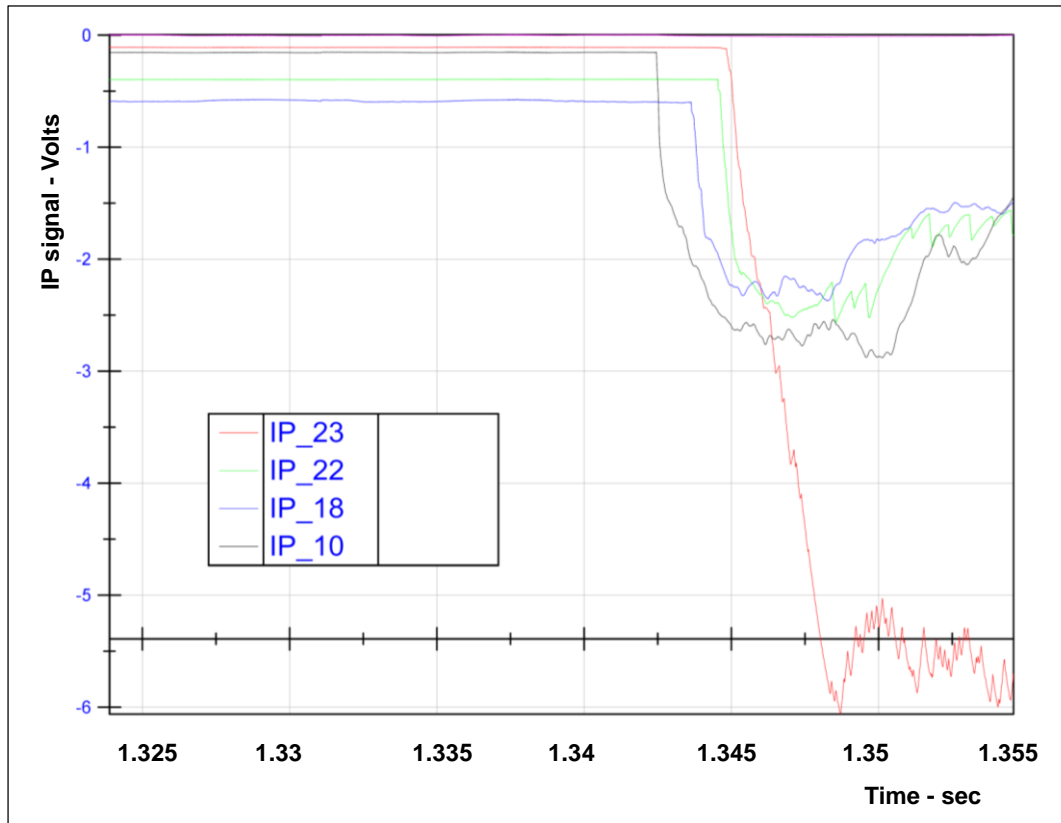


Figure 22: Ionisation sensor signals obtained for Test 29 – 100% H₂, EQR 0.6.

The initial combustion tests used IPs mounted at around 20 mm from the duct walls. During the test programme additional centrally located IPs were introduced. The resulting group of sensors then included twelve wall mounted and twelve centrally mounted, the latter being in groups of three across the duct diameter. It was noted that, since the IPs were point measurement sensors, they only provided a signal if a high temperature flame front passes their location. Depending on the complexity of the flame development, this criterion was not always met at all locations. This was particularly true for weak combustion mixtures.

6.3 OPTICAL FLAME (OP) SENSORS

The optical sensors were made in-house and four such sensors were used along the length of the duct. These used a PbSe photoconductive element for sensing radiation in the visible and near IR range. The sensing cell used a Hamamatsu P9696 device, which is 3 x 3 mm in size with a reported response time (t_{90}) of 2 - 3 μ sec. The sensor had wavelength sensitivity in the visible region and out to 4.5 μ m wavelength, which made it suitable for the detection of water vapour and carbon dioxide emissions from vibrational stretching modes at around 3 μ m. Note that this differs from UV detection from OH radicals, which would not be suitable for the present application. Water vapour is of course also present in the engine exhaust during normal running, but this only becomes visible to

the detector when the flame front is present due to the temperature difference between the exhaust gas and the combustion flame front. The detection circuit using this device is shown below as Figure 21. As with the IP devices, the OPs were tested using a hand held propane flame, which again was appropriate due to the wide detection bandwidth of the detector.

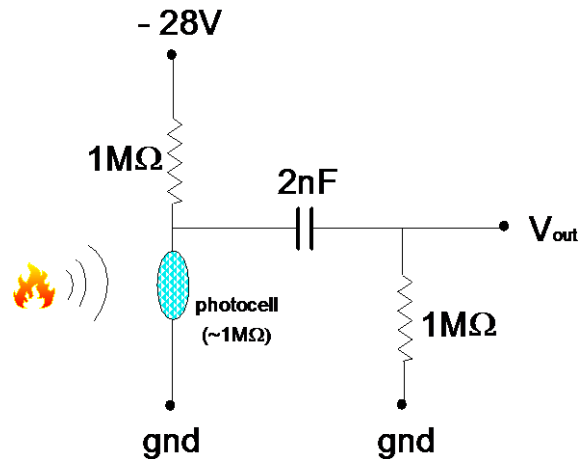


Figure 21: Optical probe detection circuit

The detection circuit was set up in order to block the large DC offset arising from the -28V power supply, so the output was basically the derivative of the input signal due to flame radiation arriving at the sensor. The input side of the photocell was sitting at around -15V and, as the resistance drops with flame radiation arriving, this voltage goes more +ve. The first change seen on the output was therefore a signal rise and for a radiation pulse input, the output was a sharp +ve pulse followed by a sharp -ve pulse. The cross-over point at zero volts corresponds to the maximum of the flame radiation (i.e. where the derivative is zero).

In general, for a flame front arriving, which is followed by high temperature combustion gases (i.e. a step change in temperature), the signal took the form of a positive pulse, where the maximum corresponded to the maximum rate of change of radiation emission within the flame front or brush. The geometry using this cell at each measurement point is shown below in figure 24.

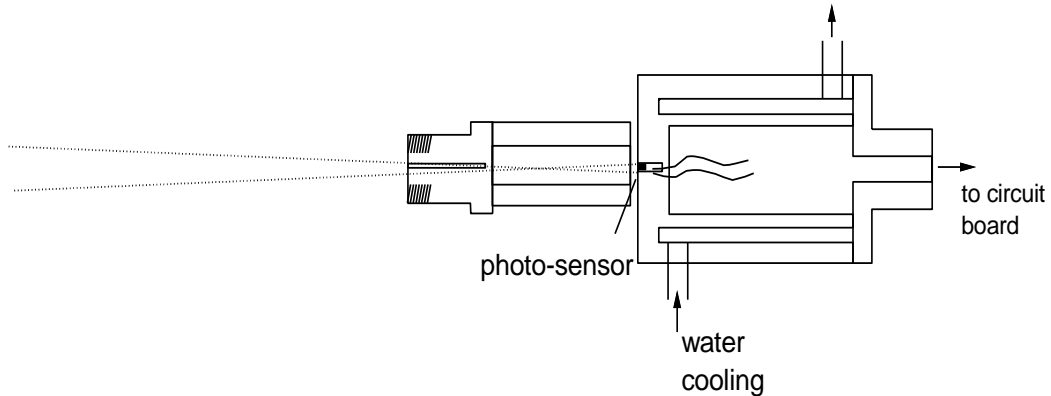


Figure 22: Optical probe mechanical layout

The viewing angle subtended from the sensor was set by the receiving aperture at the open end of the device body and this corresponded to a viewing width along the axis of the duct of around 40mm at the duct centreline. For the tests later in the series, a modified front end design was tested using a sapphire receiving lens of 50mm focal length, with the objective of creating a collimated collection path of around 15mm diameter. This was seen as particularly important for the larger scale HRSG tests when the viewing angle using simple apertures would have created too large a viewing area within the larger structure. In principle, since the OPs were collecting radiation from across the duct diameter, they provided a different flame detection opportunity from the IPs and would have generated a signal when some individual IPs did not.

It was also noted that the IPs and OPs were considered 'on' or 'off' devices with the purpose of detecting when a flame front arrived. There was no intent with these to extract any particular flame properties and therefore no calibration procedure for these was undertaken prior to use. Each of the devices was bench-tested to confirm flame detection prior to use and this process was repeated regularly to confirm correct operation. This bench test involved the use of a hand-held propane torch flame, which was passed quickly through the sensor tips in the case of the IPs and passed across the front of the aperture for the OPs. During this procedure, the data collection system sampled the signal in the normal way to confirm correct operation.

A comparison of the optical sensor outputs for a typical bench test and real rig test are given in Figures 25 and 26 below.

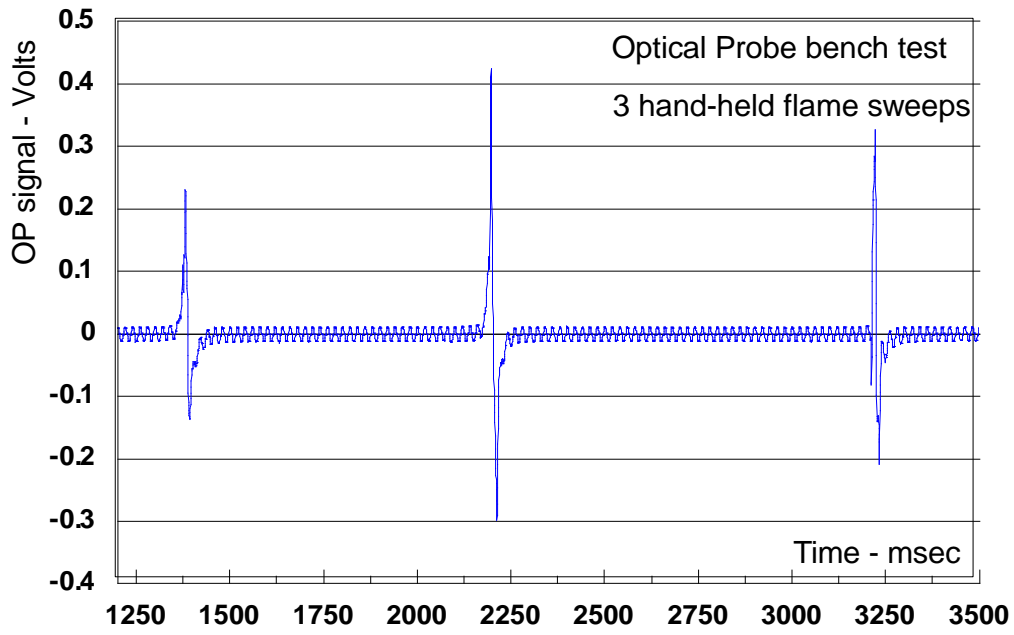


Figure 25: Example of OP sensor signal using a hand-held butane torch and 3 sweeps across the field of view of the sensor. Note that the signal is the derivative of the received intensity.

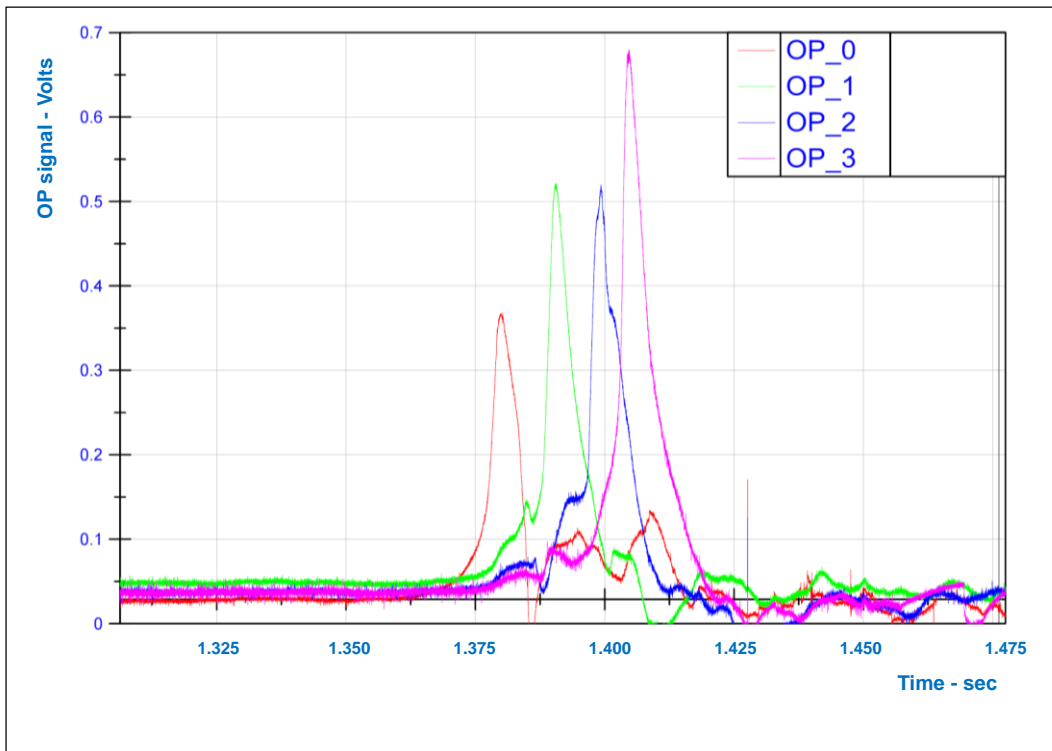


Figure 26: Optical sensor signals obtained for Test 37 – 40% H/ 60% CH, EQR 0.75

6.4 PRESSURE SENSORS

The primary type of pressure sensor used during the test programme was piezo-resistive, manufactured and supplied by Kulite in the UK. The particular series used was Kulite XTEH-10L-180 (M); see data sheet at Appendix 12.2 for the full specification. Several different sensors from this series were used depending on availability, thus sensors with different pressure ranges and threads were used. Additional protection was provided for the sensors by mounting them in water-cooled jackets. These types of sensor are able to withstand operating temperatures of up to 538 °C, thus making them more suitable for the operational environment of the experiments being conducted.

These sensors were therefore chosen because they offered a higher operating temperature range than piezo-electric alternatives, although their frequency responses were less (being typically 50-100 kHz). A protective diaphragm placed across the sensing element limited their response. This was not considered to be an issue as the sampling rate of the data logger was set at 100 kHz. This limiting value was chosen on the assumption that the tests would produce mild to fast deflagrations with flame speeds well below the sound speed of the exhaust gas mixture and with the pressure waves travelling sonically. In the event, several detonation events were observed for which the flame speeds were measured from the OP and IP data, and the peak pressures from the Kulite sensors after checking them, where possible, against a single PCB Piezotronics supplied piezo-electric sensor. It was noted in Section 6.1 that the initial choice of sensor pressure range was changed to a lower value after initial ignition tests.

The respective responses of the two sensors to water hammer pressures were also checked. These tests were carried out with both types of sensor attached to one end of a one metre long tube, water filled and with a movable piston inserted in the opposing end of the tube. The piston was struck with a hammer creating a pressure wave in the water travelling at the speed of sound in water, circa 1500 m/s. This was a similar velocity to those observed in some of the tests where it had been assumed that a detonation had occurred. The responses of the two sensors were recorded on an oscilloscope at rates above 1 MHz. The results showed that the Kulite sensors did not appear to respond as quickly as the PCB sensor and, although the waveform shapes were similar the peak levels attained by the Kulite sensor were lower. This was to be expected in view of the quoted lower frequency responses of the Kulite sensors. It was also noted that removing the front protection screen from the Kulite sensors did not appear to make any difference to the response time and the waveform shape. A detailed assessment of the test results and their implications for the relevance of the pressure measurements is given in section 9.1.

A single PCB Piezotronics-supplied 0-70 bar pressure sensor, Type 113B24, was used in some of the later tests as a check on the response times and peak pressures being attained by the Kulite sensors. This sensor was also fitted into a water cooled jacket as supplied by the sensor manufacturer. Nevertheless, one of these sensors was damaged

due to overheating as their tolerance of thermal environments appeared to be less than that of the Kulite sensors. Supporting evidence for this statement was that the maximum operating temperature quoted for the sensor was 135 °C but with the ability to withstand a flash temperature of 1649 °C. The duration of the latter, and probably the peak value, was observed to have been exceeded on several high speed video recordings of combustion events within the duct.

6.5 VELOCITY MEASUREMENTS

The velocity profiles across the duct were measured using a Kimo-supplied and calibrated pitot-static probe to measure the dynamic pressure of the flow. An RS supplied GEMS differential diaphragm pressure transducer was used for these measurements, Type 5266250LBHT1C-RS, 0 – 250 Pa. These measurements were made at the start of each test during the test programme, consequently during operation of the rig a traverse was made across one half of the duct only and its mirror image taken as representing the other half. In this way velocity profiles across the whole of the duct were obtained, from which duct mass flow rates were obtained by integration of the velocity and density profiles. A typical velocity profile is shown in Figure 27.

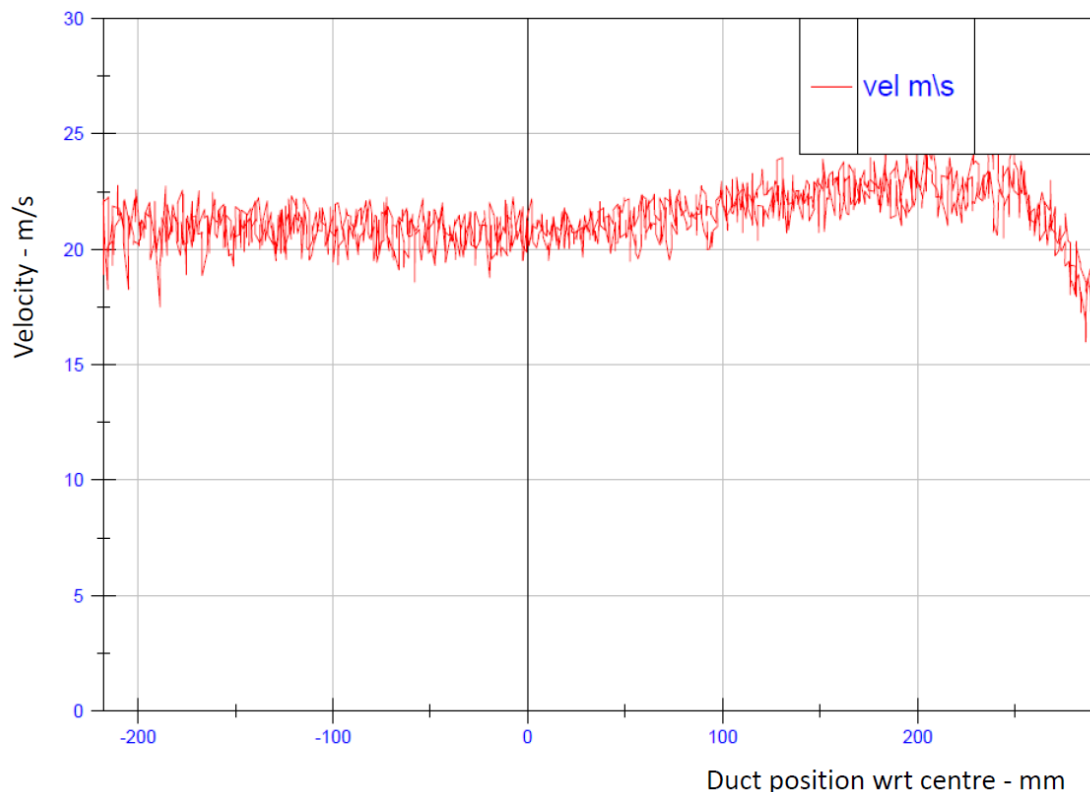


Figure 27: Typical velocity profile using the pitot-static probe during a low velocity test.

6.6 TEMPERATURE MEASUREMENTS

'K' type thermocouple were used of all of the temperature measurements made on the rig, including all the wall and gas temperatures. They were supplied calibrated as standard to be within ± 2 °C at 600 °C. They were sampled at a rate of 10 Hz and logged on the engine and control systems loggers. Their outputs were time-synchronised with the rig's high speed logging system and their locations were as shown on the format used to summarise the test results, see Appendix 12.3 for an example.

The sampling rate of 10 Hz is considered appropriate for the thermocouples given their time response of several seconds. This depends on the fluid medium, turbulence levels and resulting heat transfer coefficient. An example of the growth in temperature for two of the duct thermocouples (TC0 and TC1) located in the gas phase and following an ignition event is shown in Figure 28. The ignition is around 242.8 seconds and the gas phase temperature will be established very quickly after this (e.g. 0.2 seconds) and it can be seen that the thermocouple response grows over the following 10 seconds, which is a measure of its normal time response under the duct conditions.

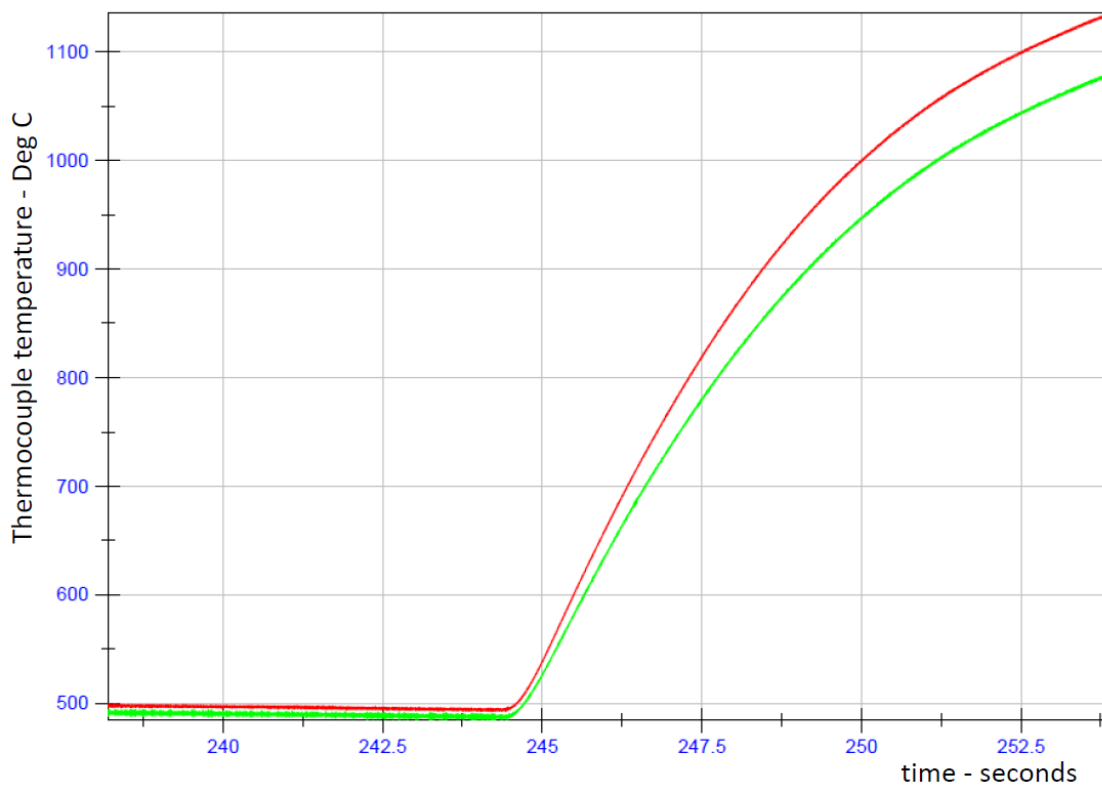


Figure 238: Growth of thermocouple response following an ignition event at T~242.8 seconds

6.7 IGNITION SYSTEM

The ignition system used to provide a spark ignition source was an 8-10 Joule spark supplied by Rolls-Royce as this was the only unit readily available at the time. Once triggered by the gas injection system it sparked repeatedly at a rate of once every 1.5-2 seconds. The spark plug was a standard gas turbine igniter as supplied by Vibrometer. It was located on the axis of the duct through a rigid plug extension which maintained it normal to the flow along the centreline. It was located in the top of the first duct section, 250 mm from the beginning of it. Other locations were available but were not used in these tests. It was noted that the discharge of the igniter capacitor produced an electrical pulse on a number of signal channels. This is not unusual on signal acquisition systems where large EM fields are present and it did not interfere with the measurements on the signal channels. Due to the narrowness of this pulse (~5 μ sec) this signal could also be used if necessary to align signal channels on different data acquisition cards, where small time shifts could arise (e.g. 200 μ sec). The occurrence of such a pulse on the signal channels after the start of data acquisition was variable due to the variable time it took for the discharge capacitor to reach discharge voltage.

6.8 DATA SYNCHRONISATION

The high speed data collection took place via several data cards, whose clocks were initially synchronised but which may drift apart by a small amount over several minutes. The drift was small, but for some aspects of data comparison it was important to make corrections for this drift. For this purpose, cards, which were operating from different internal clocks, have a single channel dedicated to receiving a reference signal that was simultaneous on each of these channels. This enabled any relative time correction to be made when necessary. An alternative, which was often applied, made use of the ignition pulse used to ignite the combustible mixture within the duct. This high voltage pulse produced a simultaneous 'noise spike' on most of the sensor channels and could also be used to make any time position adjustment when channels driven from different internal clocks were being compared.

Making such time comparisons was not seen to be necessary for most of the data analysis, where time intervals were being taken from sensors connected to the same card such as only IPs or OPs or pressure transducers, but in some cases it became particularly important. An example was for cases where detonation was suspected, e.g. where the large peak pressures and sharp shock response on some of the pressure sensors were to be compared with flame sensor response. Test 25 was one such example, where a comparison needed to be made of the arrival times of the shock and the flame front at the same location in the duct exit. In this case it was found that a time adjustment of 0.361 msec between the two channels was required, based on ignition pulse positions for each. This confirmed in this case that the flame front and shock were associated to within one data sampling interval (10 μ sec).

It should be noted that the data currently available for examination within the project has not had any adjustments made to precisely synchronise the different cards in the manner described above and this should be carried out where it is necessary to relate events within a particular test. This relates particularly to pressure and flame sensors.

7 RIG OPERATING PROCEDURES

7.1 SAFETY PROCEDURES

Several HAZOP studies and risk assessments were undertaken to explore and control the hazards associated with the operation of the rig and the subsequent trials. The initial HAZOP studies were split into three areas; the butane isolation, its separation, and the gas feed system. Further HAZOP studies were made of the fire and explosion hazards associated with the test rig and the engine. A basis of safety was established from these HAZOP studies that applied to the design and construction of the rig itself and subsequently to its routine operation. The latter included the handling of the flammable and toxic gases used for the test programme. Details of the HAZOP studies are given in (5-9).

Consequently, during the trials the main basis of safety was the exclusion of personnel from the experimental test rig and the 200 metre exclusion zone which surrounded it. This exclusion zone was calculated to ensure that personnel were protected from blast, ejected parts, thermal radiation, noise and toxic hazards. The exclusion zone was enforced by HSL staff (sentries), which is standard practice for many other experiments undertaken at the HSL site. In the unlikely event that there was an incursion into the exclusion zone, the sentries immediately advised the trials officer in the experimental control room who abandoned the experiment and placed the rig into isolation mode. This was achieved immediately, remotely and securely by key switch operation.

After a trial was completed the basis of safety shifted to the isolation of both the butane and gas feed systems. Due to the use of asphyxiating, oxidising and flammable gasses, isolation was paramount.

7.1.1 Hazards associated with the trials

The potential hazards of the trials were:

- *Fire*

There was a potential for fire as flammable fuels were used on site including butane, methane, hydrogen and carbon monoxide. The designs for the gas compounds and gas injection systems ensured that there were separated isolated states for these systems when not in use.

- *Explosion*

A study was undertaken by HSL's Explosives Team using the US NRC (US Nuclear Regulatory Commission) model. This study modelled the blast overpressure of a detonation of either methane or hydrogen in the most undesirable (i.e. a stoichiometric) mixture in the duct. The pressure resulting on the area around the rig was then determined. This modelling provided:

- Assurance that the walls erected around the rig would remain intact and therefore provide on-going protection to adjacent plant (e.g. bulk gas storage) resulting from direct blast and/or ejected parts.
- A separation distance between the rig and people that would protect against effects of blast.

- *Toxic Exposure*

A study was undertaken by HSL’s Consequence Modelling and Risk Assessment Team using the PHAST (Process Hazard Analysis Software Tool) system. This modelled a rapid release of carbon monoxide whilst the engine was running. This was based upon a release of some 9 kg of carbon monoxide, a volume of approximately 8,000 litres at NTP. A HAZOP study was then undertaken to identify and implement control measures to ensure the safe handling of potential asphyxiates.

- *Noise*


The hazard that determines the largest exclusion zone was exposure to noise. Here a minimum exclusion zone of 230 metres from the rig was indicated. The noise associated with the running of the Viper engine cannot be reduced therefore control measures such as personnel exclusion and the use of ear protection were introduced.

7.2 CALIBRATION PROCEDURES

Of the four sensor types installed in the test rig (pressure transducers, thermocouples, optical probes and ionisation probes) only the pressure transducers and thermocouples were subject to a formal calibration procedure. The optical probes and ionisation probes did not require calibration as their mode of operation effectively makes them indicators.

Calibration of the pressure transducer and thermocouple channels was carried out using a Druck DPI620 calibrator which was supplied and maintained by Scitek and calibrated annually by the Druck Standards Laboratory. The Druck unit is calibrated in accordance with the requirements of UKAS and international standards ISO/IEC 17025.

Table 1: Details of Druck calibrator used for calibration of pressure and temperature measurement channels

	Manufacturer	Druck
	Model	DPI620
	Serial Number	02918726
	Calibration number	certificate 0058874

7.2.1 Pressure Transducers

The pressure transducers were supplied complete with certificates of calibration but were re-calibrated 'in situ' as a complete unit comprising sensor, amplifier (where fitted) and data acquisition card. This calibration was carried out prior to first use and then periodically at maximum intervals of 12 months.

The gain and offset for each of the pressure sensor channels was set to 1 and 0 respectively, to effectively give a voltage output. The sensors were each then systematically subjected to known pressures using the Druck calibrator at a minimum of 5 points and across the full sensor range. The data obtained was plotted and a linear regression applied to produce scaling (gain) and offset factors which were applied to the appropriate channel output. An example of a typical calibration plot for sensor channel K0 is shown in Figure 29.

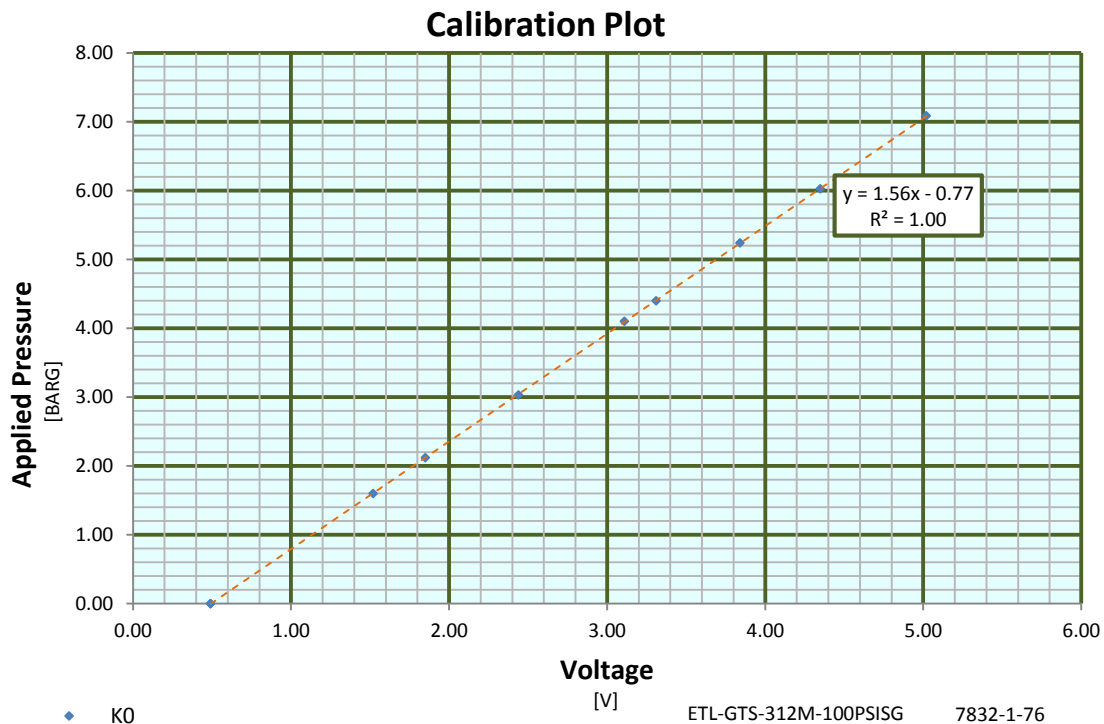


Figure 249: A typical calibration plot from a pressure measurement channel incorporating a Kulite pressure transducer

All the sensors calibrated showed excellent linearity with correlation coefficients (R^2 value) of 1.

Furthermore, periodic checks of the calibrated sensors were carried out, usually following a period of inactivity or significant change in configuration i.e. sensor relocation, using the Druck calibrator. As with calibration a known pressure was applied to the sensor and compared with the displayed value (in barg). Any significant variations in these results would require the sensor unit to be recalibrated. However, all of the calibration checks have proven to be consistently accurate and recalibration has not been necessary.

The calibration of the PCB pressure transducer was carried out in a similar way but due to drift it was essential that the application of pressure was achieved rapidly. A methodology was developed whereby a known pressure was applied to a small pressure vessel to which the sensor was attached. The output from the sensor was zeroed before rapidly discharging the stored pressure (to 0 barg), which generated a negative signal whose amplitude was proportional to the gauge pressure to which the vessel had been charged. This occurred within 10 seconds of the zeroing procedure, during which no drift was observed. This procedure was carried out at a number of pressures across the range 0 to 10 bar. The obtained data was plotted and a linear regression applied to produce scaling and offset factors that were applied to the appropriate channel output in the data acquisition software. It is noted that during normal testing, any drift on the PCB was used as the baseline from which combustion generated pressures were measured.

In addition to the calibration procedure for both pressure sensors, a comparison was made of the response of both when exposed to the same pressure transient and is further discussed in Section 9.1.

7.2.2 Thermocouples

All the 'K' type thermocouples conformed to British Standard BS EN 60584-1:2013. The temperature measurement channels were calibrated using the Druck DPI620 calibrator which supplied voltage values in accordance with standard IEC 584. The range of temperatures and measurement uncertainties are shown in Table 2.

Table 2: Temperature calibration ranges of Druck DPI620 calibrator and measurement uncertainty values

Type	Standard	Temperature Range				Total uncertainty	
		°C		°F		°C	°F
		From	To	From	To		
K	IEC584	-270.00	-220.00	-454.00	-364.00	4.00	7.20
		-220.00	-160.00	-364.00	-256.00	1.00	1.80
		-160.00	-60.00	-256.00	-76.00	0.50	0.90
		-60.00	800.00	-76.00	1472.00	0.30	0.54
		800.00	1370.00	1472.00	2498.00	0.50	0.90

Each of the temperature channels were calibrated at several temperatures and the applied value compared to the temperature reading value. The results of the calibration were recorded and in all cases showed the output value to be within ± 1 °C of the applied temperature.

7.2.3 Ionisation Probes

The ionisation probes were *not* calibrated as they are effectively indicators, sensing the arrival of the flame along the tube wall. However, functionality of the sensors was periodically checked by taking them out of the rig and applying a flame from a butane torch across each of the sensor tips.

Further details of the operation of the ionisation probes can be found in Section 6.2.

7.2.4 Optical Probes

The optical probes were *not* calibrated as they are effectively indicators, sensing the arrival of the flame front across the diameter of the horizontal centreline in the tube.

Further details of the operation of the optical probes can be found in Section 6.3 and a discussion of the performance of both the optical and ionisation probes can be found in Section 9.2.

7.3 OPERATING PROCEDURES

Operating procedures were developed during commissioning as the process developed and staff became familiar with the system's idiosyncrasies and safety requirements. After several iterations two written operational procedures were developed, one covered operation with flammable gases only, the second with toxic gases added. These were used to draw up check lists that the system operators were required to follow during the experimental test programme.

The essence of these procedures was as follows:

- On the designated test day, checks were made for, and to ensure, correct functioning of all the required instrumentation by following the procedures described in Section 7.2.
- The test gas mixture required was then made up by filling the gas reservoir with the lightest gas first then adding the next heavier component(s). The correct gas mixture ratio was obtained using partial pressures. When a toxic gas was being used any person approaching and opening the toxic gas bottle filling valve was required to wear BA.
- The gases were thoroughly mixed by recirculating through the Haskel gas pump for a minimum of one hour.
- The liquid butane, which would fuel the Viper gas turbine, was also recirculated through the butane supply system at approximately the same time.
- The engine control software and the data logging system were readied for operation.
- The appointed Trials Officer then placed lookouts at chosen points on the exclusion zone boundary. They were in radio contact.
- Given the all clear, the gas turbine was started and run up to the operating speed (usually 12,200 rpm).
- After some five to ten minutes of running to allow the gas temperature to stabilise, a pitot-static probe traverse was made of the duct. The results from this were used to calculate the required fuel mixture and oxygen injection rates needed to meet the EQR requirements of the particular test conditions being investigated. The results were logged and filed.
- After a series of safety checks, the actual test proceeded with the injection of the fuel mixture sample together with sufficient oxygen to restore the level in the exhaust stream to a maximum of 21%. These were injected at approximately the same time into the exhaust downstream of the engine turbine. This procedure reduced the exhaust stream temperature by approximately 50 °C resulting in the exhaust temperatures previously discussed above.
- The flammable gas/oxygen mixture injection process lasted for no more than 10 seconds, during which time ignition of the mixture was undertaken using an

electrical spark situated axially downstream of the fuel injection point. This also started the data recording process. Immediately after ignition the fuel and oxygen supplies were automatically stopped by the controlling software.

- If an ignition occurred the engine was slowed down and a check made of the data, which was subsequently filed and backed up.
- Up to two further runs would be undertaken before the system was shut down if the same gas mixture was being used but with different EQR values.

The operating procedure required the engine to be run for up to ten minutes in order to stabilise the gas temperature along the duct. A typical operating gas temperature, after injecting the test gas and oxygen, was expected to be about 550 °C, however both higher and lower values than this were achieved in the range of 300 °C to 600 °C. During this process the duct walls were heating up but at no point in the test did they reach thermal equilibrium. However, the heat losses to the duct walls were minimal but in any case the wall temperatures were recorded throughout the test period.

For each day of testing, an initial pitot-static probe traverse across the diameter of the duct was conducted with the engine running at 12,200 rpm for the tests conducted at the higher exhaust temperature. This provided the exhaust mass flow rate on which to base the injected mass flow rates of oxygen and fuel mixture. It was observed that the exhaust mass flow rate was very reproducible during all of the tests at a value of 2.35 kg/s. The exhaust oxygen was monitored using a Servomex analyser and this provided a repeatable value of 16.5% at the high temperature running condition. This resulted in an oxygen make-up injection rate of 0.15 kg/s. Note that a deviation from this injection rate of between 0.14 to 0.16 kg/s results in a deviation in the exhaust oxygen level from 20.7 to 21.3%. It was observed that the usual range for the oxygen injection level was 0.145 to 0.155 kg/s. For each test a target EQR was set and the fuel mass flow calculated and entered into the control system parameters. Following a test, the actual fuel mass flow rate was extracted from the data and the actual EQR re-calculated. This was the value quoted for each test.

The composition of the engine exhaust gas has been reported in the earlier Commissioning Report and these values have been used to calculate the molecular weight of exhaust gas, both for fuel injection calculation and sound speed estimation when required. The molar % values used for the exhaust are as follows: N₂ 76.46, O₂ 16.50, H₂O 3.72, CO₂ 2.47, and Ar 0.88.

The calculation of the required injection rate for oxygen and mixed fuel was carried out based on the following analysis. The variables are defined in Table 3 below.

Table 3: Symbol table for oxygen and mixed gas injection calculation

Symbol	Description
m_{ex}	mass flowrate of exhaust - specify this
M_{ex}	molecular weight of exhaust - calculated
M_f	molecular weight of fuel - calculated
F_{CO}	mole fraction of CO in fuel mixture - specify this
F_{H_2}	mole fraction of H ₂ in fuel mixture - specify this
F_{CH_4}	mole fraction of CH ₄ in fuel mixture - specify this
F_f	mole fraction of fuel in exhaust - specify this
F_{EXO_2}	mole fraction of oxygen in exhaust - given as 0.165 at engine operating condition
m_{O_2}	mass flowrate of additional oxygen
M_{O_2}	molecular weight of oxygen
m_f	mass flowrate of fuel
m_{ex}/M_{ex}	molar flowrate of exhaust
m_f/M_f	molar flowrate of fuel

Additional oxygen molar flow rate required to bring concentration in exhaust up to 0.21 mole fraction is calculated from:

$$0.21 = (\text{oxygen from exhaust} + \text{additional oxygen})/(\text{exhaust} + \text{oxygen})$$

$$0.21 = \frac{F_{EXO_2} \frac{m_{ex}}{M_{ex}} + \frac{m_{O_2}}{M_{O_2}}}{\frac{m_{ex}}{M_{ex}} + \frac{m_{O_2}}{M_{O_2}}}$$

Rearrange to give:

$$m_{O_2} = \frac{\frac{m_{ex}}{M_{ex}} (0.21 - F_{EXO_2})}{(1 - 0.21)} \quad (1)$$

Mole fraction of fuel in exhaust calculated from the flow rates of fuel and modified exhaust flow:

$$F_f = \frac{\frac{m_f}{M_f}}{\frac{m_{ex}}{M_{ex}} + \frac{m_{O_2}}{M_{O_2}} + \frac{m_f}{M_f}}$$

$$\text{Rearrange to give: } m_f = \frac{M_f F_f \left(\frac{m_{ex}}{M_{ex}} + \frac{m_{O_2}}{M_{O_2}} \right)}{1 - F_f} \quad (2)$$

Equations 1 and 2 are mass flow rates of additional oxygen and fuel - calculated in spreadsheet form and applied before each test run.

The input values to this calculation were based on the user's choices for the particular test being run. For example, the fuel mixture composition was input as the mole fractions of each gas in the mixture already prepared and the oxygen mole fraction in the exhaust was measured separately with the engine running at normal operating condition. The exhaust mass flow rate was calculated separately from a velocity traverse carried out routinely on each test day, whereby a point-by-point velocity was calculated across the duct diameter using Bernoulli's equation and the locally measured pitot pressure. The density was calculated from the temperature measured at the pitot-static probe and local atmospheric pressure at the Buxton site.

The recording system was triggered to start recording by the ignition spark and it was terminated by the closing of the mixture supply valve. During the first set of tests using carbon monoxide it was observed that auto-ignition was occurring shortly after commencing the fuel mixture injection process and before the ignition system had been triggered. As a consequence the data recording system did not record the event. A modification was therefore made to the software controlling the data recording system which allowed the recording system to be started manually. This was used for the subsequent set of carbon monoxide based tests. It resulted initially in larger data files but these were clipped to contain only the relevant data prior to being issued.

7.3.1 Additional high velocity tests

Upon completion of the original test programme two further tests were carried out as preparatory work for the follow-on WP 2.3 HRSG test programme. These tests were undertaken with a large diameter orifice plate fitted and with the engine operating at 12,200 rpm (as in previous tests). The measured velocity along the duct was some 85 to 90 m/s. The tests were undertaken with the 15 row obstruction removed, and the injected gas mixtures were ignited. A full description of the tests and the results are given in (10).

7.4 SAFETY RECORD DURING TESTING

During the course of the test programme there were no significant safety related incidents that brought into question the originally established basis of safety as identified through the HAZOP and risk assessment studies undertaken originally.

During commissioning of the rig there were some modifications made to the system that could be considered safety related. These are detailed below.

Two remotely controlled ball valves that were part of the fuel and oxygen injection systems, in accordance with the HAZOP studies and the resulting P&ID, proved to be problematic - particularly the valve supplying the oxygen line. This valve failed, jamming closed almost immediately after it was first operated. It was repaired by the supplier/manufacturer but failed again with the internal seat materials overheating and being destroyed. The cause was investigated, and the manufacturer reviewed their design and implemented some additional post-production testing of the replacement valves. The other valve in the fuel

line did not open when the system was operating even at modest pressures; consequently it was removed and returned to the supplier, who again modified and replaced the device. After this both valves functioned as intended.

A further problem occurred with the oxygen flow control valve and Coriolis flow meter when it was discovered that these components were not suitable for oxygen service. They were returned to the supplier who modified them before they were re-installed in the system.

Problems were also encountered with a three-way solenoid valve controlling the pressure being applied to the domes of the two Hale-Hamilton pressure regulators. This valve would not operate consistently at the operating pressures required to achieve high gas injection rates. An alternative valve was not available immediately from the suppliers; consequently an alternative means of controlling the dome pressures was devised using two 2-way valves. This proved satisfactory and prevented a further delay to the commissioning and test programmes.

In developing a satisfactory means of operating the gas and oxygen injection systems, three bursting discs protecting the injection components downstream of the Hale-Hamilton pressure regulators failed and had to be replaced. This was not expected but occurred as a result of the slow reaction times of these two regulators when operated in a no-flow condition with their domes pressurised. A work-round was developed and incorporated into the controlling software, which involved a change in the operating sequences for both the fuel and oxygen injection sequences.

Two hand-operated vent valves were added at the filling point of the two gas storage cylinders to enable them to be safely emptied in the event of the remotely operated main discharge valve failing to open when the cylinders were under pressure, as happened once during commissioning of the oxygen system.

A potentially serious incident occurred when running the original gas turbine at speed. The engine suddenly seized due to a bearing failure, but the resulting torque almost pulled the engine from its mountings. The engine was replaced, the replacement one proving more reliable than the original one.

8 RESULTS

8.1 INTRODUCTION

The results reported here focus on the combustion outcomes. This section presents summary data for these tests involving injected fuel composition, equivalence ratio of the fuel in the exhaust, fuel and oxygen mass flow rates and the peak pressure observed following ignition of the duct mixture.

The rationale for the test programme is discussed in output from the Imperial College study (4), noting that it is based upon the need to identify the increasing risk of detonation for the chosen test gas mixtures with increasing EQR and decreasing gas temperature. The three gases used in the test programme and the various mixture combinations used were based on the requirements of the project as identified in the original proposal and subsequently updated in the light of discussions with all the interested parties. The test programme was also updated as the tests proceeded and results became available.

8.2 PRESENTATION OF RESULTS

There were a total of 67 tests completed and numbered 1 - 67 in all of the reporting procedures. Immediately after a test was completed all of the data from a valid test was stored and backed-up on the system computers and individual storage devices. The high speed data from the rig was stored in TDMS format so that it could be analysed using the National Instruments Diadem software package. The engine data and the control and gas supply data were stored in CSV format. There was an additional pitot-static probe data file also stored in CSV format.

There was a large body of data collected for each test involving the supporting hardware including engine running conditions (rpm, internal temperatures, internal pressures, vibration etc.) and control system operation (valve positions, injected fuel and oxygen mass flow rates, exhaust oxygen concentration) and all of this data is available to the project for analysis.

The data was used initially to generate a set of data summary sheets, the first sheet of which is shown in Section 12.3. This particular sheet shows the positions of the sensors used for a particular test; following sheets summarised the test set-up, the test conditions and the actual test parameters used, such as the mixture ratio and it's EQR. Further sheets summarised the test results, such as the maximum flame speeds and pressures.

The injected mixtures tested are described in Section 8.3 and also in Section 12 (Appendix A), specifically Sections 12.4 and 12.5. The tests fall into four categories covering (a) those with no obstacles in the duct, (b) those with eight rows of obstacles, (c) those with 15 rows of obstacles and (d) those with fifteen rows of obstacles but with the exhaust running at a lower temperature, typically 340-350 °C. This resulted in exhaust temperatures, after oxygen and mixed gas injection, of 320 °C at the upstream position (TC0) and 260 °C near

the duct exit (TC15) with intermediate thermocouples at temperatures between these limits.

The eight rows of obstacles were set up in all cases with the eighth row being in a flange sandwiched between the end of duct section 3 and the beginning of section 4. The previous seven rows of obstacles were upstream of the eighth row. In the fifteen row obstacle case the additional seven rows were added downstream of the already in place eighth row, thus making the obstacles in this case equally spaced either side of the section 3 to section 4 joint. Note that of the 67 tests undertaken, the data from test 67 has been held for future investigation if necessary. A small number of the intermediate tests have not been included in the summary for varying reasons.

8.3 COMBUSTION TEST SUMMARY DATA

Summaries of the tests and the test results are presented in the following four sub-sections. They are separated into the four categories referred to in Section 8.2. The peak pressures shown were taken from any of the four/five Kulite pressure transducers used in these tests. Usually, the peak pressures were observed towards the exit from the duct. It should be noted that, due to the fact that the pressure traces were generally complex, including multiple peaks, it was considered misleading to associate the recorded peak pressure in the tables below with particular times in the event train, particularly since a secondary peak may be close in amplitude to the main one. For this reason, the occurrence times of these peak pressures have not been included in the tables.

Test 6 was found to have a fault within the control system and has therefore been removed. Tests 14, 15, 17 and 18 involve CO or H₂/CO mixtures and these were found to result in pre-ignition before stable conditions were achieved. They are included for the record but have no useful data. Later tests with this mixture used a modified procedure, see Section 7.3, that was successful and these test results can be found in the later test results, tests 47-60.

8.3.1 Combustion tests no congestion

Table 4: Combustion tests no congestion.

Mixture	Test Number	Eq. Ratio	CH ₄ (vol%)	H ₂ (vol%)	CO (vol%)	Fuel Gas Flow Rate (kg/s)	Oxygen Flow Rate (kg/s)	Peak Pressure (mbar)
CH ₄	1	1.02	100	-	-	0.143	0.155	230
CH ₄	2	1.02	100	-	-	0.142	0.156	216
CH ₄	3	1.02	100	-	-	0.143	0.152	209
CH ₄	4	1.00	100	-	-	0.144	0.152	232
CH ₄ / H ₂	5	0.67	40	60	-	0.0765	0.154	168
CH ₄ / H ₂	7	0.88	40	60	-	0.103	0.152	204
CH ₄ / H ₂	8	0.88	40	60	-	0.103	0.155	205
H ₂	9	0.42	-	100	-	0.024	0.158	73
H ₂	10	0.51	-	100	-	0.0297	0.157	130
H ₂	11	0.72	-	100	-	0.045	0.157	320
CH ₄ / H ₂	12	0.87	40	60	-	0.103	0.157	262
CH ₄ / H ₂	13	0.35	40	60	-	0.0396	0.149	43
CO	14	0.35	-	-	100	Pre-ignition		
CO / H ₂	15	0.55	-	60	40	Pre-ignition		
CO / H ₂	16	0.50	-	60	40	0.178	0.140	91
CO / H ₂	17	0.50	-	60	40	Pre-ignition		
CO / H ₂	18	0.50	-	60	40	Pre-ignition		

8.3.2 Combustion tests with eight rows of congestion

Table 5: Combustion tests with eight rows of congestion.

Mixture	Test Number	Eq. Ratio	CH ₄ (vol%)	H ₂ (vol%)	CO (vol%)	Fuel Gas Flow Rate (kg/s)	Oxygen Flow Rate (kg/s)	Peak Pressure (mbar)
CH ₄ / H ₂	19	0.36	40	60	-	0.038	0.148	75
CH ₄ / H ₂	20	0.67	40	60	-	0.076	0.150	591
CH ₄ / H ₂	21	0.85	40	60	-	0.102	0.147	1670
H ₂	22	0.32	0	100	-	0.0172	0.157	0
H ₂	23	0.40	0	100	-	0.023	0.155	0
H ₂	24	0.52	0	100	-	0.030	0.158	323
H ₂	25	0.71	0	100	-	0.044	0.160	7620
H ₂	26	0.63	0	100	-	0.0375	0.148	1950

8.3.3 Combustion tests with fifteen rows of congestion

Table 6: Combustion tests with fifteen rows of congestion.

Mixture	Test Number	Eq. Ratio	CH ₄ (vol%)	H ₂ (vol%)	CO (vol%)	Fuel Gas Flow Rate (kg/s)	Oxygen Flow Rate (kg/s)	Peak Pressure (mbar)
H ₂	27	0.53	0	100	-	0.030	0.148	1733
H ₂	28	0.42	0	100	-	0.0237	0.157	451
H ₂	29	0.63	0	100	-	0.038	0.164	7159
CH ₄ / H ₂	30	0.55	40	60	-	0.062	0.149	284
CH ₄ / H ₂	31	0.65	40	60	-	0.0757	0.148	3016
CH ₄	33	0.86	100	-	-	0.12	0.148	2620
CH ₄	34	0.76	100	-	-	0.105	0.148	650
CH ₄	35	0.65	100	-	-	0.089	0.147	300
CH ₄ / H ₂	36	0.65	60	40	-	0.0826	0.151	416
CH ₄ / H ₂	37	0.75	60	40	-	0.096	0.155	1515
CH ₄ / H ₂	38	0.60	60	40	-	0.075	0.148	363
CH ₄ / H ₂	39	0.61	40	60	-	0.07	0.154	600
CH ₄ / H ₂	40	0.66	40	60	-	0.076	0.154	1353
H ₂	41	0.40	-	100	-	0.0235	0.148	0
H ₂	42	0.50	-	100	-	0.0297	0.148	1400
H ₂	43	0.60	-	100	-	0.0366	0.148	9400
H ₂	44	0.51	-	100	-	0.03	0.151	1762
CO	46	0.44	-	-	100	0.359	0.15	130

Combustion tests with fifteen rows of congestion (continued)

Table 7: Combustion tests with fifteen rows of congestion (continued).

Mixture	Test Number	Eq. Ratio	CH ₄ (vol%)	H ₂ (vol%)	CO (vol%)	Fuel Gas Flow Rate (kg/s)	Oxygen Flow Rate (kg/s)	Peak Pressure (mbar)
CO	47	0.60	-	-	100	0.51	0.159	574
CO	48	0.77	-	-	100	0.7	0.152	3000
H ₂ / CO	49	0.65	-	40	60	0.351	0.158	10380
H ₂ / CO	50	0.41	-	40	60	0.209	0.17	227
H ₂ / CO	52	0.50	-	40	60	0.259	0.155	824
H ₂ / CO	53	0.40	-	60	40	0.142	0.19	218
H ₂ / CO	54	0.50	-	60	40	0.183	0.175	1500
H ₂ / CO	56	0.56	-	60	40	0.208	0.18	966
CH ₄ / H ₂ / CO	57	0.65	25	40	35	0.178	0.148	3128
CH ₄ / H ₂ / CO	58	0.56	25	40	35	0.147	0.148	1503
CH ₄ / H ₂ / CO	59	0.51	25	40	35	0.133	0.148	1500
CH ₄ / H ₂ / CO	60	0.45	25	40	35	0.118	0.148	214

8.3.4 Combustion tests with fifteen rows of congestion at lower exhaust temperature

Table 8: Combustion tests with fifteen rows of congestion at lower exhaust temperature.

Mixture	Test Number	Eq. Ratio	CH ₄ (vol%)	H ₂ (vol%)	CO (vol%)	Fuel Gas Flow Rate (kg/s)	Oxygen Flow Rate (kg/s)	Peak Pressure (mbar)
H ₂	61	0.50	0	100	0	0.041	0.114	2230
H ₂	62	0.45	0	100	0	0.0326	0.128	788
H ₂	63	0.35	0	100	0	0.0275	0.123	374
CH ₄ / H ₂	64	0.58	40	60	0	0.092	0.126	2774
CH ₄ / H ₂	65	0.50	40	60	0	0.0785	0.125	1579
CH ₄ / H ₂	66	0.40	40	60	0	0.0618	0.124	84
H ₂ / CO	67	0.51	0	40	60	0.369	0.123	1075

Note that the engine running condition at 8500 rpm produced the same exhaust average velocity but with lower exhaust temperatures of around 350 °C. The exhaust oxygen concentration for this condition was 18.3% and the required oxygen make-up rate was 0.125 kg/s in order to bring it up to 21%.

9 DISCUSSION OF RESULTS

This section provides an assessment of the results obtained, in particular the validity of the data, its consistency and the interpretation of the data from the various sensors. Any anomalies are highlighted and discussed. The key sensors were the pressure measuring sensors as in many cases the absolute values were important in judging the deflagration/detonation behaviour of the different gas mixtures being tested for a range of EQR values. Therefore, particular attention was given to understanding their behaviour under dynamic loading conditions as discussed in Section 9.1.

Interpretation of the optical and ionisation sensors was considered less contentious as they were essentially on/off devices. Similarly for the thermocouples, as these were calibrated at source, there was far less likelihood of their outputs being questionable.

9.1 VALIDITY OF PRESSURE SENSOR DATA

The pressure sensors used for transient measurement were of two types. Five Kulite high temperature piezoresistive pressure transducers (XTEH - 7L-190) with a range of 7 - 10 barg and full scale output of 100 mV were distributed along the walls of the duct. The signals from these were amplified using an in-house high frequency amplifier. A single piezoelectric transducer was also deployed in the third duct section, this being a PCB Piezotronics sensor, type 113B24.

The calibration of the Kulite sensors was carried out regularly using a Druck calibrator; see Section 7.2 for the actual procedure. These were found to hold their calibration well over periods of several weeks. Since the experiments were dynamic in nature, the issue of the frequency response of these sensors was important to address and to assess the effects of limitations that exist in this area.

The Kulite sensors have a quoted natural frequency, which refers to the natural frequency (f_n) of the sensing membrane. For the sensors used, this was 380 kHz. This figure was not the frequency response of the device as a whole, which was considerably lower due to constructional features. If incident pressure pulse frequencies were greater than a limiting value, then the sensor output tended to overshoot the peak incident pressure and oscillate at the resonant frequency. This limiting frequency (as defined by a $\pm 5\%$ output linearity limit) was indicated by the manufacturer to be $0.2 f_n$, implying that for the sensors used, this limiting frequency was around 75 kHz. This corresponded to a period T of this limiting wave of 13 μsec and an associated rise time of the pressure wave of around $1/4$ of the period i.e. 3 μsec . However, this performance data referred to sensors without a perforated screen over the sensing element. Discussions with Kulite indicated that the effect of this screen was to effectively reduce the resonant frequency by a factor of two. This resulted in an effective limiting frequency of 35 - 40 kHz and associated rise time limit of $\sim 6 \mu\text{sec}$. Pressure waves originating within the system will tend to coalesce into a shock wave and this will be more evident at the exit of the duct (around position K7, see Section 12.3). The pressure associated with a shock wave of even moderate strength will rise within a much

shorter time interval than this due to the shock thickness being no more than a few mean free paths.

With the exception of the pressure recorded around the exit of the duct (K7) the signals from the other Kulite sensors showed rise times which were longer than the limiting values discussed above. For those combustion cases where the peak pressures were greater (e.g. >2 barg) then there was usually evidence of ringing on the K7 sensor. This can be understood as arising from the factors discussed above. The peak of the transient pressures quoted do not attempt to make any correction for any pressure signal overshoot which may arise, e.g. on K7, as a result of this resonant behaviour. This can be considered as being a conservative approach to the statement of peak pressure. An example of the ringing evident on Kulite sensor K7 for test 33 is shown in figure 30 below.

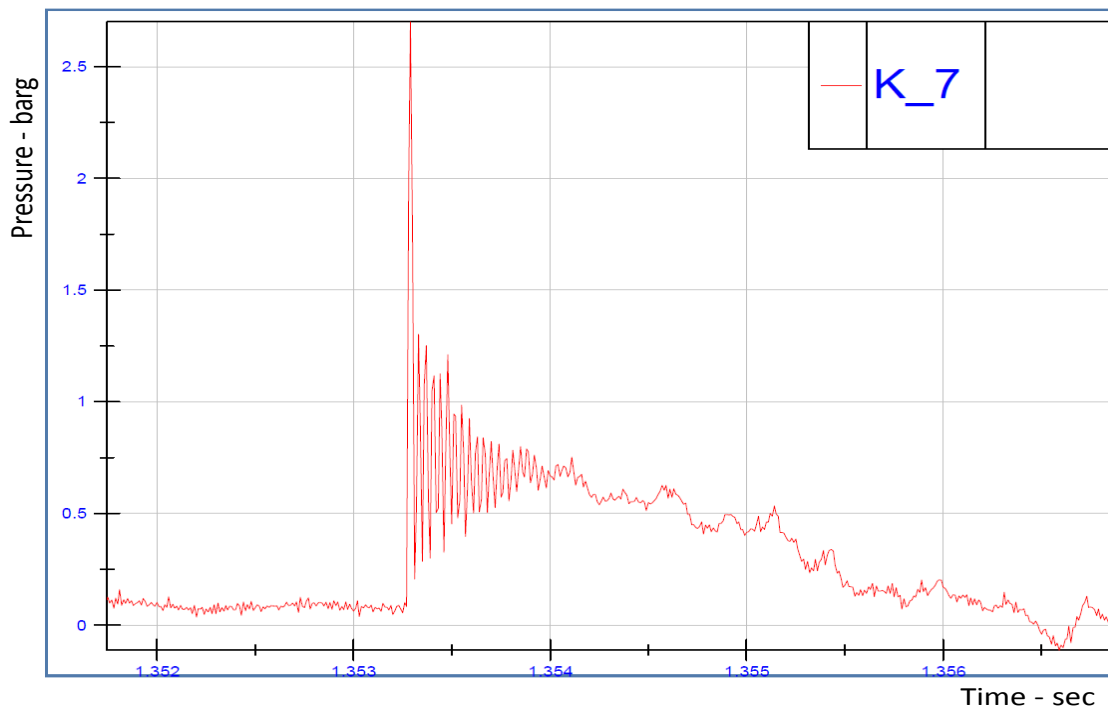


**Figure 30: Indication of ringing on K7, Kulite pressure transducer for Test 33.
Only the peak pressures are reported in the Tables.**

The PCB sensor is based on a different technology and manufacturer's data indicates that operation frequencies above 100 kHz are within the sensor's capabilities. This in turn implies that signal pressure wave rise times around 1 μ sec can be accommodated, which is consistent with quoted specifications. Calibration for these sensors is less straightforward due to medium term drift of the signal, but a procedure has been developed within HSL to use a transient pressure discharge protocol whereby a small pressure vessel with the sensor attached is charged and the sensor output is then zeroed. Discharge of the pressure then generates a negative-going signal whose magnitude is directly related to the gauge pressure to which the vessel has been charged. This procedure was applied and the calibration factor incorporated into the data acquisition software.

As part of the calibration procedure for both pressure sensors, a comparison was made of the response of both when exposed to the same pressure transient. For this purpose, the sensors were mounted at the bottom of a water-filled tube to the top of which a movable piston was connected. A transient pressure pulse was generated by striking the piston and this was recorded on an oscilloscope. It is noted that this was carried out in order to observe the time response behaviour of both sensor types and before any formal calibration procedure was undertaken.

An example of the simultaneous response behaviour of both is shown in Figure 31, where the oscilloscope time base was 2 msec/division. It can be seen from these traces that the response behaviour for both types of sensors was very similar.

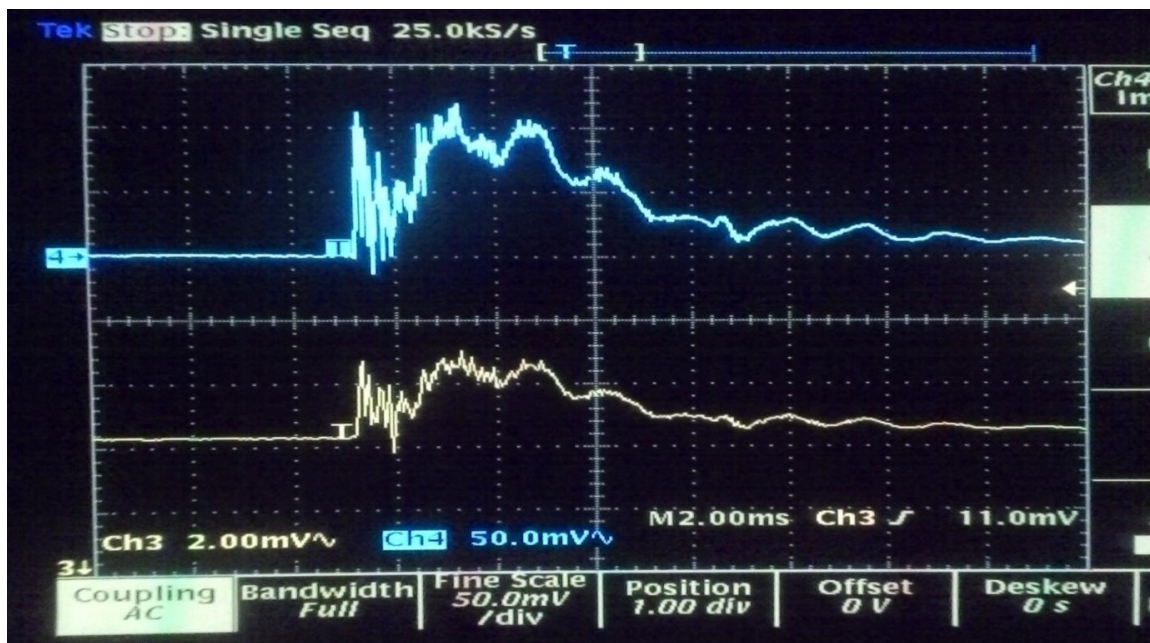


Figure 31: Response of Kulite and PCB sensors to a hydraulic pulse. Ch3 = Kulite, Ch4 = PCB. (Kulite peak pressure ~ 1.6 barg, PCB peak pressure ~ 1.4 barg.)

For larger amplitude signals and on a shorter timebase (20 μ sec /division), differences in the response behaviour was suggested by the traces in Figure 32.

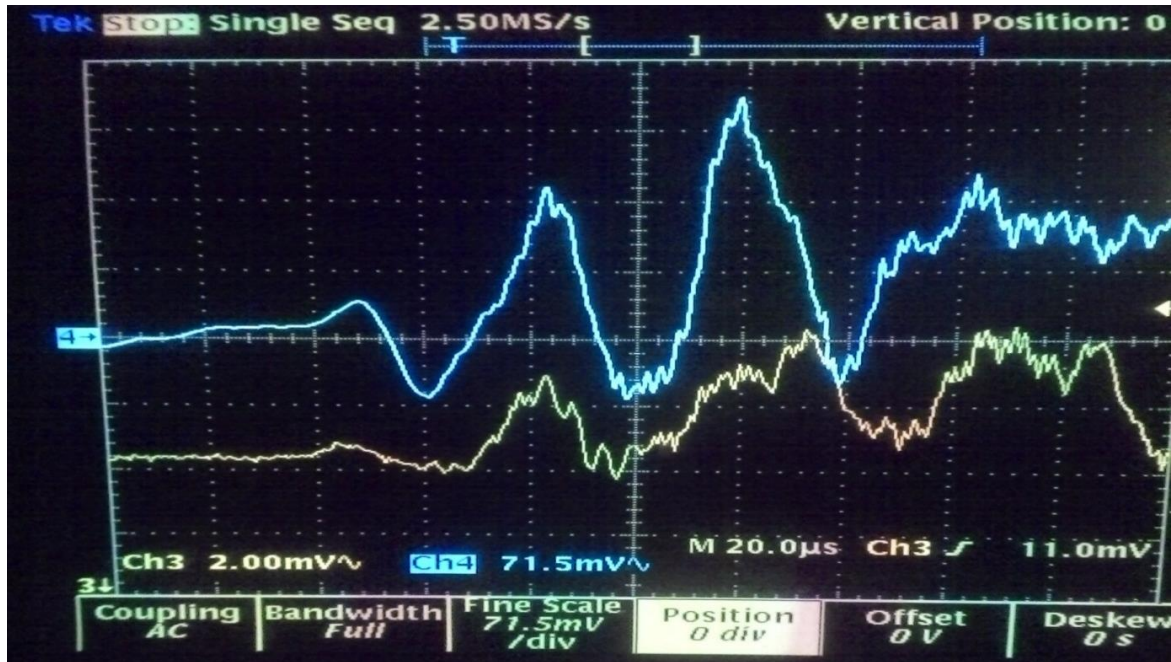


Figure 32: Response of Kulite and PCB sensors to a hydraulic pulse. Ch3 = Kulite, Ch4 = PCB. (Kulite Peak pressure ~ 2.0 barg, PCB peak pressure ~ 3.5 barg.)

In this case the PCB signal showed a larger peak pressure and a slightly earlier rise in signal. Both may reflect the faster response of the PCB sensor.

The conclusions from this comparison exercise suggest that for pressure changes with moderate rates of change then both sensor types satisfactorily reproduced both the amplitude and shape of the pressure waves. It was noted in tests that, for the PCB sensor, low pressure changes were poorly reproduced in comparison with the Kulite sensors, which may be due to the short term drift of the PCB sensors on a msec timescale. By contrast, for rapidly changing pressures associated with shock propagation, the PCB sensor signal indicated a faster rate of rise and generally a larger peak pressure than that from the Kulite sensors.

Part of the judgement in the value of the pressure signals was in identifying those areas of mixture and exhaust concentration which were safe or unsafe in respect of the over pressures they generated, and what reliance could be placed on the absolute values obtained. This in turn could to some extent be judged by the reproducibility of pressure behaviour from shot-to-shot for the same conditions. The programme did not seek to explore this variable in detail, but in the few cases that were repeated the pressures did suggest that there was such variability in peak pressures. Examples would be tests 27, 42 and 44, which were three tests with 100% hydrogen at an EQR of 0.5. The measured peak pressures were 1733, 1400, and 1762 MPa respectively. It is suggested that the differences are also a function of the reproducibility of the test conditions and these may dominate.

Nevertheless, and despite such sources of variability and the issues regarding the accuracy of the pressure sensor time response and peak amplitudes, it is clear from the data that the pressure sensors were able to identify the finely defined boundaries between moderate pressure development and high pressure development, which may in some cases differ by only 0.05 in EQR value. This was apparent from an examination of the data from increasing EQR measurements, which showed a consistent increase in peak pressure and flame speeds including those where a transition to detonation occurred.

9.2 OBSERVATIONS REGARDING THE USE OF FLAME SENSORS

It was found that the performance of the IP sensors depended on the EQR value being tested. It was expected that well-defined flame fronts would be associated with higher EQR values so, for example, tests with EQR values above 0.6 for CH₄ or 0.5 for H₂ produce well defined transitions on the IP signals for most of the sensors. For example, the high speed video record for test 44 using 100% H₂, 15 rows of obstacles and an EQR of 0.51, shows a weakening flame towards the exit and an absence of signals on the last two flame ionisation sensors.

Differences in flame arrival times between wall mounted and centrally located IPs are frequently observed, which may be attributed to differences in the flame dynamics at the wall compared to the body of the tube. For lower EQR values, approaching the combustion limit for a mixture, IP signals were frequently not seen. This may have been due to the poorly defined nature of the flame front or flame brush, or the lower flame temperature associated with the weaker mixture. It was also noted that the high speed video records taken for some of these cases confirmed that, for the weaker mixtures, flames may have been weakened before reaching the duct exit (e.g. 100% CH₄ at EQR of 0.65), which was consistent with IP and some OP observations.

The OP signals were generally more secure, being an average measure across the duct diameter and these usually provided flame arrival signals after they had been lost on the IPs with reducing EQR values. The OPs are principally used for flame speed estimation and this is most reliably achieved by using OPs as a group rather than combining OP signals with those of the IPs. This is stipulated due to the difference in the measuring nature of the OPs, i.e. line of sight across the duct rather than a point measurement. Since the sensor and circuit provide an output proportional to the rate of change of received intensity, the maximum of this signal is taken to be representative of flame passage and therefore the maximum of the OP signal has been used as a consistent measure of the flame arrival for all tests.

9.3 CONSISTENCY OF DATA

A limited number of combustion tests were undertaken for each condition spanning a range of injected mixtures and EQR values. Since the objective was to identify operational boundaries for mixture ratio and exhaust EQR that represented safe limits

with regard to peak pressures following ignition. It was also of interest to confirm that changes in these parameters produced results that followed a logical and simple trend.

In general, three exhaust EQR values were tested for each fuel mixture combination, and these were chosen to span mixtures that produced peak pressures above and below the expected operational limit of 1 - 2 barg.

A simple test of such consistent trends can be judged from the data table in Section 8.3. The first important trend to observe was the peak pressure observed in moving from no congestion to eight rows and then to fifteen rows of congestion. This is depicted in Table 9 and Table 10 below for two of the injected gas mixtures (CH₄/H₂ and pure H₂).

Table 9: Fixed EQR for CH₄ / H₂

Congestion rows	Mixture	Test Number	Eq. Ratio	CH ₄ (vol%)	H ₂ (vol%)	CO (vol%)	Peak Pressure (mbar)
0	CH ₄ / H ₂	5	0.67	40	60	-	168
8	CH ₄ / H ₂	20	0.67	40	60	-	591
15	CH ₄ / H ₂	31	0.65	40	60	-	3016

Table 10: Fixed EQR for H₂

Congestion rows	Mixture	Test Number	Eq. Ratio	CH ₄ (vol%)	H ₂ (vol%)	CO (vol%)	Peak Pressure (mbar)
0	H ₂	10	0.51	-	100	-	130
8	H ₂	24	0.52	0	100	-	323
15	H ₂	27	0.53	0	100	-	1733

These tables are just two examples from the data but are representative of the trends generally observed, i.e. that increasing congestion produced greater peak pressures due to the increased level of turbulence within and downstream of the congestion.

The second important effect observed was that in moving through increasing EQR values for a particular fuel mixture and level of congestion there was always an increase in pressure. This is depicted in Tables 6-9, and covers geometries with eight and fifteen rows of congestion.

Table 11: Fixed congestion (8 rows) and increasing EQR value.

Mixture	Test Number	Eq. Ratio	CH ₄ (vol%)	H ₂ (vol%)	CO (vol%)	Peak Pressure (mbar)
CH ₄ / H ₂	19	0.36	40	60	-	75
CH ₄ / H ₂	20	0.67	40	60	-	591
CH ₄ / H ₂	21	0.85	40	60	-	1670

Table 12: Fixed congestion (8 rows) and increasing EQR value.

Mixture	Test Number	Eq. Ratio	CH ₄ (vol%)	H ₂ (vol%)	CO (vol%)	Peak Pressure (mbar)
H ₂	23	0.40	0	100	-	0
H ₂	24	0.52	0	100	-	323
H ₂	26	0.63	0	100	-	1950
H ₂	25	0.71	0	100	-	7620

Table 13: Fixed congestion (15 rows) and increasing EQR value.

Mixture	Test Number	Eq. Ratio	CH ₄ (vol%)	H ₂ (vol%)	CO (vol%)	Peak Pressure (mbar)
CH ₄ / H ₂	38	0.60	60	40	-	363
CH ₄ / H ₂	36	0.65	60	40	-	416
CH ₄ / H ₂	37	0.75	60	40	-	1515

Table 14: Fixed congestion (15 rows) and increasing EQR value.

Mixture	Test Number	Eq. Ratio	CH ₄ (vol%)	H ₂ (vol%)	CO (vol%)	Peak Pressure (mbar)
H ₂	28	0.42	0	100	-	451
H ₂	27	0.53	0	100	-	1733
H ₂	29	0.63	0	100	-	7159

Once again the trends observed with EQR were generally observed for all of the data. These provided some confidence when judging the position in the EQR/mixture envelope of the location of an operational limit based on the peak pressures produced.

Although the trends discussed above were consistently found, there was also an element of variability between identical tests, consistent with the random nature of the turbulence generation process. This showed in differences in peak pressure for the same mixture and EQR test conditions, examples being between tests 24 and 27, 23 and 28 and 26 and 29.

9.4 HIGH SPEED VIDEO DATA

Video records were produced for the following tests, where fifteen rows of congestion were in place:

Table 15: High speed video tests

Mixture	Test Number	Eq. Ratio	CH ₄ (vol%)	H ₂ (vol%)	CO (vol%)	Peak Pressure (mbar)
CH ₄	33	0.86	100	-	-	2620
CH ₄	34	0.76	100	-	-	650
CH ₄	35	0.65	100	-	-	300
CH ₄ / H ₂	36	0.65	60	40	-	416
CH ₄ / H ₂	37	0.75	60	40	-	1515
CH ₄ / H ₂	38	0.60	60	40	-	363
H ₂	44	0.51	-	100	-	1762

Both high speed black and white at 10000 fps and colour videos at 3000 fps were taken. The camera position was such as to view along the axis of the duct from the open end towards the injection end. This view was interrupted by the rows of congestion at the mid-position of the duct.

The emission intensity for the different gas mixtures was different due both to mixture content and EQR used. In all cases the beginnings of the flame development could be seen as it illuminated the rear of the congestion array. Against this emission could also be seen a degree of chaotic flow on the downstream side of the congestion due to the turbulence generated. The apparent energy of the flame propagation event was qualitatively consistent with the peak pressures observed in each case. The pure CH₄ at an EQR of 0.86 produced the fastest flame event and also the greatest emission level. The colour video indicated more clearly that the flame emission was not uniform across

the diameter and also that flame could emerge through the congestion in an asymmetrical manner, with the wall areas often showing flame in advance of the body of the flame front. Flame acceleration downstream of the congestion could also be deduced qualitatively from the video record.

For the weakest case of test 35, there was also a suggestion from the video that the flame weakened considerably before it reached the exit of the duct, which may be consistent with turbulence decay toward this point. The cases recorded have moderate flame intensity, rather than a weak intensity, as was the case for some tests. For the weaker tests it was likely that the decay of the flame towards the exit resulted in a loss of signal strength from the OPs and IPs as was usually found to be the case for these types of sensors. Overall the video records have a value in confirming the other parameters measured in the tests, as well as having the ability to reveal any anomalous behaviour in flame development and propagation.

9.5 CONCLUSIONS RELATING TO THE OVERALL PERFORMANCE OF THE TEST RIG.

It was concluded that:

1. The rig design was successfully implemented as a fully operational test rig.
2. The rig fully met the agreed specification.
3. The rig was commissioned and operated successfully.
4. All the agreed safety standards and operational procedures were met.
5. There were no serious incidents recorded during the operation of the rig.
6. A total of 67 ignition tests were completed for a range of EQRs, gas mixtures and the number of tube banks.
7. The majority of the tests were undertaken at temperatures around 500 °C, with a small number being undertaken at a temperature of 325 °C.
8. Valid and consistent data sets were obtained over a wide range of agreed operational parameters.
9. Measurements of flame speed, pressure rise and wave speed were successfully made for the majority of the tests.
10. The completion of the test programme has paved the way for the follow-on work in which a model HRSG is to be added to the existing rig and a test programme undertaken in which the gas flow rates will be some four times those already used.
11. The results obtained thoroughly justify proceeding with the next phase of the test programme.

10 DETAILED ANALYSIS

10.1 THE SAFE OPERATING MODES FOR H₂/CH₄/CO MODEL FUEL MIXTURES.

As indicated in previous documentations and discussed at stage gate meetings, information on the upper concentration safety limit for the use of model high hydrogen content gas mixtures in the circular duct facility of work package WP2.2 was to be obtained by investigating the influence of an increase in the equivalence ratio (EQR) of selected fuel mixes on flame velocities and generated overpressures.

As summarised in Section 8.3, eight fuel mixture compositions were selected for these tests:

- (1) 100% H₂ - 100% CH₄ - 100% CO;
- (2) H₂/CH₄ 60/40 - H₂/CH₄ 40/60;
- (3) H₂/CH₄ 60/40 – H₂/CH₄ 40/60;
- (4) H₂/CH₄/CO 40/25/35

For each of these mixtures

- (a) Normally three EQRs would be tested to record flame behaviour across anticipated safe-unsafe boundaries. Starting EQR choices for such tests were based on results from the WP2, Task 1 Imperial College laboratory tests; subsequent choices were made in the light of last experience.
- (b) This procedure was carried out with, and without flow obstruction, with the obstruction provided by a model heat exchanger (MHE) arrangement of respectively 8 and 15 rows of tubes.
- (c) To simulate as closely as possible real-life conditions, the tests were carried out with the lowest flow entry velocities (≈ 20 m/s) that could be achieved with the circular duct facility (≈ 20 m/s). Unfortunately but not critically this failed to be as low as in real life situations (4 – 8 m/s).
- (d) A few tests were carried out at lower temperature, to appreciate the sensitivity of results on this parameter.
- (e) Higher exhaust flow velocity tests, essential for predicting WP2, Task 3 conditions were deferred.

Because of the exploratory nature of the work, the tests were not carried out in a fully arranged order of the investigated fuel mixtures. For the purpose of this report results have been rearranged as shown in Table 16.

Safety conclusions from these tests are mainly focussed on the over-pressures generated. As could be expected, the highest over-pressures were found in tests with the longest (15 rows of tubes) heat exchanger model. For all eight systems investigated with the complete MHE system, the corresponding over-pressures as a function of EQR are listed in column 6 of Table 16.

Table 16: Stream Fuel mixtures, EQRs, overpressures, flame velocities and temperatures from the WP2.2 circular duct test programme. (Uncorrected data from the HSL Experimental Report)

Mixture	Run	EQR	----- ΔP ----- (mbar)				V_{\max} [m/sec]	T_{\max} [K]
			0 rows	8 rows	15 rows	15 rows (low temp)		
H2-100%	22	0.32		0			0	855
	63	0.35				374	185	567*
	23	0.40		0			0	892
	41	„			0		0	1017
	9	0.42	73				93	760
	28	„			451		167	779
	42	„			1400		278	850
	62	„				788	250	616*
	61	0.50				2230	769	898
	10	0.51	130				115	839
	44	„			1762		286	847
	24	0.52		323			219	815
	27	0.53			1733		417	827
	43	0.60			9400		1724	93
	26	0.63		1950			288	874
	29	„			7159		1875	939
	25	0.71		7620			2500(?)	958
11	0.72	320				348	992	
H ₂ /CH ₄ 60/40	13	0.35	43				63	779
	19	0.36		75			49	711
	66	0.40				84	89	619*
	65	0.50				1579	312	720*
	30	0.55			284		208	1139
	64	0.58				2774	694	792*
	31	0.65			3016		556	971
	5	0.67	168				196	992
	20	„		591			353	969
	21	0.81		1670			451	1109
	12	0.87	262				357	779
	7	0.88	204				312	1172
8	„	205				310	1092	

Table 16 (continued):

Mixture	Run	EQR	----- ΔP ----- (mbar)				V_{max} [m/sec]	T_{max} [K]
			0 rows	8 rows	15 rows	15 rows (low temp)		
H ₂ /CH ₄ - 40-60	38	0.60			363		357	997
	39	0.61			600		242	944
	36	0.65			416		313	988
	40	0.66			1353		233	996
	37	0.75			1515		391	1057
CH ₄ -100%	35	0.65			300		227	1058
	34	0.76			650		548	1078
	33	0.86			2620		595	1111
	4	1.00	232				312	1172
	1	1.02	230				392	869
	2	„	216				240	1182
	3	„	209				366	1172
H ₂ /CO- 60/40	53	0.40			218		129	800
	54	0.50			1500		286	842
	56	0.56			966		185	824
H ₂ /CO- 40/60	50	0.41			227		176	845
	17	0.50	Pre-ig					
	18	„	Pre-ig					
	16	„	91				90	858
	52	„			824		286	1046
	67	„				1075	366	881*
	15	0.55	Pre-ig					
49	0.65			10380		2500	1218	
CO-100%	14	0.35	Pre-ig					
	46	0.44			130		158	705
	47	0.60			574		417	1181
	48	0.77			3000		1000	1268
H ₂ /CH ₄ /CO 40/25/35	60	0.45			214		96	720
	59	0.51			1500		275	899
	58	0.56			1503		313	1029
	57	0.65			3128		385	1308

Note: Test 14,15,17 and 18 pre ignited.

The same information is also given in Figures 33(a–c). As reactivity tends to increase exponentially with concentration, the vertical axes of the diagrams have a logarithmic scale, which allows trends to be approximated with straight lines.

The maximum over-pressures recorded were almost always not at EQR levels that represent the lower and upper limits respectively of hazardous and safe operating conditions, i.e.: those causing respectively unacceptably high or acceptable over-pressures from unintended ignition of not-combusted CCTG or CCGE exhaust flow. What these limits are in practice will depend on a number of factors.

- (i) The results of Figures 33 do not lie all on a single line; even a power trendline could not achieve that. For the high overpressures this is in a minor part due to the accuracy of the recordings. Overwhelmingly it reflects the stochastic nature of the combustion process especially in such turbulent environments. For the definition of practical safety margins, the hazardous limit can only be set against the lowest EQR for which unacceptable over-pressures are recorded.
- (ii) The extent of a practical Δ -EQR safety margin will first of all depend on the stability of the composition of the industrial process stream which in turn is decided by the nature of the process. Waste gas streams are likely to be less reliable than process discharges. Increasing the concentration of generated hydrogen will increase stability.
- (iii) Another important consideration is what the maximum pressure excursion is that the industrial facility can accommodate without being damaged and whether a distinction needs to be made between very short duration pressure peaks and more extended pressure waves. Quite apart from metal choice and wall thickness, ductile materials tend to stand up better to the former than brittle ones, the shock sensitivity and accuracy of recording instruments can be very dependent to both.
- (iv) Finally environment and operator preference may be deciding factors. In congested areas there is limited scope for relief and venting. Location, guaranteed operator availability and skills, industrial and national safety standards may all be of influence.

However, from advisory comments received during the project it was provisionally concluded that over-pressures above 3 bar would be likely to cause permanent damage to some part of the installations, while 0.4 bar was generally regarded as safe and otherwise acceptable. These over-pressure levels have been indicated on the diagrams of Figures 33.

Figure 1.(a): H_2/CH_4

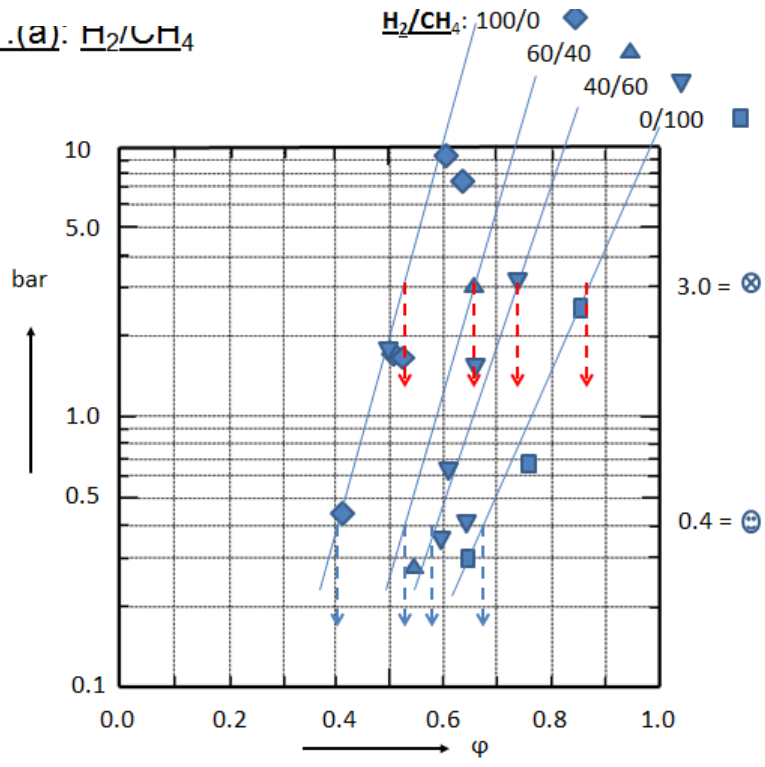


Figure 33(a): H_2/CH_4

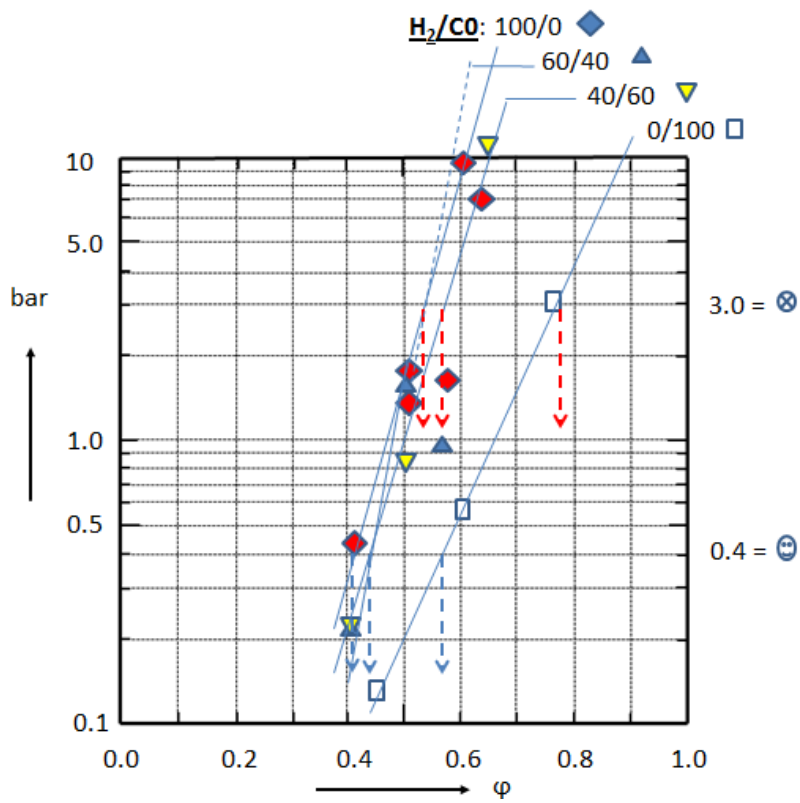


Figure 1(c): $H_2/CO/CH_4$

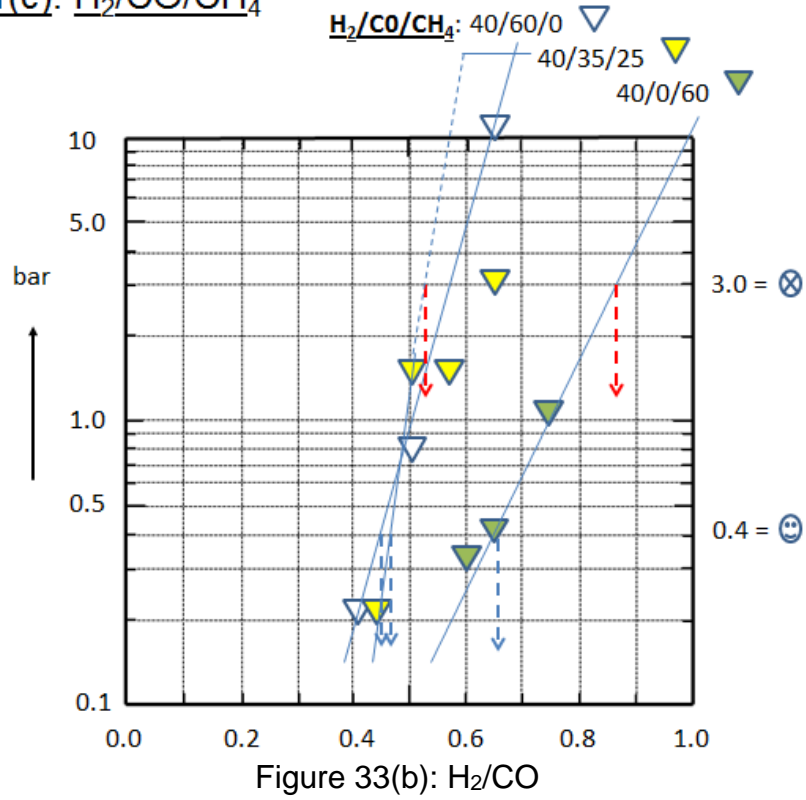


Figure 33(c): $H_2/CO/CH_4$

The conclusions from Figures 33 are summarised in Table 17 on the next page. It shows that the EQR gap between the two identified levels varies from about 0.10 to 0.20. Given the uncertainties listed above and the general ability to control fuel mixture composition and all times, it would seem reasonable to assume a safe gap at the higher 0.20 Δ -EQR level. This results in the recommendation of Table 17, column 5.

The data from Table 17 have also been used to construct the trapezoid diagram of hazardous and safe operating planes previously anticipated at Stage Gate 3 and in VAR027 and here shown as Figure 34.

Table 17: Equivalence ratios of model fuel mixtures for respectively “highest safe” and “lowest hazardous” concentrations in air and recommendations for safe operating EQR of these mixtures in practical situations.

Fuel Mixture	EQR 0.4 bar	EQR 3.0 bar	Δ EQR	Recommended max. EQR for safe operation.
100% H ₂	0.41	0.53	0.12	0.35
H ₂ /CH ₄ 60/40	0.53	0.67	0.14	0.45
H ₂ /CH ₄ 40/60	0.58	0.74	0.16	0.55
100% CH ₄	0.67	0.86	0.19	0.65
H ₂ /CO 60/40	0.43	0.53	0.10	0.35
H ₂ /CO 40/60	0.44	0.57	0.13	0.35
100% CO	0.57	0.77	0.202	0.55
H ₂ /CO/CH ₄ 40/35/25	0.45	0.55	0.10	0.35

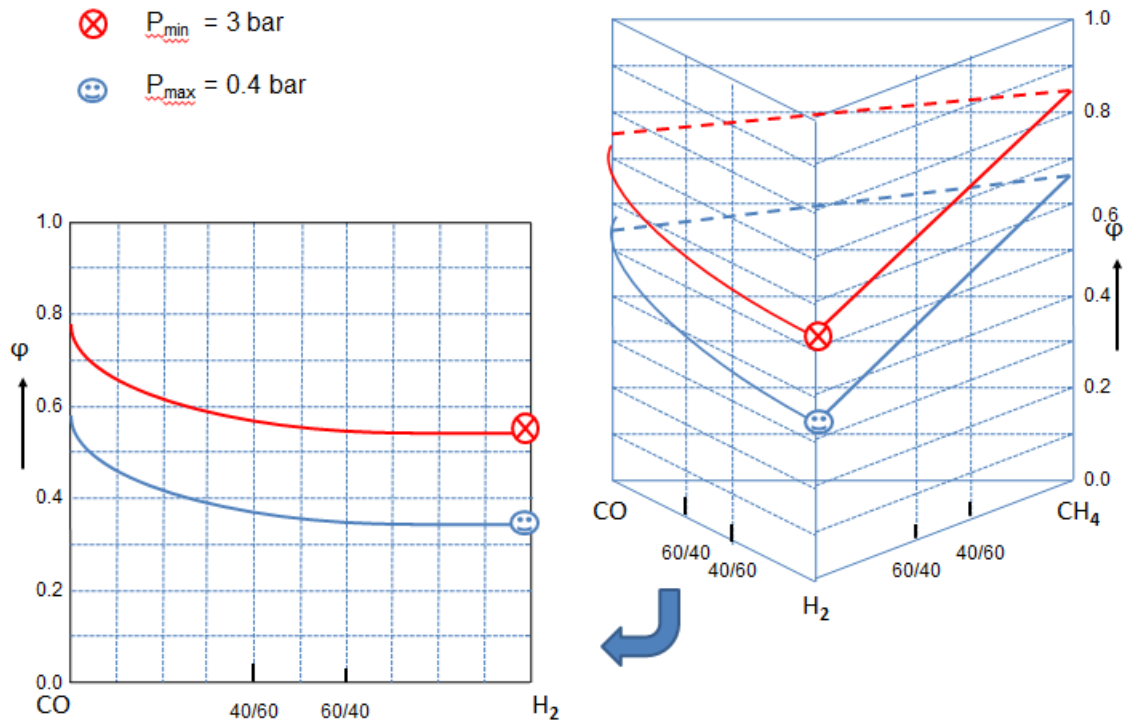


Figure 34: Ternary diagram to illustrate advisable boundaries for minimum hazardous and maximum safe operation conditions to avoid explosion in CCGT and CCGE model experiments with H₂/CH₄/CO fuel mixtures in air.

Some interesting evidence derives from these results and presentations.

- (i) The laboratory tests of WP2.1 have demonstrated some important differences between the binary systems of H₂/CH₄ and H₂/CO. Whereas the reactivity of the former appears to be a linear function of the concentration ratio, that for the hydrogen/carbon monoxide system demonstrated a disproportionate enhanced reactivity as result of hydrogen addition, which became apparent before the 50/50 mix was reached.
- (ii) Scaling up to the cylindrical duct, results of WP2.2 bear out the same evidence. In Figure 33a the lines of constant fuels ratio for H₂/CH₄ run more or less parallel as do the linear boundaries of the “safe” and “unsafe” planes concentration planes in Figure 33. By contrast, these boundaries are curved in Figure 33, while in Figures 33b the H₂/CO lines converge with those for 100% H₂, except for 100% CO. The extent of this coalescence is shown in Table 17. Clearly, hydrogen has a special activating influence on carbon monoxide, which from the equi-molar concentration makes their combined reactivity virtually indistinguishable from that of pure hydrogen. As Figure 33c and Table 17 show, the presence of even 25% CH₄ seems to have little effect on this and a more fundamental study of this behaviour is fully justified.

10.2 THE INFLUENCE OF HEAT EXCHANGER MODEL OBSTRUCTIONS ON THE CHARACTER OF COMBUSTING FLOW.

In Section 10.1 the information from the experimental results was used for a general determination of hazardous and relatively safe operating equivalence ratios for the model H₂/CH₄/CO fuel mixtures in their various concentrations. These have also been summarised in Figure 34. This result was obtained making use of the results of almost all WP2.2 tests 1 – 61. However, dealt with in this way, using maximum and average over-pressures recorded, the results do not fully consider the nature and therefore the role and potential hazards from flame development under the varying conditions or compare the dependence of its unobstructed progress with its character in the presence of obstructing heat exchanger models of varying length/depth.

To achieve this a more detailed analysis was done of the evidence from a limited number of tests that highlight this difference between free and obstructed flame development for fuel mixtures of constant composition and varying equivalence ratios in the oxygen enriched turbine exhaust flow.

For this purpose a primary list of 16 tests were identified from the 61 performed at low flow inlet velocity and constant inlet temperature, for which the results could be compared with those of at least one other test at a different obstruction level but with the same equivalence ratio ($\phi \pm 0.01$). The latter margin was judged to be within the accuracy with which equivalence ratios could have been determined. Collectively, this selection provided the 7 comparative sets, shown in Table 18, of which two incorporate all three of the obstruction levels investigated in the WP2.2 test programme. From the Experimental Report data the recorded maximum over pressures (Δp) and evaluated flame velocities (v_{flame}) are also listed.

As shown, the sets are not ordered around set mixture compositions, but on the basis of increasing over-pressure and flame speed of the un-obstructed test mixture. Where more than one number is shown as “XX/YY” the different maxima relate to the output from two different sensors along the length of the WP2.2 circular duct rig. In some instances the differences appear not to be from process variations, but due to malfunction of one of the two recording sensors.

Table 18: Test mixtures selected from the WP2.2 test programme best suited to investigate the influence on over-pressure and flame velocity on combustion in the CCGT and CCGE model arrangements of WP2.23

	No Obstruction			8 tube rows			15 tube rows		
	Run	Δp	v_{flame}	Run	Δp	v_{flame}	Run	Δp	v_{flame}
	[No]	[mbar]	[m/sec]	[No]	[mbar]	[m/sec]	[No]	[mbar]	[m/sec]
H ₂ /CH ₄ 60/40; $\phi=0.35$	13	43	63/0	19	75	49			

H ₂ 100%; $\phi=0.42$	9	73	0/93				28	451	167
H ₂ /CO 40/60; $\phi=0.50$	16	91	0/90				52	824	286
H ₂ 100%; $\phi=0.52$	10	130	0/115	24	323	123	27	1733	416
H ₂ /CH ₄ 60/40; $\phi=0.66$	5	168	169/170	20	591	353	31	3016	556
H ₂ 100%; $\phi=0.63$	26	1050	(288?)				29	7159	1754
H ₂ 100%; $\phi=0.72$	11	320	312/348	25	7620	1944			

The immediate and obvious evidence from the above is that, regardless of the fuel mix, the maximum over-pressures and flame velocities generated depend directly on the presence and extent of obstruction in the WP2.2 circular duct.

10.2.1 Problems limiting a comprehensive analysis based on all data collected.

As presented in the Experimental Report, the results from the tests referred to in Table 18 were found not to be suitable for a detailed and accurate analysis of the combustion enhancing influence and effects from the model heat exchanger on the enriched turbine exhaust flows. The reasons are in part structural, in part related to the manner of presentation in the Experimental Report. It must be added that, while obvious now, these barriers to optimal result analysis were in many ways 'unforseeable', mainly because of inadequate up-front experience with the extensive and complex recording and analysing system.

As for the structural problems: because of the very large number of sensors required and the significant cost of having these purchased (if available), all except the pressure sensors were 'custom-made'. However, despite best design and manufacturing efforts, the ionisation probes proved not to be as reliable as intended, especially in the earlier tests. Understandably also affected by low ionisation levels for slow and marginal combustion and combined with the difficulties of this large and complex rig, information from probes was for some of the more challenging tests less than 50%, leaving significant information gaps for the overall understanding required. As for the optical probes: their initial design proved not fully successful in excluding stray and advancing

source light. Additionally, interaction between sensor outputs and signal overlap and signal noise could make identification of individual signals an arduous and lengthy task.

The provision of arrays of different types of sensors was intended to provide detailed comprehensive rather than just supplementary information on a number of distinctive details of flame development. To do this efficiently the positions of at least two different types of sensors should have coincided at a satisfactory number of locations with respect to the long axis of circular duct. Given the available resources and the need to collect information along the full length of the 12 m long duct, such opportunities were limited: with mostly separated positions, the combined individual information on a normally changing flame process could not readily be interpreted coherently. Having said this, at four distances from the point of ignition the axial location of an ionisation probe aligned with that of a pressure transducer and at two positions did they coincide with the plane of view of an optical probe. The latter is unfortunate as first responses in the optical probe records to the ignition are mostly at variance with that of the other sensors, while the response signals could be viewed as not well defined. The latter is in part a result of the light reflections in the recesses that house the sensors; in part it is also clearly due to signal input overload. With hindsight it must be admitted that - because of design or installation imperfections - predominantly complementary rather than comprehensive information could readily be obtained, which is a lesson for the WP2.3 programme.

Additionally, as already pointed out in the experimental section of the report, the time-bases of the pressure and optical sensors did not accurately agree with that of the ionisation probes. This is due to the individual characteristics of different cards in the recording system.

Thus the suitability of the experimental report data for combustion analysis, was adequate for the more *general* evaluations, where identification of maximum and acceptable over pressures anywhere in the WP2.2 facility was required to determine too hazardous and relatively safe operating conditions for the H₂/CH₄/CO fuel mixtures. However, for *detailed* analysis of combustion behaviour the results from the experimental report needed to be reviewed and adjusted. Specifically, to achieve the necessary accuracy improvements that were required, including:

1. In 10.1 the mean flame velocities were quoted and graphically shown at the end of a distance interval over which these had been calculated rather than the mid-distance point;
2. Locations of maximum overpressures were time markers, rather than the onset of pressure rise, which in particular for sonic pressure waves indicates the arrival of the 'combustion wave' and is for combustion progress assessment the important moment;
3. Software analysis of the data could show ionisation probe responses preceding the arrival of the pressure wave, which is scientifically unsound;
4. The times of optical sensor responses sometimes precede those of other sensors at an upstream position;
5. Optical probe and pressure transducer responses are frequently distorted because of interference from the response from earlier sensors in the same group, which commonly lifts the baseline;

6. Downstream of the heat exchanger model location, the distances of sensors to the beginning or ignition point of the circular duct needed to be increased by 100 mm allowance for the width of the flange that supported the heat exchanger tube holder.

For the more detailed analysis and interpretation, that would highlight the nature of the combustion process and in particular conditions or locations for its enhancement, the causes for such discrepancies first had to be identified and the relevant data from the Experimental Report improved.

Following early discussion between members of the Consortium this was attempted by considering the data output files from the tests, where possible and necessary, by trying to adjust the data and to see whether from this a coherent image of flame development for the particular test could be extracted. Unfortunately, despite very extensive trying, this was not achieved with the available data set because of clarity and accuracy of signals and/or the problems outlined previously. It was concluded that only a complete new analysis and inter-comparison of all the sensor outputs from the tests of interest might be able to provide the information and insight required. The procedures for this are outlined below in Section 10.3 and Appendix B.

10.3 DETAILED ANALYSIS OF TASK 2 EXPERIMENTAL DATA.

The basis required for a more detailed analysis and understanding of flame development and its hazards in a free or obstructed facility such as the circular duct model facility of WP2.2 has to be a clear and sufficiently accurate display of the distance versus time progression of the flame front. Once this is obtained, additional information on the flame front, flame structure and overpressures generated can be obtained from contributing responses of the different types of sensors employed. In turn this can then be interpreted in the light of the compositions and conditions of the mixture investigated and the influence of the confinement and obstructions of the test facility.

This adaptation of the experimental results data-set for more 'advanced' analysis has been carried out for five selected tests from those listed in Table 18.

The successive data evaluation steps required for such an optimal analysis and interpretation of the results in terms of revealed combustion behaviour are complex and are described in Appendix B for Test 27. This test was one of the 100% H₂ tests, which with a heat exchanger model obstruction of fifteen rows of pipes caused flame velocities and over-pressures suggestive of detonative behaviour.

10.4 RESULTS: CONSTRUCTION OF DISTANCE VERSUS TIME DIAGRAMS.

With the creation of these best achievable time data, there remain two further requirements to enable display of distance vs time functions.

The first is the listing of sensor positions. This requires,

- (a) for appreciation of overall upstream combustion development and function creation: distances of probe positions to the point of ignition,
- (b) for appreciation of overall downstream combustion development and function creation, distances to the first sensor downstream of the heat exchanger model
- (c) for estimates of local flame velocities and flame development within the areas of (a) and (b), inter probe distances.

The second are time differences for each of the distances listed under (a) – (c).

In the first instance, this report has focussed on creating the database from which all above options can readily be developed and a relatively accurate graphical oversight can be given. To this end distances to point of ignition from the experimental results data and time intervals from Table B1.1 (Appendix B), column 4 less column 1, are respectively listed in columns 5 and 6. In the former, the inter-probe distances are also given. These last two tasks are also summarised by Figure B1.1 (see Appendix B), boxes 12 and 13.

Completion of Table B1.1 then finally allows construction of the distance vs time diagram. For all 5 tests discussed in this first report such diagrams and the results of such parallel calculations as detailed in Section 3 are shown as follows:

- Test 10: 100% H₂ at $\phi = 0.52$, & no HE model; Figure 35 and Appendix C
- Test 24: 100% H₂ at $\phi = 0.52$, & 7 row HE model: Figure 36 and Appendix D
- Test 27: 100% H₂ at $\phi = 0.52$, & 15 row HE model: Figure 37 and Appendix B
- Test 29: 100% H₂ at $\phi = 0.63$, & 15 row HE model: Figure 38 and Appendix E
- Test 25: 100% H₂ at $\phi = 0.72$, & 7 row HE model: Figure 39 and Appendix F

10.5 EVALUATION OF RESULTS.

The results show that the very methodology of the analysis of this report has paid off. The number of 46 NS (no signal) and NA sensor responses for the five 5 Tests in the experimental results section (28%) has been reduced to ONE (0.6%).

The slopes of straight lines drawn by eye through the results indicate approximate overall velocities of the pressure and/or combustion waves. These demonstrate the validity of scaling approach used, the test mixtures selected for Task 2 building on the findings of the laboratory experiments carried out in Task 1. The success of this approach gives confidence for the next stage in the Task 3 HRSG rig.

For these 100% H₂ tests the undisturbed flame (Test 10) and therefore the flame upstream of the HE model (other tests) develops very much according to expectation. With an increase in the equivalence ratio from about 0.5 to 0.7 the overall flame velocity rises from approximately 80 to 120 m/sec.

The diagrams of the HE model constrained tests, e.g. Tests 24 and 27, Figures 36 and 37 show that a linear extrapolation of the correlation line back to the ignition point does not go through the diagram origin. This is as it should be because the flame needs some distance to accelerate from 0 – approximately 80 m/sec.

The very early pressure sensor responses, e.g. Tests 10 and 24, Figures 35 and 36, are records of the passage of the pressure wave caused by the initial explosion and the expanding initial flame.

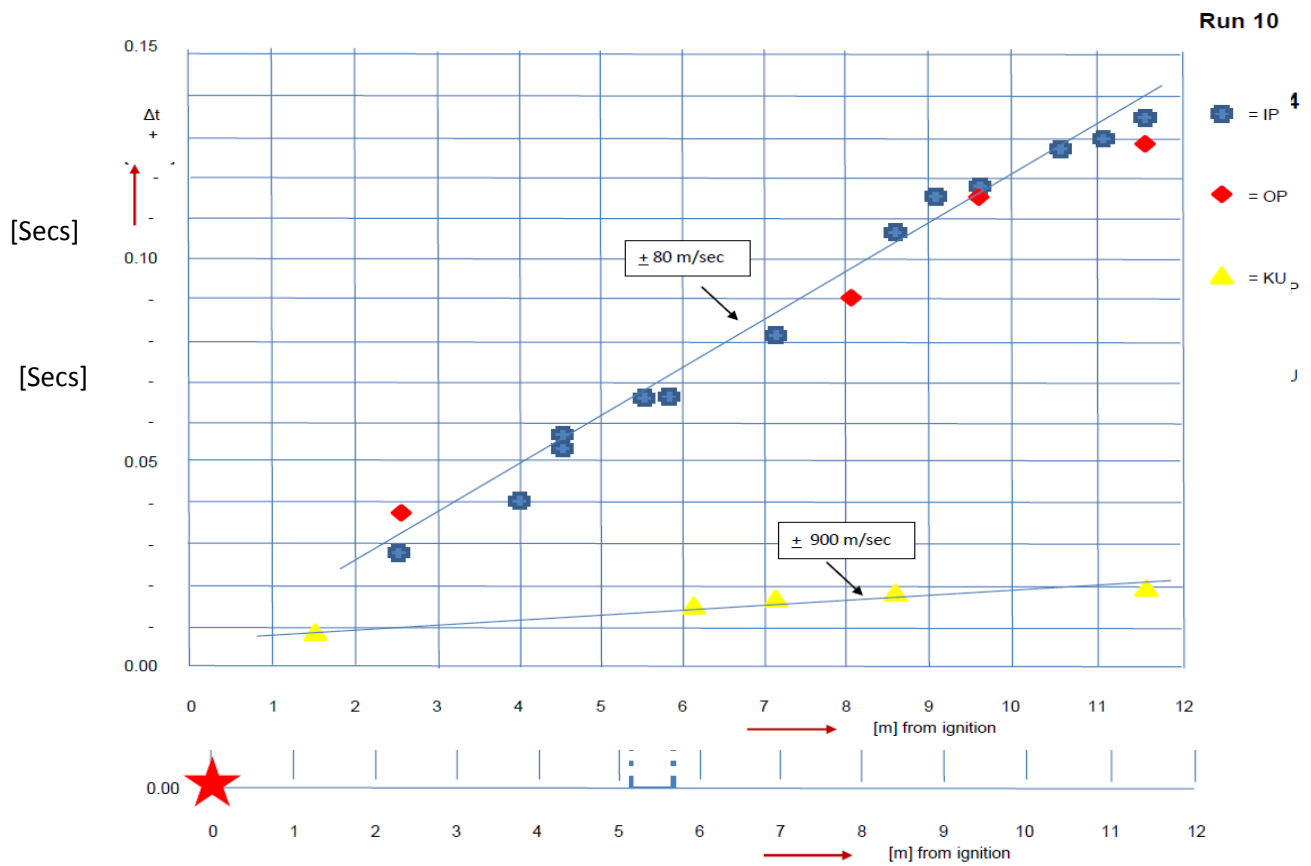
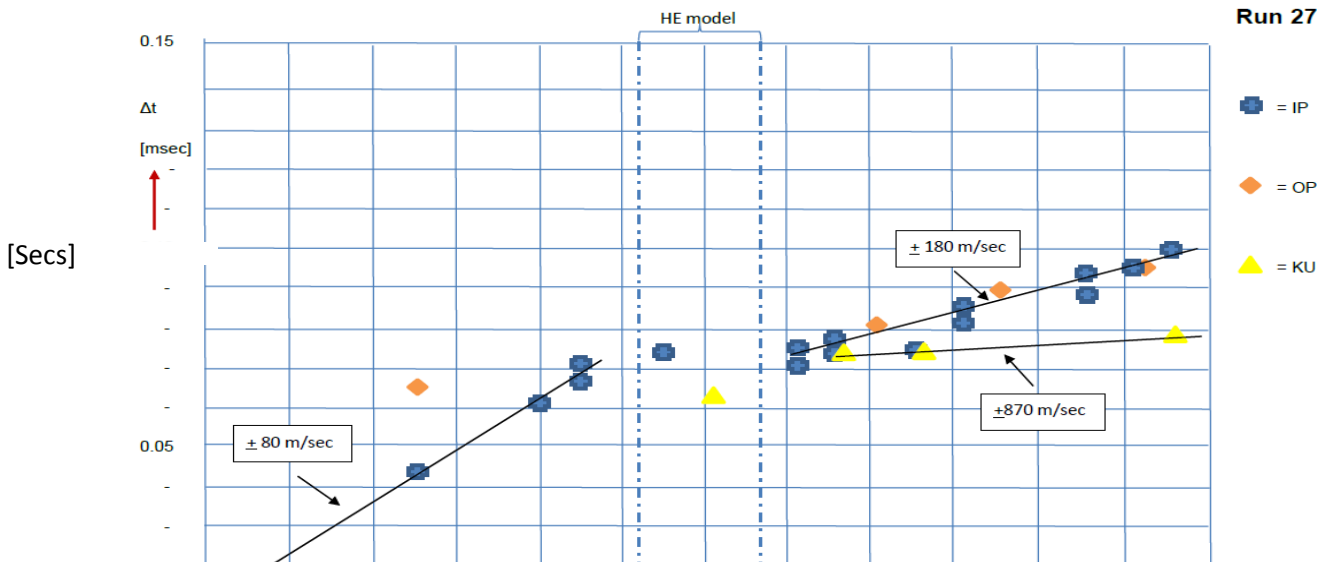
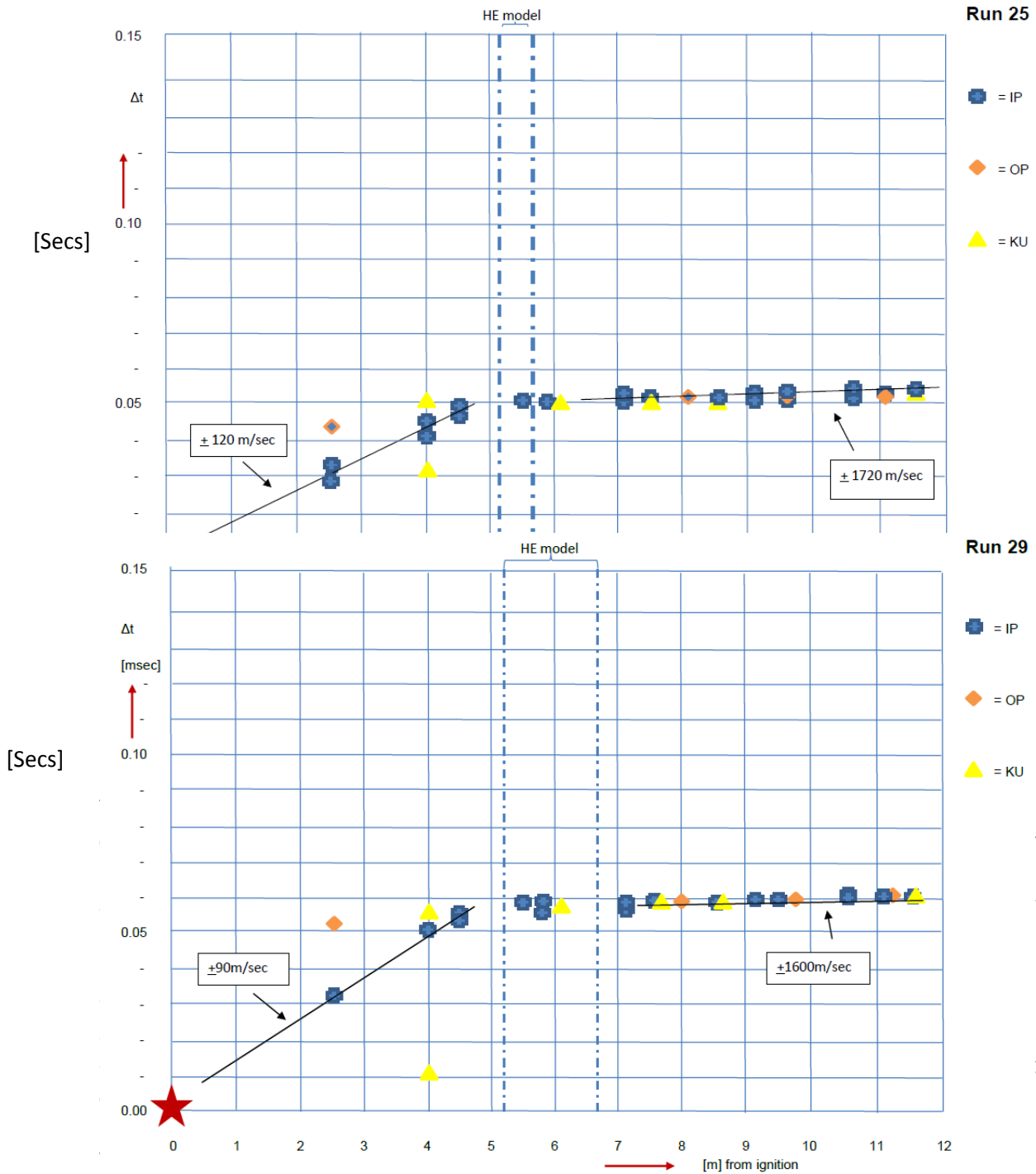


Figure 36: Distance vs Time for 100% H₂ at $\phi = 0.52$ and 7 row heat exchanger





length = effect of the HE model. When If high enough, the shock from the intensely powerful gas release and explosivity exiting the HE model will set off a detonation process with shock wave, ionisation and combustion following each other very closely as shown for Test 29 ($\phi \approx 0.7$) by the close proximity of the outputs from the three types of sensors and the overall combustion velocity of around 1700 m/sec. It is also consistent with the maximum over-pressure recorded of 7 - 8 bar.

When the length of the HE model is reduced, i.e. a 7 row HE model, but all other conditions remain the same, its impact on the same 100% H₂ mixture is clearly less severe, see Test 24, Figure 36. After the temporary velocity fall at exit the flame will accelerate again but the less intense and slower pressure wave (~ 550 m/sec) fails to support the flame sufficiently and decouples, while the flame continues at its own enhanced but overall subsonic flame velocity of around 100 m/sec.

In 10.2 of this report it was concluded that for a particular fuel mixture a safe operating gap between a “lowest hazardous” and “highest safe” concentration in air would be $\Delta\phi = 0.2$, see Table 17. For 100% H₂ these levels were respectively $\phi_{\text{haz}} = 0.55$ and $\phi_{\text{safe}} = 0.35$. Detailed analysis of the results actually confirms that **what really matters is to ensure that for a given size, type and length of heat exchanger the fuel mixture is not so energetic that it will generate an overpressure/shock at the exit that is powerful enough to auto-ignite the mixture sufficiently rapidly for a detonation type reaction to be maintained.** Test 27 (Figure 37) shows that for 100% H₂ and the 15 row heat exchanger the hazardous limit is indeed at $\phi = 0.52 + 0.01$, where the near-exit over-pressure of 0.8 bar (KU3) was not able to set up a detonation, which resulted in a maximum recorded downstream over pressure of 1.7 bar (KU4 and Table 16).

We have as yet no similar telling results for the 7 row heat exchanger but **it will be very important for the WP2.3 test programme that the over-pressure at the exit of the heat exchanger can be recorded and monitored. The recommended safety margin of $\Delta\phi = 0.2$ remains reasonable.**

10.6 FURTHER SUGGESTED WORK

The above are early appreciations of the enhanced results and further development and interpretation will follow. The first task will be to transfer the data from the appendices to excel spreadsheets so that curve fitting can take place and the overall velocity correlations be expressed as functions for future use. The sheets will be formatted to allow also for velocity calculation over shorter distances/time intervals and to incorporate the over-pressure values recorded. The velocities calculated will be averages and must therefore be assigned to the half-way point of the length interval for which they have been calculated.

Results from other tests in Table 18 that should/will be analysed in the same way include:

- the set of Tests 5, 20 and 31 for the H₂/CH₄ 60/40 mixture is essential to look more closely at flame behaviour between the high risk and safe limits at the H₂-CH₄ boundary of the three dimensional model of Figure 34.
- and Tests 16 and 53 for the same purpose for H₂/CO
- Analysis of the few lower temperature tests will also have to be conducted
- Results for the high gas velocity tests will first have to be considered as essential for completion of WP2.2 or as a preliminary for WP2.3

Finally on an ongoing basis, methods will have to be considered to see if this successful but time-consuming analysis method,

- Can be simplified and/or speeded up by using more cp based aid

- And/or remains necessary with the improvements that are being made in the detection and signal processing methods currently effected at the HSL.

In addition, the results obtained and the analysis achieved illustrate how the HRSG rig might be used post WP2.3 to understand the phenomena within the congested area, and the impact of different arrangements and systems (such as duct burners) on these phenomena as means of preventing or mitigating conditions that might lead to damaging overpressures.

11 REFERENCES

1. Basis of Design Document for HSL WP2 Task 2 Test rig for ETI. K. Moodie 20th March 2014. Version 2.02.
2. Commissioning Report HSL WP2 Task 2 Test Rig. K. Moodie and B.C.R. Ewan. 9th May 2014. Version 0.01.
3. Operation of ETI HiH2 test rig with carbon monoxide. MHUA 32, R. Gibson. 02/04/2015.
4. Analysis of data from ETI WP 2.2 tests. H. Michels. July 2015.
5. MHU0139 – PE02162 – ETI HiH2. General area and visitor risk assessment. M. Clay. 2014.
6. MHU0125 – PE02162 – ETI HiH2. Oxygen system risk assessment. M. Clay. 2014.
7. MHU0068 – PE02162 – ETI HiH2. Hydrogen test rig. Mixed gas system. M. Clay. 2014.
8. MHU0193 – PE02162 – ETI HiH2. Hydrogen project. Toxic (CO) risk assessment. M. Clay. 2014.
9. MHU0100 – PE02162 – ETI HiH2. Modification of rig. Operational risk assessment. M. Clay. 2014.
10. High velocity tests in preparation for the WP 2.3 HRSG test programme. K. Moodie and B.C.R. Ewan. July 2015.

APPENDIX A: RIG DETAILS AND RESULTS

11.1 CONTRACTUAL REQUIREMENTS

The Participants acknowledge that a critical purpose of the project is to demonstrate, to the reasonable satisfaction of the ETI, that the Project meets the Value Objective as set out in Clauses 3.2, 3.3 and 3.4 of this Part 1 of Schedule 5.

The Project will provide a more detailed and reliable evidence base and advance the state-of-the-art in the safe and efficient use of high hydrogen gas mixtures for energy production in order to contribute critically to the following outcomes:

- Identification for a range of CHP/CCGT applications of the boundaries for safe design and operation with proposed high hydrogen fuel mixtures to avoid the unintended presence in their exhaust systems of fuel mixtures that constitute a risk on the grounds of their limits of flammability, and ignition and significant overpressure potential.
- Operation of existing systems with more confidence within safe boundaries in order to optimise energy production, while avoiding trips, for example by enabling gas engines to run at higher fuel/air mixture ratios or CCGT systems to operate with higher trip-point settings.
- Improvements in detailed design and instrumentation of high hydrogen systems in order to deliver more robust and inherently safer designs.
- Outline of the scope and specific limitations of the application of the Project results to larger duct dimensions and other geometries and of opportunities for further work to increase confidence in such extrapolations.

During the project, the participants provide the following outputs:

- A summary on previous work on limits of flammability, ignition characteristics and potential for significant overpressure generation, including from DDT, of high hydrogen systems under varying conditions, including how this information is applicable to exhaust systems of engines/turbines, particularly with respect to CHP/CCGT systems which may include duct burners for turbine applications. The summary should highlight recognised shortfalls, gaps, and development opportunities including for inherently safer designs and indicate which aspects of these area addressed by the project.
- The results from laboratory experiments into the limits of flammability, ignition characteristics and significant overpressure potential, including from DDT, and from the further investigation in the approved larger geometries, including for any agreed temperatures and pressures and from any modelling work;
- An assessment of any recognized and relevant remaining gaps in the experimental and additional modelling work.

- An interpretation of the implications and recommendations from the results for the design and operation of CCGE and CCGT systems as understood from the findings obtained from the first deliverable above, own knowledge and any additional information provided by the Participants.
- A review and summary of methods and devices for assessing the composition of gases entering the exhaust system, with identification of any technologies that have a sufficiently high response time to allow an engine or turbine to adapt to changes in gas composition within a critical time span. Where acquisition of additional information or work has been approved, the outcome or results from such investigations or other work and any validation resulting from these will be included.
- An evaluation of identified and recognized remaining areas of greatest concern for the design, operation and control of CCGE and CCGT systems.
- An outline scope for the future development of understanding of such areas of concern and recommendations for further experimental, theoretical or modelling work that follows directly from and/or complements the outcome of the Project.

The Parties agree that the Project is intended to meet the following critical success factors, which shall characterise or are required to facilitate a successful Project outcome:

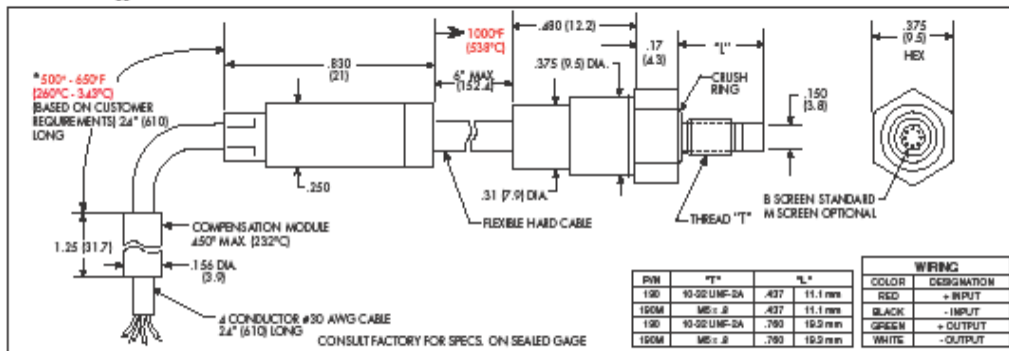
- The Project should make a significant step forward in developing the evidence base and tools for the safe and more economical design and operation of gas engines and gas turbines using high hydrogen fuels.
- The Project must provide sufficient information and present it in such a manner as to enable the ETI to make informed decisions at the end of the Project regarding follow-on work that may be required.

11.2 KULITE PRESSURE SENSOR DATA SHEET



- XTEH-10L-190 (M) SERIES**
- -65°F To 1000°F Temperature Capability*
 - Patented Leadless Technology VIS®
 - High Natural Frequency
 - Suitable For Stall Avoidance Application

The XTEH Series pressure transducers feature a very wide operating temperature range. These characteristics make these devices ideal for Turbine engine testing especially in the areas of stall avoidance and active stability control. Other equally demanding applications in the industry may also benefit from the ruggedness of these devices.



INPUT Pressure Range	1.7 25	3.5 50	7 100	14 200	21 300	35 500	70 1000	140 2000	210 BAR 3000 PSI
Operational Mode	Absolute, Sealed Gage								
Over Pressure	2 Times Rated Pressure								
Burst Pressure	3 Times Rated Pressure								
Pressure Media	All Nonconductive, Noncorrosive Liquids or Gases (Most Conductive Liquids and Gases - Please Consult Factory)								
Rated Electrical Excitation	10 VDC/AC								
Maximum Electrical Excitation	15 VDC/AC								
Input Impedance	1000 Ohms (Min.)								
OUTPUT Output Impedance	1000 Ohms (Nom.)								
Full Scale Output (FSO)	100 mV (Nom.)								
Residual Unbalance	± 5 mV (Typ.)								
Combined Non-Linearity, Hysteresis and Repeatability	± 0.1% FSO BFSL (Typ.) ± 0.5% FSO (Max.)								
Resolution	Infinitesimal								
Natural Frequency (KHz) (Typ.)	240	300	380	500	575	700	1000	1400	1650
Acceleration Sensitivity % FS/g Perpendicular Transverse	5.0x10 ⁻⁴ 6.0x10 ⁻⁶	3.0x10 ⁻⁴ 4.0x10 ⁻⁶	1.5x10 ⁻⁴ 2.0x10 ⁻⁶	1.1x10 ⁻⁴ 1.5x10 ⁻⁶	9.0x10 ⁻⁵ 1.0x10 ⁻⁶	6.5x10 ⁻⁵ 7.0x10 ⁻⁶	4.0x10 ⁻⁵ 4.0x10 ⁻⁶	2.5x10 ⁻⁵ 3.0x10 ⁻⁶	1.9x10 ⁻⁵ 2.0x10 ⁻⁶
Insulation Resistance	100 Megohm Min. @ 50 VDC								
ENVIRONMENTAL Operating Temperature Range	-65°F to +1000°F* (-55°C to +538°C) - Cable Area								
Compensated Temperature Range	+80°F to +850°F (+25°C to +454°C)								
Thermal Zero Shift	± 1.5% FS/100°F (Typ.)								
Thermal Sensitivity Shift	± 1.5% /100°F (Typ.)								
Steady Acceleration and Linear Vibration	1,000g. Sine								
PHYSICAL Electrical Connection	4 Conductor 30 AWG Shielded Cable (24" After Module)								
Weight	8 Grams (Nom.) Excluding Cable								
Pressure Sensing Principle	Fully Active Four Arm Wheatstone Bridge Dielectrically Isolated Silicon on Silicon Patented Leadless Technology								
Mounting Torque	15 Inch-Pounds (Max.) 1.7 N-m								

* Limited life above 850°F (455°C), dependent on operating conditions.
 Note: Custom pressure ranges, accuracies and mechanical configurations available. Dimensions are in inches. Dimensions in parentheses are in millimeters.
 Note: Requires external compensation module (Max. temp. 450°F). Please refer to outline drawing.
 Continuous development and refinement of our products may result in specification changes without notice - all dimensions nominal (N)
 KULITE SEMICONDUCTOR PRODUCTS, INC. • One Willow Tree Road • Lodi, New Jersey 07605 • Tel: 201 461-0000 • Fax: 201 461-0000 • <http://www.kulite.com>

11.4 COMBUSTION TESTS SUMMARY OF DATA

Combustion tests with no congestion

Mixture	Vol% ratio	Test number	Comments
CH ₄ / H ₂	100/0	1	1 No obstacles in duct. Pure methane starting test mixture. Stoichiometric condition and oxygen met satisfactorily, however flame speeds from IPs not considered reliable. OPs provide flame speeds but latter value appears high. Test 3 will repeat this condition.
CH ₄ / H ₂	100/0	2	2 No obstacles in duct. Repeat of Test 1 conditions. Stoichiometric condition and oxygen met satisfactorily. Flame speeds and pressures provide satisfactory measurements.
CH ₄ / H ₂	100/0	3	1a [Repeat of 1] No obstacles in duct. Further repeat of Test 1 conditions. Stoichiometric condition and oxygen met satisfactorily. Data is not considered to be fully satisfactory, e.g. IP flame sensors appear to carry high level of noise. Some OP sensors provide flame speed data. Pressures are consistent with previous test.
CH ₄ / H ₂	100/0	4	2a [Repeat of 2] No obstacles in duct. Completion of data set for CH ₄ at equivalence ratio of 1.0. Stoichiometric condition and oxygen met satisfactorily. Data set is satisfactory.
CH ₄ / H ₂	40/60	5	6a No obstacles in duct. First of series using 40/60 CH ₄ /H ₂ . Stoichiometric condition and oxygen met satisfactorily. Useful data obtained although low equivalence and weak flame results in incomplete record for IPs and OPs. Flame speeds are low as are peak pressures.

Mixture	Vol% ratio	Test number	Comments
CH ₄ / H ₂	40/60	7	Test added following engine replacement and to provide further data with 40/60 CH₄/H₂ mixture 62 No obstacles in duct. Target equivalence ratio was 0.85. 2nd equivalence ratio for this mixture (40/60 CH ₄ /H ₂). Stoichiometric condition and oxygen met satisfactorily. Useful data obtained and strong flame provides good flame speeds on both IP and OP sensors.
CH ₄ / H ₂	40/60	8	Test added to provide further data with 40/60 CH₄/H₂ mixture 62a No obstacles in duct. Target equivalence ratio was 1.0. However, decreasing available pressure in mixed gas reservoir resulted in actual equivalence ratio of 0.86. This is nearly identical to test 7. Oxygen target met satisfactorily. As for test 7, the equivalence ratio for this mixture (60/40 H ₂ / CH ₄) resulted in a strong flame and provides good flame speeds on both IP and OP sensors
CH ₄ / H ₂	0/100	9	No obstacles in duct. Target equivalence ratio is 0.4 First of series using 100% H ₂ . Stoichiometric condition and oxygen met satisfactorily. Useful data obtained although low equivalence and weak flame results in an absence of signals for the IPs suggesting flame front doesn't travel along side walls. OP sensors show clear signals and provide a flame speed record. Flame speeds are low as are peak pressures. (41)
CH ₄ / H ₂	0/100	10	No obstacles in duct. Target equivalence ratio is 0.5 Increased equivalence ratio from test 9. Stoichiometric condition and oxygen met satisfactorily. Useful data obtained although low equivalence and weak flame results in an absence of signals for the IPs suggesting flame front doesn't travel along side walls. OP sensors show clear signals and provide a flame speed record. Flame speeds are low as are peak pressures. (51)
CH ₄ / H ₂	0/100	11	Change of Equivalence Ratio compared with test matrix - overpressure and flame speeds from test 9 and 10 low therefore E.R. changed from 0.3 to 0.7 No obstacles in duct. Target equivalence ratio is 0.7

Mixture	Vol% ratio	Test number	Comments
			Stoichiometric condition and oxygen met satisfactorily. Sensors show strong flame front progression on IPs and OPs. Peak pressure (0.3 bar) highest yet seen)
CH ₄ / H ₂	40/60	12	No obstacles in duct. Target equivalence ratio is 1.0. Target equivalence ratio not fully reached for this mixture (60/40 H ₂ / CH ₄). Oxygen met satisfactorily. Useful data obtained and stronger flame provides good flame speeds on both IP and OP sensors. Pressures consistent with other tests on this mixture at the same equivalence.
CH ₄ / H ₂	40/60	13	Test added to matrix to investigate EQRs nearer to 'real world conditions' . No obstacles in duct. Target equivalence ratio is 0.35 Weakest equivalence tested for this mixture. Stoichiometric condition and oxygen met satisfactorily. Useful data obtained although low equivalence and weak flame results in an absence of signals for the IPs suggesting flame front doesn't travel along side walls. 3/4 of the OP sensors show clear signals and provide a flame speed record. Flame speeds are low as are peak pressures.
CO / H ₂	100/0	14	No obstacles in duct. First test of pure CO injection. Mass flow condition met for CO. Due to dome valve pressure required to obtain CO mass flow, the oxygen dome pressure is at limit of operation and oxygen mass flow found to be oscillating. There is some evidence of ignition but test is not considered to provide useful data.
CO / H ₂	40/60	15	Oxygen flow control valve not stabilising at 0.152 kg/s No obstacles in duct. Target equivalence ratio was 0.55 First test of H ₂ / CO injection (60/40). Mass flow condition met for CO but for oxygen, the mass flow shows instability for the same reasons as test 14 (dome valve pressure limit for oxygen). Sensor data on the IPs, OPs and pressure transmitters is absent but the thermocouples show a high temperature at the start of data collection (triggered on the igniter start). The conclusion is that pre-ignition has occurred for this mixture (despite the oxygen being below the 21% level).

Mixture	Vol% ratio	Test number	Comments
CO / H ₂	40/60	16	Oxygen flow control valve not stabilising at 0.152 kg/s. No obstacles in duct. Target equivalence ratio was 0.7. Further test of H ₂ / CO injection (60/40). Mass flow condition is not met for CO due to depleting reserve and for oxygen, a similar instability is showing for the same reasons as test 14 (dome valve pressure limit for oxygen). The resultant equivalence ratio is 0.5 for the mixture (but oxygen is indeterminate but above baseline exhaust value of 16.3%). Sensor data on the IPs is absent but OPs are showing a satisfactory signal indicating that the mixture ignited in the normal controlled way. The thermocouples also show initially low values which rise during the combustion event. Therefore no pre-ignition (autoignition) is in evidence for this test.
CO / H ₂		17	No obstacles in duct. Target equivalence ratio was 0.7. Continued testing of H ₂ / CO injection (60/40). Due to instability in the oxygen injection rate on previous tests due to the dome valve pressure being too close to its limit, the dome pressure for both control valves was reduced. The mass flow condition is now met for oxygen, but the lower available mixed gas pressure now limits the mass flow available for the fuel injection. This results in an effective equivalence ratio of 0.5, but with the correct oxygen make-up level. Sensor data on the IPs, OPs and pressure transmitters is absent but the thermocouples show a high temperature at the start of data collection (triggered on the igniter start). The conclusion is that pre-ignition has again occurred for this mixture.
CO / H ₂		18	No obstacles in duct. Target equivalence ratio is 0.7. RE-RUN OF TEST 17 TO CONFIRM AUTO-IGNITION. TEST ADDED TO MATRIX FOLLOWING AUTOIGNITION EVENT OF PREVIOUS TEST RESULTED IN ALMOST IDENTICAL OUTCOME. Note: due to auto-ignition all future tests with CO should allow for pre-triggering the data collection to 'catch' the autoignition event and subsequent pressure and flame speed data. Continued testing of H ₂ / CO injection (60/40). Due to instability in the oxygen injection rate due to the dome valve pressure being too close to its limit, the dome pressure for both

Mixture	Vol% ratio	Test number	Comments
			control valves is reduced. The mass flow condition is now met for oxygen, but the lower available mixed gas pressure now limits the mass flow available for the fuel injection. This results in an effective equivalence ratio of the 0.5, but with the correct oxygen make-up level. Sensor data on the IPs, OPs and pressure transmitters is absent but the thermocouples show a high temperature at the start of data collection (triggered on the igniter start). The conclusion is that pre-ignition has again occurred for this mixture.

Combustion tests: Eight rows of congestion

Mixture	Vol% ratio	Test number	Comments
CH ₄ / H ₂	40/60	19	Test added to matrix to compare with tests on same mixtures of gas without congestion. Tests on mixture of 40% CH ₄ and 60% H ₂ with intent to start at low equivalence ratio (0.35) Experiment gave relatively weak flame speeds and overpressure but data set is satisfactory. Limited data set from IPs due to weak event but gave flame speeds consistent with those from OPs
CH ₄ / H ₂	40/60	20	Test added to matrix (as above) Second test with congestion in place. Eight (8) rows of congestion in place from central flange (between tube sections 2 and 3). Tests on mixture of 40% CH ₄ and 60% H ₂ at higher EQR Pressure transducers and optical probes provided reliable data showing significant increase in overpressure and some higher flame speeds which correlated well with data from ionisation probes. Highest overpressures yet recorded in any tests.
CH ₄ / H ₂	40/60	21	Third test with congestion in place. Eight (8) rows of congestion in place from central flange (between tube sections 2 and 3). Tests on mixture of 40% CH ₄ and 60% H ₂ at highest EQR Pressure transducers and optical probes provided reliable data showing significant increase in overpressure and some higher flame speeds which correlated well with data from ionisation probes.
CH ₄ / H ₂	0/100	22	Test with congestion in place. Eight (8) rows of congestion in place from central flange (between tube sections 2 and 3). Very weak flame - only evidence being the rise of temperature on the gas thermocouples. No flame front signals present on the ionisation, optical or pressure sensors.
CH ₄ / H ₂	0/100	23	Test with congestion in place. Eight (8) rows of congestion in place from central flange (between tube sections 2 and 3). Very weak flame - only evidence being the rise of temperature on the gas thermocouples. No flame front signals present on the ionisation, optical or pressure sensors.

Mixture	Vol% ratio	Test number	Comments
CH ₄ / H ₂	0/100	24	Test with congestion in place. Eight (8) rows of congestion in place from central flange (between tube sections 2 and 3). This 100% H ₂ test with higher equivalence ratio shows a more definite flame development and pressure signature. Optical probes give a clear flame velocity indication. The IPs carry more uncertainty with flame fronts being difficult to assign definite arrival times in all cases. This gives more uncertainty about flame speeds derived from these sensors. Pressure shows growth in advance of the flame front arriving at the obstacle array at 6000mm and after arrival a pressure wave develops strongly in the downstream region. Some evidence of the pressure wave sharpening downstream of the obstacles. As noted for test 21, the some weak oscillation at 20 kHz shown on the downstream pressure sensors awaits further explanation.
CH ₄ / H ₂	0/100	25	Test added to matrix to compare with test 11 (same EQR but without congestion) Test with congestion in place. Eight (8) rows of congestion in place from central flange (between tube sections 2 and 3). With highest equivalence ratio for pure H ₂ , there is strong evidence of a rapid combustion and strong pressure wave development following flame impingement on the congestion region. Signals on most IPs and all OPs give a good indication of flame speed along the duct. These are in the region of 2000 - 2500 m/s. This case shows a step rise in flame speeds and associated pressures compared to the weaker mixtures so far tested. The peak pressures show a sharpening to shock behaviour downstream. The average pressure wave velocity between the last two sensors is 1818 m/s, which corresponds to a predicted wave speed for the observed pressure pulse of 1703 m/s. The exit flame speed is 1724 m/s which suggests that this test case has given rise to a weak detonation wave event. As noted for test 21, the some weak oscillation at 20 kHz shown on the downstream pressure sensors awaits further explanation.
CH ₄ / H ₂	0/100	26	Test added to matrix Test with congestion in place. Eight (8) rows of congestion in place from central flange (between tube sections 2 and 3). This case represents an intermediate equivalence ratio for pure H ₂ to explore the region prior to the strong combustion event with equivalence of 0.7. There is clear

Mixture	Vol% ratio	Test number	Comments
			evidence of a rapid combustion and a significant pressure wave development following flame impingement on the congestion region. Signals on most IPs and all OPs give a good indication of flame speed along the duct. These however are lower in the 200-300 m/s range. The peak pressures show a sharpening to shock behaviour downstream with a shock speed of around 900 m/s. The flame speed is much lower than this as shown for both IPs and OPs. As noted for test 21, the some weak oscillation at 20 kHz shown on the downstream pressure sensors awaits further explanation.

Combustion tests: Fifteen rows of congestion

Mixture	Vol% ratio	Test number	Comments
CH ₄ / H ₂	0/100	27	Pure hydrogen only starting at EQR 0.50 This case represents an intermediate equivalence ratio for pure H ₂ to compare with the same equivalence ratio with 8 congestion tubes in place, in anticipation of a stronger event. Most signals on the IPs and OPs provide flame arrival information, although there is some ambiguity for some positions leading to some uncertainty with the flame speed behaviour. The peak pressures show a sharpening after the congestion with a decrease in peak pressure towards the exit and a Mach number of around 1.25. The flame speed is much lower than this as shown for both IPs and OPs. As noted for other tests, where the pressure wave sharpens, the same weak oscillation at 20 kHz is shown on the downstream pressure sensors.
CH ₄ / H ₂	0/100	28	Test with 15 rows of congestion (row 8 on central flange with 7 rows projecting upstream into tube 2 and 7 rows projecting downstream into tube 3 This case represents a lower equivalence ratio for pure H ₂ to compare with the same equivalence ratio with 8 congestion tubes in place. The combustion event provides poorly defined flame fronts with resulting absence of good signals on the IPs. The OPs provide some arrival information, and flame speeds.
CH ₄ / H ₂	0/100	29	Test with 15 rows of congestion (row 8 on central flange with 7 rows projecting upstream into tube 2 and 7 rows projecting downstream into tube 3 This case represents an increased equivalence ratio for pure H ₂ to compare with the same equivalence ratio with 8 congestion tubes in place. With this ratio and 15 rows of tube congestion, there is strong evidence of a rapid combustion and strong pressure wave development following flame impingement on the congestion region. Signals on most IPs and all OPs give a good indication of flame speed along the duct. These are in the region of 1660 - 1870 m/s. This case shows a step rise in flame speeds and associated pressures compared to the 0.4 and 0.5 equivalence ratio mixtures so far tested. The peak pressures show a sharpening to shock behaviour downstream. The average pressure wave velocity between the last two sensors is 1648 m/s. The exit

Mixture	Vol% ratio	Test number	Comments
			flame speed is 1667 m/s which suggests that this test case has given rise to a weak detonation wave event. Further support for this comes from the observation that the pressure wave and flame front at the exit of the tube arrive within a single sampling interval of one another. As noted for test 21, the some weak oscillation at 20 kHz shown on the downstream pressure sensors awaits further explanation.
CH ₄ / H ₂	40/60	30	Observation is that the combustion is a relatively weak event with this EQR based on peak pressures and flame speeds.
CH ₄ / H ₂	40/60	31	Stronger combustion event compared with EQR of 0.55 as evidenced by peak pressure of 3 bar (vs 0.2 bar) and higher exit flame speed.
CH ₄	100	33	A moderately strong combustion event at an EQR of 0.86 and showing a peak pressure of 2.6 bar. his should be contrasted with the corresponding pure methane case with no obstacles where the peak pressure was around 0.2 bar. Note that OP3 was later found to have loosened in its mounting, resulting in no signal for this sensor.
CH ₄	100	34	A weaker combustion event at an EQR of 0.76 and showing a peak pressure of 0.65 bar. This can be compared with the corresponding pure methane case with no obstacles where the peak pressure was around 0.2 bar.
CH ₄	100	35	A weak combustion event at an EQR of 0.65 and showing a peak pressure of 0.3 bar. This is comparable with the pure methane case with an EQR of 1 with no obstacles where the peak pressure was around 0.2 bar, giving an indication of the relation between increasing obstacles and decreasing EQR.

Mixture	Vol% ratio	Test number	Comments
CH ₄ / H ₂	60/40	36	The first test of this new mixture. Combustion event is fairly weak with a peak pressure of 416 mbar. Prior to this test, the IPs sensor tips were treated to a blowtorch treatment raising them to yellow heat to attempt to remove any residual moisture. This was found in pre-checks to greatly improve their sharpness of performance. The results for this combustion test confirm this, with many more giving good flame transition signatures. The flame speeds are modest (~200 m/s at the exit) but it is also clear from the arrival times that the flame propagation is complex with arrival times at some of the locations being out of the expected sequence.
CH ₄ / H ₂	60/40	37	This is the highest EQR used for this mixture. The combustion event is moderate in intensity with a peak pressure of 1500 mbar. Note that for this group of tests, the IPs sensor tips were treated to a blowtorch treatment raising them to yellow heat to attempt to remove any residual moisture. This was found in pre-checks to greatly improve their sharpness of performance. The results for this combustion test confirm this, with many more giving good flame transition signatures. The flame speeds are modest (~250 m/s at the exit) but there is also some evidence for this concentration that the flame propagation is complex with arrival times at some of the locations being out of the expected sequence. Flame speeds on the centreline are not always equal to the values measured with the wall sensors. The OPs provide an overall perspective across the tube diameter.

Mixture	Vol% ratio	Test number	Comments
CH ₄ / H ₂	60/40	38	<p>This is the lowest EQR used for this mixture. The combustion event is weak in intensity with a peak pressure of 363 mbar. Note that for this group of tests, the IPs sensor tips were treated to a blowtorch treatment raising them to yellow heat to attempt to remove any residual moisture. This was found in pre-checks to greatly improve their sharpness of performance. The results for this combustion test confirm this, with many more giving good flame transition signatures. The flame speeds are modest (~200 m/s at the exit) but there is also some evidence for this concentration that the flame propagation is complex with arrival times at some of the locations being out of the expected sequence. Flame speeds on the centreline are not always equal to the values measured with the wall sensors. For this reason, the flame speeds based on the IPs are in two sets, one being based on the intervals between the wall sensors and the other based on the intervals between the array sensors within the body of the duct. The OPs provide an overall perspective across the tube diameter.</p>
CH ₄ / H ₂	40/60	39	<p>This is an intermediate EQR for this mixture. The combustion event is weak in intensity with a peak pressure of 600 mbar. Note that for this group of tests, the IPs sensor tips were treated to a blowtorch treatment raising them to yellow heat to attempt to remove any residual moisture. This was found in pre-checks to greatly improve their sharpness of performance. It is noted that the IP signals carry more noise than usual making flame arrival difficult for some positions. The complexity of the flame propagation leads to some uncertainty in the calculation of this for some locations. However flame speeds are very modest (~100 -200 m/s). The OPs provide an overall perspective across the tube diameter, although OP3 at the exit does not provide a signal. It is also noted that the photographic record did not show flame front emergence from the tube exit.</p>

Mixture	Vol% ratio	Test number	Comments
CH ₄ / H ₂	40/60	40	This is a repeat of Test 31 and is the highest EQR tested for this 40/60 CH ₄ / H ₂ mixture. By comparison this combustion event is relatively weak in intensity with a peak pressure of 1353 mbar compared previously with 3016 mbar. Note that for this group of tests, the IPs sensor tips were treated to a blowtorch treatment raising them to yellow heat to attempt to remove any residual moisture. This was found in pre-checks to greatly improve their sharpness of performance. It is noted however that the IP signals carry more noise than usual, making flame arrival difficult for some positions. The complexity of the flame propagation leads to some uncertainty in the calculation of this for some locations. The flame speeds are very modest (~100 -200 m/s) and the overall combustion event appears weaker than that for test 31. This is also confirmed by the absence of a flame on the exit OP3. It is also noted that the photographic record did not show flame front emergence from the tube exit. It should also be noted that the tdms file for this case contains two sets of data as this case was repeated during the data collection. The second data set shows very similar combustion behaviour, e.g. in terms of peak pressure and OP behaviour.
H ₂	100	41	This is lowest EQR value for the repeat tests with pure H ₂ . The combustion has occurred on the evidence of the gas thermocouples. However the combustion is very weak and there is no evidence of a flame front propagating or of a pressure rise following ignition. No pressures or flame speeds are recorded for this case.
H ₂	100	42	This is the intermediate EQR value for the repeat tests with pure H ₂ . The combustion is of moderate strength and the IP signals are variable in their presence and relative order in time. The OP3 signal is weak and not included (to be investigated) and the velocity from these is consistent with that from the IPs in the region. The peak pressures is 1.4 bar and exit flame velocity is around 200 m/s

Mixture	Vol% ratio	Test number	Comments
H ₂	100	43	This is the highest EQR of the repeat tests pure H ₂ . The combustion is strong and the IP signals are almost a complete set. Only two of the OPs have given a useful signal (to be investigated) and the velocity from these is consistent with that from the IPs in the region. The peak pressures (9.4 bar) and exit flame velocity (1666 m/s) indicated a detonation condition has been reached for this case.
H ₂	100	44	This is an intermediate EQR using pure H ₂ . The combustion is moderate and the IP and OP signals provide a basis for interpretation. All of the OP signals are present and velocities are generally consistent with those from the IPs at around 200m/s. The arrival times of flame fronts based on IP data suggests that flame development is complex with axis and wall sensors behaving differently. The peak pressure is moderate at 1.7 bar.
CO	100	46	This is the first test of pure CO combustion but with a low EQR. The combustion is very weak and the IP and OP signals indicate low flame speeds (~ 100m/s). Some evidence of the flame weakening towards the exit of the duct (e.g. no signal on OP3). The peak pressures confirm a very weak event.
CO	100	47	This represents an intermediate EQR using pure CO injection. The combustion is relatively weak and the IP and OP signals indicate moderate flame speeds (~200 - 300m/s). There is inconsistency in velocity estimates among the IPs on axis and on the walls, suggesting complex flame development behaviour. The peak pressure is intermediate with that from adjacent EQR tests.

Mixture	Vol% ratio	Test number	Comments
CO	100	48	This is the highest EQR value using pure CO combustion. The combustion is of moderate strength and the IP and OP signals indicate high flame speeds (up to 1000m/s). There is inconsistency in velocity estimates among the IPs on axis and on the walls, suggesting complex flame development behaviour. It is noted that the flame signal on IP23 at the exit is effectively coincident in time with the shock wave arrival on K7 at the exit.
H ₂ /CO	40/60	49	This test uses a 40/60 H ₂ /CO mixture at a relatively high EQR. The combustion is very strong with very clear signals on both IPs and OPs. Exit flame speed is around 2000 m/s and the evidence is for the existence of a detonation where the pressure is high (10.3 bar) and the exit shock wave is coincident with the exit flame front.
H ₂ /CO	40/60	50	This is the first test of pure 40/60 H ₂ /CO mixture combustion but with a low EQR. The combustion is very weak and the IP and OP signals are very incomplete. They indicate low flame speeds (~ 100m/s) but with considerable variability between axial and wall sensors. Some evidence of the flame weakening towards the exit of the duct (e.g. no signal on OP3). The peak pressure of 227 mbar confirms a very weak event.
H ₂ /CO	40/60	52	This is an intermediate EQR value using this H ₂ /CO mixture. The combustion is relatively weak with the OP signals indicate low flame speeds (~ 200m/s). IP signals are not strong and clear but generally confusing with no clear pattern of flame passage based on relative timings. The peak pressures of 824 mbar confirm a weak event.
H ₂ /CO	60/40	53	This is the first test of the H ₂ /CO mixture but with a low EQR. The combustion is very weak and the IP signals are mostly absent. Three OP signals indicate low flame speeds (~ 100m/s). The peak pressures confirm a very weak event.

Mixture	Vol% ratio	Test number	Comments
H ₂ / CO	60/40	54	This is an intermediate test of the H ₂ /CO mixture with a raised EQR. The combustion is rather very weak and the IP signals are of poor quality or absent. Four OP signals indicate low flame speeds (< 200m/s). The peak pressure is increased significantly compared with an EQR of 0.4 and is close to a likely industrial application limit.
H ₂ / CO	60/40	56	This test represents a small increase in the previous EQR value using the 60 H ₂ /40 CO mixture. This cautious increase was due to the large increase in peak pressure in moving from EQR 0.4 to EQR 0.5. However, the combustion in this case is weaker than expected and there is evidence of a (a) a weak pre-ignition giving a peak pressure of 200mbar followed 40msec later by (b) the main ignition giving a peak pressure of 1069 mbar. This main ignition occurs at the target mixture EQR of 0.56 but it appears that this is also an auto-ignition event. The peak pressure is lower than expected and may be due to the exhaust mixture ahead of the flame front being depleted by the previous weak pre-ignition. The IP signals are of poor quality or absent. Three OP signals indicate low flame speeds (< 200m/s).
CH ₄ / H ₂ / CO	25/40/35	57	This test represents the first using a 3 component mixture of H ₂ /CO/ CH ₄ with an upper limit chosen for the EQR. The combustion in this case is of medium strength at a peak pressure of 3.12 bar. The OP signals indicate an exit flame speed of ~ 300m/s and the IPs generally agree. Differences remain in flame arrival times associated with the wall and centre of the duct.
CH ₄ / H ₂ / CO	25/40/35	58	This test represents a reduced value of EQR compared to the initial test with this 3 component mixture of H ₂ /CO/ CH ₄ . The combustion in this weaker than that of the highest EQR with a peak pressure of 1.5 bar. The OP signals indicate an exit flame speed of 200- 300m/s and the IPs generally agree. Differences remain in flame arrival times associated with the wall and centre of the duct.

Mixture	Vol% ratio	Test number	Comments
CH ₄ / H ₂ / CO	25/40/35	59	This test represents a reduction in value of EQR to 0.51 from the previous value of 0.56 with the 3 component mixture of H ₂ /CO/ CH ₄ . The combustion is fairly weak and it is noted that the peak pressure is similar to that of the previous higher EQR value of 1.5 bar. The OP signals indicate an exit flame speed of 200- 300m/s and the IPs generally agree. Some of the OP and IP signals are missing indicating a weak event and differences remain in flame arrival times associated with the wall and centre of the duct.
CH ₄ / H ₂ / CO	25/40/35	60	This test represents the lowest value of EQR of 0.45 tested in order to confirm the lowest peak pressure likely to be achieved by this mixture of H ₂ /CO/ CH ₄ . The combustion is very weak as indicated by the limited IP and OP signals. Flame speed is very low at ~100 m/s

Combustion tests: Fifteen rows of congestion at lower exhaust temperature

Mixture	Volume % ratio	Test number	Comments
CH ₄ / H ₂ / CO	0/100/0	61	This test represents the initial test with pure H ₂ at a lower exhaust temperature of 350 C (but with the same exhaust duct velocity) and using a modest EQR value of 0.5. The high temperature equivalent case for this condition produced a peak pressure of 1.76 bar. For this test the exit pressure, which is usually the highest, is 2.23 bar but it should be noted that the PCB transducer at position 3-6 indicates a much higher pressure of 9.7 bar. Multiple peaks associated with the PCB sensor raise the question as to whether 9.7 bar is correct. The time difference to the pressure wave arriving at the exit is around 2.5 ms, which would be too long for a wave associated with a 9.7 bar shock wave travelling at around 1600 m/s. A lower pressure value is therefore taken as representative as the peak pressure for this case (2.23 bar). The combustion is moderate in other respects with flame speeds around 200 m/s although it is noted that several sensors suggest much higher speeds in the region of the obstacle arrays of around 700 m/s.
CH ₄ / H ₂ / CO	0/100/0	62	This test represents an EQR reduced by 0.05 units from the initial test with pure H ₂ at the lower exhaust temperature of 350 C (but with the same exhaust duct velocity). The combustion is fairly weak with a peak pressure of 0.78 bar. The OPs indicate a flame speed in the range 150 - 200 m/s, however the IP sensors show very little evidence of a clearly defined flame front and no sensible flame speeds have been provided by these.

Mixture	Volume % ratio	Test number	Comments
CH ₄ / H ₂ / CO	0/100/0	63	This test represents the lowest EQR value tested for pure H ₂ at the lower exhaust temperature of 350 C (but with the same exhaust duct velocity). The combustion is very weak with a peak pressure of 0.37 bar. The OPs indicate a flame speed in the range 150 - 200 m/s, however the IP sensors show very little evidence of a clearly defined flame front and no sensible flame speeds have been provided by these.
CH ₄ / H ₂ / CO	40/60/0	64	This test represents the first test of the 60 H ₂ /40 CH ₄ mixture at an upper EQR value and at the lower exhaust temperature of 350 C (but with the same exhaust duct velocity). The combustion is moderately strong with a peak pressure of 2.8 bar. A spurious noise spike has appeared within the data and upset the OP signals and the last two of the IPs. However there is evidence of elevated flame speeds within the middle section of the duct and the pressure signals are reproduced correctly.
CH ₄ / H ₂ / CO	40/60/0	65	This test represents an intermediate EQR value using the 60 H ₂ /40 CH ₄ mixture and at the lower exhaust temperature of 350 C (but with the same exhaust duct velocity). The combustion is of medium strength with a peak pressure of 1.6 bar. Useful flame speed data is available from both OPs and IPs with these in the range up to 300 m/s, although some inconsistency exists between wall and centreline IP sensors.
CH ₄ / H ₂ / CO	40/60/0	66	This test represents the lowest EQR value using the 60 H ₂ /40 CH ₄ mixture and at the lower exhaust temperature of 350 C (but with the same exhaust duct velocity). The combustion is extremely weak with a peak pressure of only 0.08 bar. Usefully, the OPs provide flame arrival information at each station and this is very low at 50 - 90 m/s. The flame structure is not sufficiently sharp or intense to enable flame IP sensor signals.

Mixture	Volume % ratio	Test number	Comments
CH ₄ / H ₂ / CO	0/40/60	67	This test represents an intermediate EQR value using the 40H ₂ /60CO mixture and at the lower exhaust temperature of 350 C (but with the same exhaust duct velocity). The combustion is of modest strength with a peak pressure of only 1.1 bar. This pressure is 50% higher than the value obtained at the higher temperature and same EQR and this trend is consistent with the other low temperature results obtained with other gas mixtures. Usefully, the OPs provide flame arrival information at each station and this is in the 200 - 300 m/s range. The flame structure is not sufficiently sharp or intense to enable useful flame speeds from the IP sensor signals and the relative timings of these suggest a complex flame development process.

11.5 FLAME SPEED, TEMPERATURE AND PRESSURE HIGHLIGHTS

Combustion tests: No congestion

Note - initial temperatures are after oxygen and mixed gas injection but before ignition.

Test Number	1
Mixture Composition (%H ₂ /%CH ₄ /%CO)	0/100/0
Ambient Temperature (°C)	14
Ambient Pressure (mbar)	957
Wind Speed (m/s)	5
Wind direction	W
Relative Humidity (%)	92
Equivalence Ratio	1
Max. overpressure (mbar)	230
Max. pressure location (m)	6.25
Max. flame speed (ionisation sensors, m/s)	0
Max. flame speed (optical sensors, m/s)	392
Max. temperature (°C)	869
Initial temperature (°C)	512

Test Number	2
Mixture Composition (%H ₂ /%CH ₄ /%CO)	0/100/0
Ambient Temperature (°C)	14
Ambient Pressure (mbar)	957
Wind Speed (m/s)	5
Wind direction	W
Relative Humidity (%)	92
Equivalence Ratio	1
Max. overpressure (mbar)	216
Max. pressure location (m)	6.25
Max. flame speed (ionisation sensors, m/s)	0
Max. flame speed (optical sensors, m/s)	240
Max. temperature (°C)	1182
Initial temperature (°C)	512

Test Number	3
Mixture Composition (%H ₂ /%CH ₄ /%CO)	0/100/0
Ambient Temperature (°C)	14
Ambient Pressure (mbar)	957
Wind Speed (m/s)	5
Wind direction	W
Relative Humidity (%)	92
Equivalence Ratio	1
Max. overpressure (mbar)	209
Max. pressure location (m)	6.25
Max. flame speed (ionisation sensors, m/s)	366
Max. flame speed (optical sensors, m/s)	312
Max. temperature (°C)	1165
Initial temperature (°C)	512

Test Number	4
Mixture Composition (%H ₂ /%CH ₄ /%CO)	0/100/0
Ambient Temperature (°C)	14
Ambient Pressure (mbar)	957
Wind Speed (m/s)	5
Wind direction	W
Relative Humidity (%)	92
Equivalence Ratio	1
Max. overpressure (mbar)	232
Max. pressure location (m)	6.25
Max. flame speed (ionisation sensors, m/s)	312
Max. flame speed (optical sensors, m/s)	258
Max. temperature (°C)	1172
Initial temperature (°C)	512

Test Number	5
Mixture Composition (%H ₂ /%CH ₄ /%CO)	60/40/0
Ambient Temperature (°C)	15
Ambient Pressure (mbar)	958
Wind Speed (m/s)	5
Wind direction	W
Relative Humidity (%)	84
Equivalence Ratio	0.65
Max. overpressure (mbar)	168
Max. pressure location (m)	1.75
Max. flame speed (ionisation sensors, m/s)	196
Max. flame speed (optical sensors, m/s)	170
Max. temperature (°C)	992
Initial temperature (°C)	512

Test Number	7
Mixture Composition (%H ₂ /%CH ₄ /%CO)	60/40/0
Ambient Temperature (°C)	14
Ambient Pressure (mbar)	965
Wind Speed (m/s)	5
Wind direction	NW
Relative Humidity (%)	97
Equivalence Ratio	0.85
Max. overpressure (mbar)	204
Max. pressure location (m)	6.25
Max. flame speed (ionisation sensors, m/s)	294
Max. flame speed (optical sensors, m/s)	291
Max. temperature (°C)	845
Initial temperature (°C)	512

Test Number	8
Mixture Composition (%H ₂ /%CH ₄ /%CO)	60/40/0
Ambient Temperature (°C)	14
Ambient Pressure (mbar)	965
Wind Speed (m/s)	3
Wind direction	NE
Relative Humidity (%)	100
Equivalence Ratio	0.86
Max. overpressure (mbar)	205
Max. pressure location (m)	1.75
Max. flame speed (ionisation sensors, m/s)	296
Max. flame speed (optical sensors, m/s)	310
Max. temperature (°C)	1092
Initial temperature (°C)	512

Test Number	9
Mixture Composition (%H ₂ /%CH ₄ /%CO)	100/0/0
Ambient Temperature (°C)	14
Ambient Pressure (mbar)	965
Wind Speed (m/s)	3
Wind direction	NE
Relative Humidity (%)	100
Equivalence Ratio	0.4
Max. overpressure (mbar)	73
Max. pressure location (m)	1.75
Max. flame speed (ionisation sensors, m/s)	0
Max. flame speed (optical sensors, m/s)	93
Max. temperature (°C)	760
Initial temperature (°C)	512

Test Number	10
Mixture Composition (%H ₂ /%CH ₄ /%CO)	100/0/0
Ambient Temperature (°C)	14
Ambient Pressure (mbar)	965
Wind Speed (m/s)	3
Wind direction	NE
Relative Humidity (%)	100
Equivalence Ratio	0.5
Max. overpressure (mbar)	130
Max. pressure location (m)	6.25
Max. flame speed (ionisation sensors, m/s)	0
Max. flame speed (optical sensors, m/s)	115
Max. temperature (°C)	839
Initial temperature (°C)	512

Test Number	11
Mixture Composition (%H ₂ /%CH ₄ /%CO)	100/0/0
Ambient Temperature (°C)	14
Ambient Pressure (mbar)	965
Wind Speed (m/s)	5
Wind direction	W
Relative Humidity (%)	92
Equivalence Ratio	0.69
Max. overpressure (mbar)	320
Max. pressure location (m)	6.25
Max. flame speed (ionisation sensors, m/s)	312
Max. flame speed (optical sensors, m/s)	348
Max. temperature (°C)	992
Initial temperature (°C)	512

Test Number	12
Mixture Composition (%H ₂ /%CH ₄ /%CO)	60/40/0
Ambient Temperature (°C)	14
Ambient Pressure (mbar)	970
Wind Speed (m/s)	5
Wind direction	W
Relative Humidity (%)	92
Equivalence Ratio	0.85
Max. overpressure (mbar)	262
Max. pressure location (m)	6.25
Max. flame speed (ionisation sensors, m/s)	328
Max. flame speed (optical sensors, m/s)	357
Max. temperature (°C)	1186
Initial temperature (°C)	512

Test Number	13
Mixture Composition (%H ₂ /%CH ₄ /%CO)	60/40/0
Ambient Temperature (°C)	14
Ambient Pressure (mbar)	970
Wind Speed (m/s)	5
Wind direction	W
Relative Humidity (%)	92
Equivalence Ratio	0.37
Max. overpressure (mbar)	43
Max. pressure location (m)	1.75
Max. flame speed (ionisation sensors, m/s)	-
Max. flame speed (optical sensors, m/s)	63
Max. temperature (°C)	779
Initial temperature (°C)	512

Test Number	16
Mixture Composition (%H ₂ /%CH ₄ /%CO)	60/0/40
Ambient Temperature (°C)	11
Ambient Pressure (mbar)	970
Wind Speed (m/s)	1.3
Wind direction	NE
Relative Humidity (%)	97
Equivalence Ratio	0.5
Max. overpressure (mbar)	91
Max. pressure location (m)	1.75
Max. flame speed (ionisation sensors, m/s)	-
Max. flame speed (optical sensors, m/s)	90
Max. temperature (°C)	858
Initial temperature (°C)	512

Combustion tests: Eight rows of congestion

Test Number	19
Mixture Composition (%H ₂ /%CH ₄ /%CO)	60/40/0
Ambient Temperature (°C)	11
Ambient Pressure (mbar)	980
Wind Speed (m/s)	3.6
Wind direction	SSW
Relative Humidity (%)	84
Equivalence Ratio	0.34
Max. overpressure (mbar)	75
Max. pressure location (m)	6.25
Max. flame speed (ionisation sensors, m/s)	40
Max. flame speed (optical sensors, m/s)	49
Max. temperature (°C)	711
Initial temperature (°C)	512

Test Number	20
Mixture Composition (%H ₂ /%CH ₄ /%CO)	60/40/0
Ambient Temperature (°C)	11
Ambient Pressure (mbar)	980
Wind Speed (m/s)	3.6
Wind direction	SSW
Relative Humidity (%)	84
Equivalence Ratio	0.64
Max. overpressure (mbar)	591
Max. pressure location (m)	6.25
Max. flame speed (ionisation sensors, m/s)	353
Max. flame speed (optical sensors, m/s)	246
Max. temperature (°C)	969
Initial temperature (°C)	512

Test Number	21
Mixture Composition (%H ₂ /%CH ₄ /%CO)	60/40/0
Ambient Temperature (°C)	11
Ambient Pressure (mbar)	980
Wind Speed (m/s)	3.6
Wind direction	SSW
Relative Humidity (%)	84
Equivalence Ratio	0.84
Max. overpressure (mbar)	1670
Max. pressure location (m)	6.25
Max. flame speed (ionisation sensors, m/s)	451
Max. flame speed (optical sensors, m/s)	381
Max. temperature (°C)	1109
Initial temperature (°C)	512

Test Number	22
Mixture Composition (%H ₂ /%CH ₄ /%CO)	100/0/0
Ambient Temperature (°C)	10
Ambient Pressure (mbar)	972
Wind Speed (m/s)	2.5
Wind direction	S
Relative Humidity (%)	95
Equivalence Ratio	0.3
Max. overpressure (mbar)	-
Max. pressure location (m)	-
Max. flame speed (ionisation sensors, m/s)	-
Max. flame speed (optical sensors, m/s)	-
Max. temperature (°C)	855
Initial temperature (°C)	512

Test Number	23
Mixture Composition (%H ₂ /%CH ₄ /%CO)	100/0/0
Ambient Temperature (°C)	5
Ambient Pressure (mbar)	964
Wind Speed (m/s)	2.2
Wind direction	S
Relative Humidity (%)	92
Equivalence Ratio	0.4
Max. overpressure (mbar)	-
Max. pressure location (m)	-
Max. flame speed (ionisation sensors, m/s)	-
Max. flame speed (optical sensors, m/s)	-
Max. temperature (°C)	889
Initial temperature (°C)	512

Test Number	24
Mixture Composition (%H ₂ /%CH ₄ /%CO)	100/0/0
Ambient Temperature (°C)	5
Ambient Pressure (mbar)	964
Wind Speed (m/s)	2.2
Wind direction	S
Relative Humidity (%)	92
Equivalence Ratio	0.5
Max. overpressure (mbar)	323
Max. pressure location (m)	11.75
Max. flame speed (ionisation sensors, m/s)	219
Max. flame speed (optical sensors, m/s)	123
Max. temperature (°C)	815
Initial temperature (°C)	512

Test Number	25
Mixture Composition (%H ₂ /%CH ₄ /%CO)	100/0/0
Ambient Temperature (°C)	9
Ambient Pressure (mbar)	971
Wind Speed (m/s)	3.5
Wind direction	S
Relative Humidity (%)	97
Equivalence Ratio	0.7
Max. overpressure (mbar)	7620
Max. pressure location (m)	8.75
Max. flame speed (ionisation sensors, m/s)	1944
Max. flame speed (optical sensors, m/s)	2500
Max. temperature (°C)	958
Initial temperature (°C)	512

Test Number	26
Mixture Composition (%H ₂ /%CH ₄ /%CO)	100/0/0
Ambient Temperature (°C)	9
Ambient Pressure (mbar)	971
Wind Speed (m/s)	3.5
Wind direction	S
Relative Humidity (%)	97
Equivalence Ratio	0.6
Max. overpressure (mbar)	1950
Max. pressure location (m)	11.75
Max. flame speed (ionisation sensors, m/s)	250
Max. flame speed (optical sensors, m/s)	288
Max. temperature (°C)	874
Initial temperature (°C)	512

Combustion tests: Fifteen rows of congestion

Test Number	27
Mixture Composition (%H ₂ /%CH ₄ /%CO)	100/0/0
Ambient Temperature (°C)	1
Ambient Pressure (mbar)	949
Wind Speed (m/s)	2.5
Wind direction	S
Relative Humidity (%)	97
Equivalence Ratio	0.5
Max. overpressure (mbar)	1733
Max. pressure location (m)	8.75
Max. flame speed (ionisation sensors, m/s)	416
Max. flame speed (optical sensors, m/s)	238
Max. temperature (°C)	824
Initial temperature (°C)	512

Test Number	28
Mixture Composition (%H ₂ /%CH ₄ /%CO)	100/0/0
Ambient Temperature (°C)	1
Ambient Pressure (mbar)	949
Wind Speed (m/s)	2.5
Wind direction	S
Relative Humidity (%)	97
Equivalence Ratio	0.4
Max. overpressure (mbar)	451
Max. pressure location (m)	6.25
Max. flame speed (ionisation sensors, m/s)	-
Max. flame speed (optical sensors, m/s)	167
Max. temperature (°C)	776
Initial temperature (°C)	512

Test Number	29
Mixture Composition (%H ₂ /%CH ₄ /%CO)	100/0/0
Ambient Temperature (°C)	1
Ambient Pressure (mbar)	949
Wind Speed (m/s)	2.5
Wind direction	S
Relative Humidity (%)	97
Equivalence Ratio	0.6
Max. overpressure (mbar)	7159
Max. pressure location (m)	8.75
Max. flame speed (ionisation sensors, m/s)	1667
Max. flame speed (optical sensors, m/s)	1875
Max. temperature (°C)	939
Initial temperature (°C)	512

Test Number	30
Mixture Composition (%H ₂ /%CH ₄ /%CO)	60/40
Ambient Temperature (°C)	3
Ambient Pressure (mbar)	955
Wind Speed (m/s)	10
Wind direction	N
Relative Humidity (%)	97
Equivalence Ratio	0.55
Max. overpressure (mbar)	284
Max. pressure location (m)	6.25
Max. flame speed (ionisation sensors, m/s)	208
Max. flame speed (optical sensors, m/s)	161
Max. temperature (°C)	1139
Initial temperature (°C)	493

Test Number	31
Mixture Composition (%H ₂ /%CH ₄ /%CO)	60/ 40
Ambient Temperature (°C)	3
Ambient Pressure (mbar)	955
Wind Speed (m/s)	10
Wind direction	N
Relative Humidity (%)	97
Equivalence Ratio	0.65
Max. overpressure (mbar)	3016
Max. pressure location (m)	11.75
Max. flame speed (ionisation sensors, m/s)	556
Max. flame speed (optical sensors, m/s)	300
Max. temperature (°C)	971
Initial temperature (°C)	493

Test Number	33
Mixture Composition (%H ₂ /%CH ₄ /%CO)	0/100/0
Ambient Temperature (°C)	3
Ambient Pressure (mbar)	983
Wind Speed (m/s)	5
Wind direction	N
Relative Humidity (%)	97
Equivalence Ratio	0.86
Max. overpressure (mbar)	2620
Max. pressure location (m)	11.75
Max. flame speed (ionisation sensors, m/s)	595
Max. flame speed (optical sensors, m/s)	385
Max. temperature (°C)	1111
Initial temperature (°C)	493

Test Number	34
Mixture Composition (%H ₂ /%CH ₄ /%CO)	0/100/0
Ambient Temperature (°C)	3
Ambient Pressure (mbar)	983
Wind Speed (m/s)	5
Wind direction	N
Relative Humidity (%)	97
Equivalence Ratio	0.76
Max. overpressure (mbar)	650
Max. pressure location (m)	11.75
Max. flame speed (ionisation sensors, m/s)	548
Max. flame speed (optical sensors, m/s)	248
Max. temperature (°C)	1078
Initial temperature (°C)	493

Test Number	35
Mixture Composition (%H ₂ /%CH ₄ /%CO)	0/100/0
Ambient Temperature (°C)	3
Ambient Pressure (mbar)	983
Wind Speed (m/s)	5
Wind direction	N
Relative Humidity (%)	97
Equivalence Ratio	0.65
Max. overpressure (mbar)	300
Max. pressure location (m)	11.75
Max. flame speed (ionisation sensors, m/s)	227
Max. flame speed (optical sensors, m/s)	190
Max. temperature (°C)	1058
Initial temperature (°C)	493

Test Number	36
Mixture Composition (%H ₂ /%CH ₄ /%CO)	40/60/0
Ambient Temperature (°C)	8
Ambient Pressure (mbar)	975
Wind Speed (m/s)	0
Wind direction	-
Relative Humidity (%)	65
Equivalence Ratio	0.65
Max. overpressure (mbar)	416
Max. pressure location (m)	11.75
Max. flame speed (ionisation sensors, m/s)	313
Max. flame speed (optical sensors, m/s)	221
Max. temperature (°C)	988
Initial temperature (°C)	493

Test Number	37
Mixture Composition (%H ₂ /%CH ₄ /%CO)	40/60/0
Ambient Temperature (°C)	8
Ambient Pressure (mbar)	975
Wind Speed (m/s)	0
Wind direction	-
Relative Humidity (%)	65
Equivalence Ratio	0.75
Max. overpressure (mbar)	1515
Max. pressure location (m)	11.75
Max. flame speed (ionisation sensors, m/s)	391
Max. flame speed (optical sensors, m/s)	283
Max. temperature (°C)	1057
Initial temperature (°C)	493

Test Number	38
Mixture Composition (%H ₂ /%CH ₄ /%CO)	40/60/0
Ambient Temperature (°C)	8
Ambient Pressure (mbar)	975
Wind Speed (m/s)	0
Wind direction	-
Relative Humidity (%)	65
Equivalence Ratio	0.6
Max. overpressure (mbar)	363
Max. pressure location (m)	7.75
Max. flame speed (ionisation sensors, m/s)	357
Max. flame speed (optical sensors, m/s)	216
Max. temperature (°C)	997
Initial temperature (°C)	493

Test Number	39
Mixture Composition (%H ₂ /%CH ₄ /%CO)	60/40
Ambient Temperature (°C)	8
Ambient Pressure (mbar)	969
Wind Speed (m/s)	0
Wind direction	-
Relative Humidity (%)	65
Equivalence Ratio	0.61
Max. overpressure (mbar)	600
Max. pressure location (m)	11.75
Max. flame speed (ionisation sensors, m/s)	242
Max. flame speed (optical sensors, m/s)	205
Max. temperature (°C)	944
Initial temperature (°C)	493

Test Number	40
Mixture Composition (%H ₂ /%CH ₄ /%CO)	60/40
Ambient Temperature (°C)	8
Ambient Pressure (mbar)	969
Wind Speed (m/s)	0
Wind direction	-
Relative Humidity (%)	65
Equivalence Ratio	0.66
Max. overpressure (mbar)	1353
Max. pressure location (m)	11.75
Max. flame speed (ionisation sensors, m/s)	224
Max. flame speed (optical sensors, m/s)	233
Max. temperature (°C)	996
Initial temperature (°C)	493

Test Number	41
Mixture Composition (%H ₂ /%CH ₄ /%CO)	100/0/0
Ambient Temperature (°C)	8
Ambient Pressure (mbar)	987
Wind Speed (m/s)	1
Wind direction	N
Relative Humidity (%)	65
Equivalence Ratio	0.4
Max. overpressure (mbar)	0
Max. pressure location (m)	-
Max. flame speed (ionisation sensors, m/s)	0
Max. flame speed (optical sensors, m/s)	0
Max. temperature (°C)	1017
Initial temperature (°C)	493

Test Number	42
Mixture Composition (%H ₂ /%CH ₄ /%CO)	100/0/0
Ambient Temperature (°C)	8
Ambient Pressure (mbar)	987
Wind Speed (m/s)	1
Wind direction	N
Relative Humidity (%)	65
Equivalence Ratio	0.5
Max. overpressure (mbar)	1400
Max. pressure location (m)	11.75
Max. flame speed (ionisation sensors, m/s)	278
Max. flame speed (optical sensors, m/s)	273
Max. temperature (°C)	850
Initial temperature (°C)	493

Test Number	43
Mixture Composition (%H ₂ /%CH ₄ /%CO)	100/0/0
Ambient Temperature (°C)	8
Ambient Pressure (mbar)	987
Wind Speed (m/s)	1
Wind direction	N
Relative Humidity (%)	65
Equivalence Ratio	0.6
Max. overpressure (mbar)	9400
Max. pressure location (m)	11.75
Max. flame speed (ionisation sensors, m/s)	1724
Max. flame speed (optical sensors, m/s)	1667
Max. temperature (°C)	930
Initial temperature (°C)	493

Test Number	44
Mixture Composition (%H ₂ /%CH ₄ /%CO)	100/0/0
Ambient Temperature (°C)	8
Ambient Pressure (mbar)	962
Wind Speed (m/s)	1
Wind direction	N
Relative Humidity (%)	65
Equivalence Ratio	0.5
Max. overpressure (mbar)	1762
Max. pressure location (m)	11.75
Max. flame speed (ionisation sensors, m/s)	208
Max. flame speed (optical sensors, m/s)	286
Max. temperature (°C)	847
Initial temperature (°C)	493

Test Number	46
Mixture Composition (%H ₂ /%CH ₄ /%CO)	0/0/100
Ambient Temperature (°C)	8
Ambient Pressure (mbar)	961
Wind Speed (m/s)	2
Wind direction	N
Relative Humidity (%)	65
Equivalence Ratio	0.44
Max. overpressure (mbar)	130
Max. pressure location (m)	8.75
Max. flame speed (ionisation sensors, m/s)	100
Max. flame speed (optical sensors, m/s)	158
Max. temperature (°C)	705
Initial temperature (°C)	493

Test Number	47
Mixture Composition (%H ₂ /%CH ₄ /%CO)	0/0/100
Ambient Temperature (°C)	3
Ambient Pressure (mbar)	968
Wind Speed (m/s)	2
Wind direction	SW
Relative Humidity (%)	65
Equivalence Ratio	0.6
Max. overpressure (mbar)	574
Max. pressure location (m)	11.75
Max. flame speed (ionisation sensors, m/s)	417
Max. flame speed (optical sensors, m/s)	300
Max. temperature (°C)	1181
Initial temperature (°C)	493

Test Number	48
Mixture Composition (%H ₂ /%CH ₄ /%CO)	0/0100
Ambient Temperature (°C)	3
Ambient Pressure (mbar)	965
Wind Speed (m/s)	2
Wind direction	SW
Relative Humidity (%)	65
Equivalence Ratio	0.77
Max. overpressure (mbar)	3000
Max. pressure location (m)	11.75
Max. flame speed (ionisation sensors, m/s)	1000
Max. flame speed (optical sensors, m/s)	789
Max. temperature (°C)	1268
Initial temperature (°C)	493

Test Number	49
Mixture Composition (%H ₂ /%CH ₄ /%CO)	40/0/60
Ambient Temperature (°C)	3
Ambient Pressure (mbar)	961
Wind Speed (m/s)	2
Wind direction	SW
Relative Humidity (%)	65
Equivalence Ratio	0.65
Max. overpressure (mbar)	10380
Max. pressure location (m)	11.75
Max. flame speed (ionisation sensors, m/s)	2500
Max. flame speed (optical sensors, m/s)	2500
Max. temperature (°C)	1218
Initial temperature (°C)	493

Test Number	50
Mixture Composition (%H ₂ /%CH ₄ /%CO)	40/0/60
Ambient Temperature (°C)	3
Ambient Pressure (mbar)	961
Wind Speed (m/s)	2
Wind direction	SW
Relative Humidity (%)	65
Equivalence Ratio	0.41
Max. overpressure (mbar)	227
Max. pressure location (m)	6.25
Max. flame speed (ionisation sensors, m/s)	133
Max. flame speed (optical sensors, m/s)	176
Max. temperature (°C)	845
Initial temperature (°C)	493

Test Number	52
Mixture Composition (%H ₂ /%CH ₄ /%CO)	40/0/60
Ambient Temperature (°C)	3
Ambient Pressure (mbar)	965
Wind Speed (m/s)	2
Wind direction	SW
Relative Humidity (%)	65
Equivalence Ratio	0.5
Max. overpressure (mbar)	824
Max. pressure location (m)	11.75
Max. flame speed (ionisation sensors, m/s)	0
Max. flame speed (optical sensors, m/s)	286
Max. temperature (°C)	1046
Initial temperature (°C)	493

Test Number	53
Mixture Composition (%H ₂ /%CH ₄ /%CO)	60/0/40
Ambient Temperature (°C)	6
Ambient Pressure (mbar)	965
Wind Speed (m/s)	2
Wind direction	SW
Relative Humidity (%)	65
Equivalence Ratio	0.4
Max. overpressure (mbar)	218
Max. pressure location (m)	8.75
Max. flame speed (ionisation sensors, m/s)	0
Max. flame speed (optical sensors, m/s)	129
Max. temperature (°C)	800
Initial temperature (°C)	493

Test Number	54
Mixture Composition (%H ₂ /%CH ₄ /%CO)	60/0/40
Ambient Temperature (°C)	6
Ambient Pressure (mbar)	965
Wind Speed (m/s)	2
Wind direction	SW
Relative Humidity (%)	65
Equivalence Ratio	0.5
Max. overpressure (mbar)	1500
Max. pressure location (m)	11.75
Max. flame speed (ionisation sensors, m/s)	286
Max. flame speed (optical sensors, m/s)	197
Max. temperature (°C)	842
Initial temperature (°C)	493

Test Number	56
Mixture Composition (%H ₂ /%CH ₄ /%CO)	60/0/40
Ambient Temperature (°C)	6
Ambient Pressure (mbar)	965
Wind Speed (m/s)	2
Wind direction	SW
Relative Humidity (%)	65
Equivalence Ratio	0.56
Max. overpressure (mbar)	966
Max. pressure location (m)	11.75
Max. flame speed (ionisation sensors, m/s)	185
Max. flame speed (optical sensors, m/s)	183
Max. temperature (°C)	824
Initial temperature (°C)	493

Test Number	57
Mixture Composition (%H ₂ /%CH ₄ /%CO)	40/25/35
Ambient Temperature (°C)	6
Ambient Pressure (mbar)	970
Wind Speed (m/s)	2
Wind direction	SW
Relative Humidity (%)	65
Equivalence Ratio	0.65
Max. overpressure (mbar)	3128
Max. pressure location (m)	11.75
Max. flame speed (ionisation sensors, m/s)	385
Max. flame speed (optical sensors, m/s)	313
Max. temperature (°C)	1308
Initial temperature (°C)	493

Test Number	58
Mixture Composition (%H ₂ /%CH ₄ /%CO)	40/25/35
Ambient Temperature (°C)	6
Ambient Pressure (mbar)	970
Wind Speed (m/s)	2
Wind direction	SW
Relative Humidity (%)	65
Equivalence Ratio	0.56
Max. overpressure (mbar)	1503
Max. pressure location (m)	11.75
Max. flame speed (ionisation sensors, m/s)	313
Max. flame speed (optical sensors, m/s)	238
Max. temperature (°C)	1029
Initial temperature (°C)	493

Test Number	59
Mixture Composition (%H ₂ /%CH ₄ /%CO)	40/25/35
Ambient Temperature (°C)	6
Ambient Pressure (mbar)	970
Wind Speed (m/s)	2
Wind direction	SW
Relative Humidity (%)	65
Equivalence Ratio	0.51
Max. overpressure (mbar)	1500
Max. pressure location (m)	11.75
Max. flame speed (ionisation sensors, m/s)	275
Max. flame speed (optical sensors, m/s)	214
Max. temperature (°C)	899
Initial temperature (°C)	493

Test Number	60
Mixture Composition (%H ₂ /%CH ₄ /%CO)	40/25/35
Ambient Temperature (°C)	6
Ambient Pressure (mbar)	970
Wind Speed (m/s)	2
Wind direction	SW
Relative Humidity (%)	65
Equivalence Ratio	0.45
Max. overpressure (mbar)	214
Max. pressure location (m)	6.25
Max. flame speed (ionisation sensors, m/s)	70
Max. flame speed (optical sensors, m/s)	96
Max. temperature (°C)	720
Initial temperature (°C)	493

Combustion tests: Fifteen rows of congestion at lower exhaust temperature

Test Number	61
Mixture Composition (%H ₂ /%CH ₄ /%CO)	100/0/0
Ambient Temperature (°C)	6
Ambient Pressure (mbar)	977
Wind Speed (m/s)	2
Wind direction	SW
Relative Humidity (%)	65
Equivalence Ratio	0.5
Max. overpressure (mbar)	2230
Max. pressure location (m)	8.75
Max. flame speed (ionisation sensors, m/s)	769
Max. flame speed (optical sensors, m/s)	211
Max. temperature (°C)	898
Initial temperature (°C)	325

Test Number	62
Mixture Composition (%H ₂ /%CH ₄ /%CO)	100/0/0
Ambient Temperature (°C)	6
Ambient Pressure (mbar)	977
Wind Speed (m/s)	2
Wind direction	SW
Relative Humidity (%)	65
Equivalence Ratio	0.45
Max. overpressure (mbar)	788
Max. pressure location (m)	11.75
Max. flame speed (ionisation sensors, m/s)	55
Max. flame speed (optical sensors, m/s)	250
Max. temperature (°C)	616
Initial temperature (°C)	325

Test Number	63
Mixture Composition (%H ₂ /%CH ₄ /%CO)	100/0/0
Ambient Temperature (°C)	6
Ambient Pressure (mbar)	977
Wind Speed (m/s)	2
Wind direction	SW
Relative Humidity (%)	65
Equivalence Ratio	0.35
Max. overpressure (mbar)	374
Max. pressure location (m)	11.75
Max. flame speed (ionisation sensors, m/s)	52
Max. flame speed (optical sensors, m/s)	185
Max. temperature (°C)	567
Initial temperature (°C)	325

Test Number	64
Mixture Composition (%H ₂ /%CH ₄ /%CO)	60/40/0
Ambient Temperature (°C)	6
Ambient Pressure (mbar)	977
Wind Speed (m/s)	2
Wind direction	SW
Relative Humidity (%)	65
Equivalence Ratio	0.58
Max. overpressure (mbar)	2774
Max. pressure location (m)	8.75
Max. flame speed (ionisation sensors, m/s)	694
Max. flame speed (optical sensors, m/s)	0
Max. temperature (°C)	792
Initial temperature (°C)	325

Test Number	65
Mixture Composition (%H ₂ /%CH ₄ /%CO)	60/40/0
Ambient Temperature (°C)	6
Ambient Pressure (mbar)	977
Wind Speed (m/s)	2
Wind direction	SW
Relative Humidity (%)	65
Equivalence Ratio	0.5
Max. overpressure (mbar)	1579
Max. pressure location (m)	8.75
Max. flame speed (ionisation sensors, m/s)	303
Max. flame speed (optical sensors, m/s)	312
Max. temperature (°C)	720
Initial temperature (°C)	325

Test Number	66
Mixture Composition (%H ₂ /%CH ₄ /%CO)	60/40/0
Ambient Temperature (°C)	6
Ambient Pressure (mbar)	977
Wind Speed (m/s)	2
Wind direction	SW
Relative Humidity (%)	65
Equivalence Ratio	0.4
Max. overpressure (mbar)	84
Max. pressure location (m)	4.25
Max. flame speed (ionisation sensors, m/s)	0
Max. flame speed (optical sensors, m/s)	89
Max. temperature (°C)	619
Initial temperature (°C)	325

Test Number	67
Mixture Composition (%H ₂ /%CH ₄ /%CO)	40/0/60
Ambient Temperature (°C)	10
Ambient Pressure (mbar)	972
Wind Speed (m/s)	2
Wind direction	S
Relative Humidity (%)	65
Equivalence Ratio	0.51
Max. overpressure (mbar)	1075
Max. pressure location (m)	11.75
Max. flame speed (ionisation sensors, m/s)	212
Max. flame speed (optical sensors, m/s)	366
Max. temperature (°C)	881
Initial temperature (°C)	325

APPENDIX B: DETAILED ANALYSIS FOR TEST 27

This appendix describes the detailed analysis carried out, and understanding of flame development and its hazards in the free or obstructed circular duct model facility of WP2.2 for Test 27. The very thorough approach developed can be applied to other systems and data to produce a sufficiently accurate display of the distance versus time progression of the flame front. Additional information on the flame front, flame structure and overpressures generated can be obtained from contributing responses of the different sensor types, which can then further interpreted in the light of the compositions and conditions of the mixture investigated and the influence of the confinement and obstructions of the test facility.

The successive data evaluation steps required for such an optimal analysis and interpretation of the ER results in terms of revealed combustion behaviour are described in Appendix 1 for Test 27, which was one of the 100% H₂ tests, which with a heat exchanger model obstruction of fifteen rows of pipes caused flame velocities and overpressures suggestive of part-detonative behaviour.

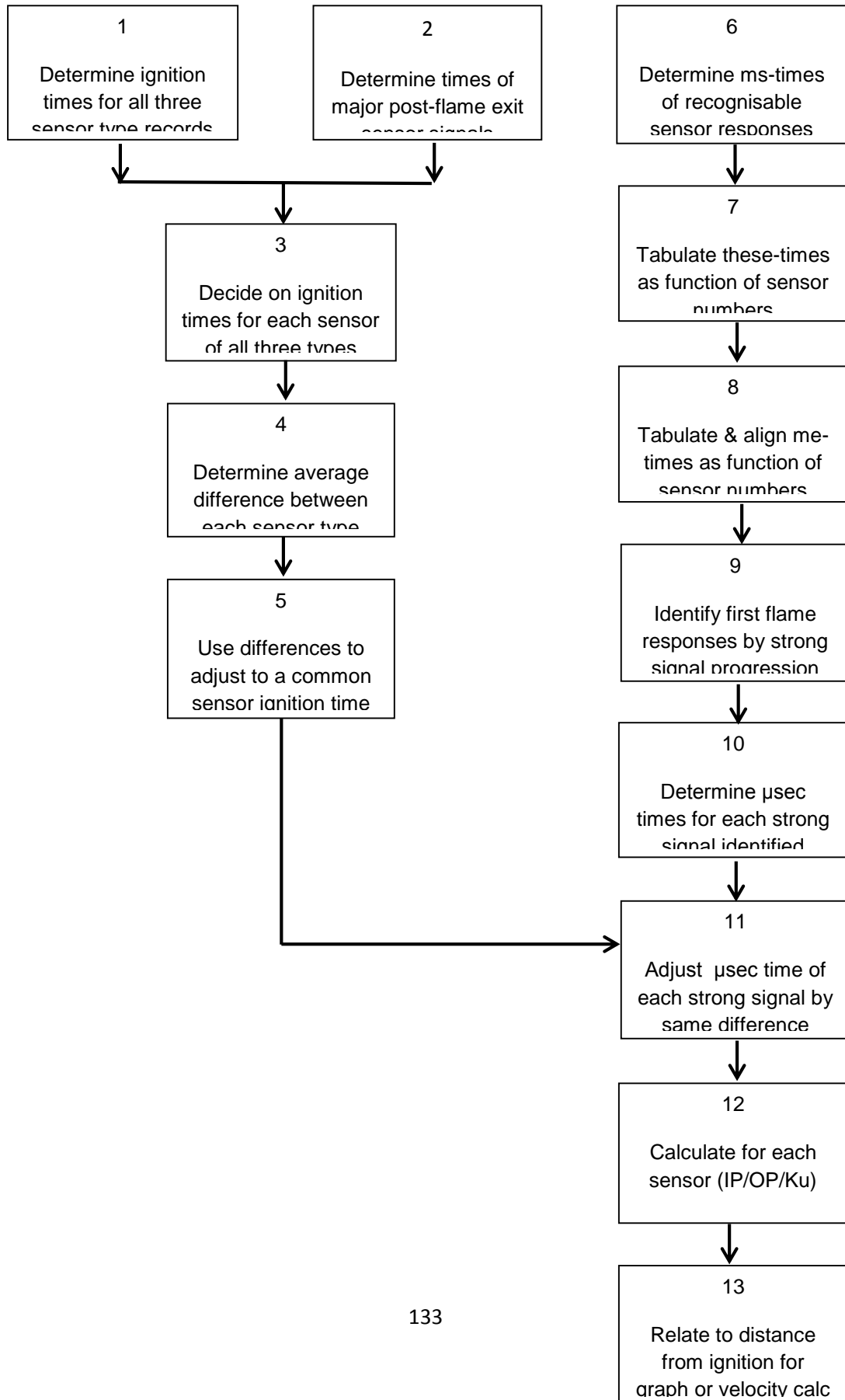
The detailed approach developed is described in Figure B1.1; in what follows these are there also demonstrated for Test 27.

As also shown in Table B1.1, the nature of the combustion process at various stages of the WP2.2 facility is directly related to the flame velocity. For this reason its evaluation requires accurate specification of distances and time at successive measuring positions with respect to the axis of the rig.

The *distances* used in this analysis are those given with the test results of the Experimental Report, except for two changes.

- The first is that - as pointed out in the last issue of the list of paragraph 2.2.4 - the in- and post-heat exchanger locations of the Experimental Report require adjustment for the 100 mm width of the flange supporting the heat exchanger model (and a ionisation probes rake). These changes have been incorporated.
- The second is that for flame development analysis, in first instance only the distances from the point of ignition matter. The location of the igniter was 250 mm from the leading end of the first straight 3 m section of the circular duct. All distances quoted from hereon have therefore been adjusted to this point.

Figure B1.1: How to construct a time/distance graph from results for WP2.2 test runs



The *time data* provided with the tests are taken from all related to the experimental test records. Their last digit given was variably in the (0.1 – 0.01) millisecond range. As the minimum distance between two sensors downstream of the HE model is 0.5 m, this means that the highest flame velocities around 1700 m.s-1 could for such sections only be calculated with an accuracy of 30 (ms-1)? – 3%. It was therefore important to express all times to at least the lower value and also to review the accuracy of times provided by the recording system's time-base.

Maximum magnification of the Diadem TDMS records shows that for the ionisation probes the time between two successive peaks of the base signal is 20 microseconds, i.e. the positive and negative peaks of basic noise are separated by 10 microseconds. The moment of an event is not at the peak of a signal excursion above or below the width of the noise signal. The time of its arrival is when the sensor starts to respond to the change in external conditions. When this external input changes slowly, the sensor and recording system will follow it to its maximum value; when it is fast the rate of response is limited by the characteristics of sensor and/or recording system. When the signal is seen to rise positively above, respectively negatively drop below the preceding common maximum/minimum level of the noise signal band, the event will have arrived within the last half of the preceding noise excursion.

For ionisation probes this means that the initial sensor response indicates that the event arrived within the preceding 10 microseconds. Thus, by taking the arrival within that half cycle as occurring at the centre of the noise band width, the event arrival time for the ionisation probes can be determined with an accuracy of ± 5 microseconds. For the optical probes and pressure transducers the duration of the noise cycles were found to be approximately 35 microseconds; the accuracy of the output data for these sensors is therefore about ± 10 microseconds.

With this information, our analysis of the TDMS files can be illustrated with the example of Test 27.

The first task listed at the top of Figure B1.1 was the determination of a common ignition time for all three sensors types employed. Like all such records there is an abundance of signals on each track, in about one quarter of cases half or completely obscured by the continuous output noise, when this is unfortunately relatively high compared to the strength of a sensor output. However, displaying a few sensor records simultaneously on the TDMS screen, a common single and sharp spike is usually readily found ahead of the first major peak and identified as the time of ignition. For test 27 such times in seconds, given to the microsecond digit, are shown in the first column of Table B1.1. As can be seen: the numbers for the ionisation probes are stable around 1.283 722, although gradually dropping by almost 20 microseconds.

Table B1.1: ETI WP2.2.Times [sec] Updates Run 27

Run	Ignition [sec]	Ignition I adjust. [μsec]	Main Signal	Adjusted main signal	Distance from previous/ ignition [mm]	Time from ignition [sec]	Final signal
IGN	1.238 722	-2	1.238 722	1.238 720			
IP1	1.238 722		1.282 302	1.282 300	2500/2500	0.043 580	2.774 864
IP2	1.238 722		1.301 612	1.301 610	1500/4000	0.062 411	2.744 864
			1.314 383	1.314 381			2.744 864
IP3	1.238 722		1.306 502	1.306 500	500/4500	0.067 780	2.744 864
IP4	1.238 722		1.305 972	1.305 970		0.067 250	2.744 864
IP5	1.238 722		1.310 802	1.310 800		0.072 080	2.744 864
.....							
IP6	1.238 722		1.314 637	1.314 635	1000/5500	0.075 915	2.744 864
IP7	1.238 722		1.314 002	1.314 000		0.075 280	2.744 864
IP8	1.283 722		1.314 002	1.314 000	300/5800	0.075 280	2.744 863
IP9	1.283 722		1.314 002	1.314 000		0.075 280	2.744 863
.....							
IP11	1.283 722		1.314 742	1.314 740		0.076 020	2.744 863
IP12	1.283 722		1.312 562	1.312 560	1300/7100	0.073 840	2.744 863
IP13	1.283 722		1.315 068	1.315 066		0.076 346	2.744 863
IP10	1.283 719	+1	1.313 349	1.313 350	500/7600	0.074 630	2.744 863
			1.317 233	1.317 234		0.078 514	
IP14	1.283 720			1.314 529	1000/8600	0.075 809	2.744 863

Commercial

IP15	1.283 720		1.322 620	1.322 636	500/910	0.083 916	2.744 863
			1.326 899	1.327 000		0.088 280	
IP16	1.238 704	+16	1.322 594	1.322 610		2.744 842	2.744 842
			1.325 794	1.325 810		0.087 090	
IP17	1.238 704		1.322 620	1.322 636		0.083 916	2.744 842
			1.326 128	1.326 144	0.087 408		
IP18	1.238 704		????????		500/9600		2.744 842
			1.329 107	1.329 123	1000/10600	0.090 403	
IP19	1.238 704		1.327 906	1.327 922		0.089 202	2.744 842
			1.333 564	1.333 580		0.094 860	
IP20	1.238 704		1.328 012	1.328 028		0.089 308	2.744 842
			1.332 695	1.332 711		0.093 991	
IP21	1.238 704		1.327 996	1.328 012			2.744 842
			1.333 686	1.333 702		0.094 982	
IP22	1.238 704		1.335 568	1.335 584	500/11100	0.096 864	2.744 842
IP23	1.238 704		1.338 546	1.338 562	500/11600	0.099 842	2.744 842
OP0``	1.238 349	+371	1.304 900	1.305 271	2500/2500	0.066 551	2.744 510
OP1	1.238 349		1.318 100	1.318 471	5600/8100	0.079 751	2.744 510
OP2	1.238 342		1.326 468	1.326 839	1500/9600	0.088 119	2.744 510
OP3	1.238 340	+380	1.333 446	1.333 835	1500/11100	0.095 115	2.744 510
KU0	1.238 350	+370	1.253 350	1.253 720	4000/4000	0.015 000	2.744 510
KU3	1.238 344	+376	1.301 900	1.302 276	2100/6100	0.063 556	2.744 503
KU5	1.238 344		1.312 000	1.312 376	1500/7600	0.073 656	2.744 502
KU6	1.238 344		1.313 935	1.314 311	1000/8600	0.075 591	2.744 503
KU7	1.238 344		1.317 740	1.318 116	3000/11600	0.079396	2.744 503

Another reliable comparison of the time records of the three types of sensors could be obtained from the massive signal that appears on all time-records after the combustion front has passed IP 23 and must have exited the duct. The delay varies from test to test in a 50 – 1000 msec range. Leaving aside the cause of this impact on the recording system, it was found that – as readily appreciated - this occurred also at exactly the same time for each of the three sensor types. Given its strength and clarity, this signal is an alternative reference for harmonising the ignition times and hence the time records of the different sensor sets. This alternative is summarised in the second box of B1.1. The choice is represented by box 3 in Figure B1.1, which in our case was made to be the direct ignition time reading from the Diadem TDMS file at maximum magnification.

Whichever option was chosen, the next step in the analysis, represented by box 4 in Figure B1.1, was to check for any differences in event recording times between the pressure and/or optical sensors and the ionisation probes. As mentioned in para 2.4.4 of the main text, it had already been established by the HSL test team that the real time ignition moments for the various sensors employed are not aligned, which was ascribed to the characteristics of individual cards in the separate recording systems employed. The signal available for comparison is the pick-up from the condenser discharge that causes ignition. From this and analysis of time records of all Test 27 sensors, average ignition times are approximately

- Ionisation probes: 1.283 715 sec \pm 10 μ sec
- Optical probes: 1.283 345 sec \pm 5 μ sec = IP time less 370 μ sec
- Pressure sensors: 1.283 346 sec \pm 4 μ sec = IP time less 369 μ sec.

Note that the variations are genuine and systematic and are not the uncertainties of the previous paragraph.

For the purpose of a detailed and comprehensive analysis and interpretation of the experimental results, these time records of data and therefore the ignition times recorded by individual sensors needed to be brought in agreement (Figure B1.1, Box 5) For our evaluations time difference rather than absolute time is important, as is also to retain a point of reference with the information from the Experimental Report. In the analysis of all test results except those of Test 5, the output data from all three sensor types were therefore adjusted to agree with those of the (ionisation probe) ignition record of Test 27 shown in the Experimental Report, which was 1.283 470 seconds. Thus the ignition and sensors response times given above would on average have to be adjusted as follows:

- Ionisation probes: 1.283 715 sec + 5 μ sec = 1.283 720 sec
- Optical probes: 1.283 345 sec + (370 + 5) μ sec = 1.283 470 sec
- Pressure sensors: 1.283 346 sec + (369 + 5) μ sec = 1.283 470 sec.

In practice it was preferable to consider individual corrections for each sensor. Thus for all Test 27 ignition time records obtained from the experimental results the following actual additions had to be made in the following ranges:

- Ionisation probes: + -2 to + 16 μ sec
- Optical probes: + 371 to 380 μ sec
- Pressure sensors: + 385 μ sec

The appropriate corrections are listed in the second column of Table B1.1.

With a common ignition time agreed, progress needed to turn to an agreement on times of sensor responses to the passage of the flame so that these can be used for a more fundamental analysis: this has been the main problem in using the test results from the Experimental Report. A summary of reasons for this includes:

- Difficulties to derive from a single set of the time data given a consistent in picture of flame development, especially upstream of any HE insertions;
- the number of NS (no signal) and NA responses, varying from 3/32 sensors (test 25) to 23/32 (test 10; no ionisation probe responses);
- the limited accuracy for higher velocities;
- the occasional inconsistency between signal sequence and expected flame development, although this may have been caused by a strongly deformed flame front;
- the disagreement between response times from the few aligned different types of probes; this includes optical probe responses preceding signal from pressure transducers, which is difficult to comprehend;
- the use of times of maximum sensor outputs which takes no account of the difference in time-width

Unable to accommodate all these issues in re-arranging the experimental results data, it was ultimately decided to start the effort from afresh and the procedure followed is summarised in the right hand column of Figure B1.1, starting with box 6 and 7

First the output signals of all ionisation probes in individual TDMS Test matrices were scanned at Diadem intermediate magnification from ignition time to the response of the last sensor IP23. First noticeable deflection of each strong and evident signal recorded with to an accuracy of one millisecond. In Table B1.2.a such data are listed for Test 27. By bold print these strong signals were provisionally identified as likely primary sensor responses. For about 20% of sensors even the most important signal could be hidden in the noise. In some instances it was not possible to find an identifiable signal. The data were placed in rows associated with rising IP numbers (box 8).

Given that the three ionisation probes on rakes were likely to have closely similar response times, such sets of responses would then be assumed to also represent flame passage and shown in bold print, although on occasions such sets could demonstrate agreement around more than one time, sometimes close to another set.

Table B1.2.a WP2.2 Run 27; matching IP sensor response times

IP1	1.295	1.370						
IP 2	1.302							
IP 3	1.306	1.311						
IP4	1.305	1.311	1.332					
IP5	1.295	1.311	1.312	1.322	1.333			
IP6	1.292	1.302	1.307	1.314	1.320	1.334		
IP7	1.292	1.313	1.317	1.337	1.343	1.356	1.363	1.370
IP8	1.311	1.314						
IP9	1.311	1.315	1.342					
IP11	1.315	1.319	1.323					
IP12	1.313	1.319	1.324					
IP13	1.315	1.319	1.323					
IP10	1.313	1.317	1.321					
IP14	1.320	1.339	1.347	1.372				
IP15	1.323	1.327	1.339	1.347	1.371			
IP16	1.315	1.323	1.326	1.334	1.349	1.358	1.372	
IP17	1.315	1.323	1.329	1.338	1.348	1.372		
IP18	1.315	1.329	1.337	1.347				
IP19	1.329	1.333	1.348	1.360	1.373			
IP20	1.310	1.320	1.326	1.333	1.342	1.345	1.361	1.374
IP21	1.310	1.320	1.328	1.333	1.345	1.360	1.374	
IP22	1.335	1.347	1.375					
IP23	1.338	1.348	1.360	1.374				

Table B1.2.b: Run 27; matching IP sensor response times

IP1	1.295																		1.370
IP 2		1.302																	1.381
IP3			1.306		1.311														
IP4			1.305		1.311				1.332										
IP5	1.295		1.311		1.312			1.322		1.333									
IP6	1.292		1.302	1.307	1.314			1.320				1.334							
IP7	1.292				1.313	1.317						1.337	1.343		1.356	1.363	1.370		
IP8					1.311	1.314													
IP9					1.311	1.315						1.342							
IP11						1.315	1.319	1.323											
IP12						1.313	1.319	1.324											
IP13						1.315	1.319	1.323											
IP10						1.313	1.317	1.321											
IP14								1.320				1.339	1.347						1.372
IP15								1.323	1.327			1.339	1.347						1.371
IP16						1.315		1.323	1.326	1.334			1.349	1.358					1.372
IP17						1.315		1.323	1.329			1.338	1.348						1.372
IP18						1.315				1.329		1.337	1.347						

Commercial

IP19										1.329	1.333				1.348	1.360		1.373
IP20					1.310			1.320		1.326	1.333			1.342	1.345	1.361		1.374
IP21					1.310			1.320		1.328	1.333				1.345	1.360		1.374
IP22												1.335			1.347			1.375
IP23													1.338		1.348	1.360		1.374

All millisecond results would then be aligned in columns of closely similar sensor response times, bearing in mind that in any event the times would have to rise with the increase of the IP number. By trial and error this would then produce a table of matching response times (box 9), such as also illustrated for Test 27 in Table B1.2.b. From this the bold figures would then be provisionally assumed to be the correct flame arrival time at the probe of the respective table row.

For each of the ionisation probes the probe signal record was then scanned again at Diadem maximum magnification to determine from the bold sensor time response and as closely the start of the combustion wave passage. Double expansion was used and time coordinates recorded to the microsecond digit. This part of the procedure is summarised in Figure B1.1, box 10; For Test 27 the results are given in Table B1.2, column 3. As shown, new high resolution results from optical and pressure sensors analysis has been added to the table. Deciding on the correct instant of the arrival of the combustion wave was however not straightforward and was guided by the following basic understanding.

Whatever the state of flame propagation, at a sensor position the first sign of its approach should always be that of an increase in the pressure sensor signal. At sub-sonic flame velocities this is indicated by a slow/extended precursor rise caused by the volume increase of the combustion zone. This rise will become steeper and more significant the further downstream the sensor is positioned, due to the accumulation of the pressure waves. Arrival/passage of the combustion wave proper is identified by the onset of a much steeper pressure rise, which starts from the top of the local pressure precursor level. When velocity exceeds the local sound velocity by more than about 5+%, the pressure rise is effectively instantaneous, regardless of whether this is linked to a following detonation wave. Thus at sub-sonic combustion it is the additional rise to higher pressure levels that indicate the arrival of combustion and with sonic combustion the more or less instantaneous rise from a single shock.

The next indicator is a response from an ionisation probe. This can have two forms. The main and common one is the detection of ionisation due to temperature rise caused mainly by radiation from the following combustion. This will promote continuing combustion once sufficient ionisation becomes available around 1500 K. However, ionisation starts well below that temperature and it depends on the sensitivity of the probe at what level it will respond.

When a shock is formed ionisation will also occur as result of the very rapid pressure and temperature rise that causes ignition, such as in a detonation. This precedes and will be followed by the response to the much higher ionisation levels in the following supporting flame. Thus ionisation sensors responses should always follow pressure sensors signals and a response from an ionisation probe is not an indication of the passage of the front of a combustion wave. In a detonation at initially ambient pressure the distance between the shock front and the first ionisation band can readily be 100 – 200 mm, but at relatively low flame velocities with negligible pressure rise it may be the first detectable indicator.

Ideally, optical sensors should signal the passage of the combustion zone proper across its central line of view and are therefore used where a response is sought from anywhere across the diameter of gas mixture containment. Unfortunately, they are extremely difficult to collimate and even deeply recessed are sensitive to reflections from upstream flames, triggering a response at times that occasionally are even ahead of that from a pressure sensor at the same location. Their best indicator of the moment of actual flame arrival is the point on the signal track where a gradually rising response suddenly takes on a much steeper slope as the flame proper gets into direct view.

Overall optical sensor records have been very problematic to interpret because of:

- the early responses to reflected light,
- which may come from different sides of the duct
- and the complication that successive responses may not cause all track responses to head in the same direction.
- Additionally, the flame proper is of course always following the pressure front but without visual records there seems to be no reliable way to decide what the time or distance difference is.

We have found it very difficult to relate optical sensor responses to the more reliable time information and combustion wave velocity evaluations from the ionisation and pressure sensors. The optical sensors were intended to advise on flame passage across the diameter of the duct, but in the present work this has been much more reliably indicated by the ionisation sensors rake. A review of the design of optical probes has since taken place and their efficiency is being evaluated with the last duct inlet velocity tests.

As indicated by Figure B1.1, box 11, the sensor response times of Table B1.1, column 3 must of course be adjusted and brought into agreement in the same ways and for the same reasons as outlined in paras 3.4 – 3.7 for the sensor ignition times. As illustrated in the table for Test 27, the corrections of column 2 have therefore also been applied to all individual readings of column 3 to result in the amended main signal times of column 4. Note:

- The three results evaluated for rake probes have been bracketed by accolades
- The position of the model heat exchanger is indicated by two horizontal dotted lines.
- IP 10 was consistently positioned further downstream than the rake containing IP 11,12 and 13.

APPENDIX C: DETAILED ANALYSIS FOR TEST 10

Appendix C: WP2.2.Start Times [sec] Updates Run 10

Run	Ignition [sec]	Ignition l adjust. [μsec]	Main Signal [sec]	Adjusted main signal	Distance from previous Or ignition [mm]	Time from ignition [sec]	Final signal [sec]
IGN	1.251 970	+ 10	1..251 970	1.251 980			2.783 460
IP1	1.251 970				2500/2500	0.028 171	2.783 460
IP2	1.251 970				1500/4000	0.043 804	2.783 460
IP3	1.251 970		1.305 356	1.305 366		0.053 386	2.783 460
IP4	1.251 970		1.309 899	1.309 909	500/4500	0.057 929	2.783 460
IP5	1.251 970		1.304 824	1.304 834		0.023 230	2.783 460
IP6	1.251 970		1.318 600	1.318 610	1000/5500	0.066 630	2.783 460
IP7	1.251 970		1.298 408	1.298 418		0.046 438	2.783 460
IP8	1.251 960	+20			300/5800		
IP9	1.251 960		1.317 600	1.317 620		0.065 640	2.783 452
IP11	1.251 960		1.339 400	1.339 420		0.087 440	2.783 450
IP12	1.251 960		1.339 000	1.339 020	500/7600	0.087 040	2.783 450
IP13	1.251 960		1.336 100	1.336 120		0.081632	2.783 451
IP10	1.251 960		1.333 935	1.333 955	1300/7100	0.081 975	2.783 451
IP14	1.251 960		1.358 660	1.358 680	1000/8600	0.106 700	2.783 451
IP15	1.251 960		1.380 410	1.380 430		0.128 450	2.783 451
IP16	1.251 950	+30	1.380 403	1.380 433	500/9100	0.128 453	2.783 432
IP17	1.251 950		1.380 410	1.380 440?		0.128 460	2.783 432
IP18	1.251 950				500/9600		2.783 432
IP19	1.251 950		1.380 871	1.380 901		0.128 921	2.783 432
IP20	1.251 950		1.380 670	1.380 700	1000/10600	0.128 720	2.783 432
IP21	1.251 950		1.380 665	1.380 695		0.128 715	2.783 431
IP22	1.251 950		1.381 623	1.381 653	500/11100	0.129 673	2.783 432
IP23	1.251 950		1.387 000	1.387 030	500/11600	0.135 050	2.783 432

APPENDIX D: DETAILED ANALYSIS FOR TEST 24

Appendix D: WP2.2.Times [sec] Updates Run 24

Run	Ignition [sec]	Ignition adjust. [µsec]	Main Signal [sec]	Adjusted main signal	Distance from previous Or ignition [mm]	Time from ignition [sec]	Final signal [sec]
IGN	1.450 620	+0	1.450 620				
IP1	1.450 620		1.500 437	1.500 437	2500/2500	0.049 817	2.946 702
IP2	1.450 620		1.507 000	1.507 000	1500/4000	0.056 380	2.946 702
			1.512 748	1.542 748		0.062 128	
IP3	1.450 620		1.527 000	1.527 000		0.076 380	2.946 702
			(Reflected? :	1.539 250			
IP4	1.450 620		1.526 745	1.526 745	500/4500	0.076 125	2.946 702
IP5	1.450 620		1.524 379	1.524 379		0.073 759	2.946 698
.....							
IP6	1.450 620		1.529 793	1.529 793	1000/5500	0.079 173	2.946 700
.....							
IP7	1.450 620		1.528 503	1.528 503		0.077 883	2.946 700
IP8	1.450 620		1.529 069	1.529 069	300/5800	0.078 449	2.946 685
IP9	1.450 620		1.528 838	1.528 838		0.078 218	2.946 685
IP11	1.450 620		1.534 937	1.534 937		0.084 317	2.946 685
IP12	1.450 620		1.535 152	1.535 152	1300/7100	0.084 532	2.946 685
IP13	1.450 630		1.535 288	1.535 288		0.084 668	2.946 685
IP10	1.450 620		1.540 208	1.540 208	500/7600	0.089 588	2.946 685
IP14	1.450 630				1000/8600		2.946 685
IP15	1.450 630		1.553 750	1.553 750		0.103 130	2.946 685
IP16	1.450 620		1.551 470	1.551 470	500/9100	0.100 850	2.946 683
IP17	1.450 620		1.556 000	1.556 000		0.105 380	2.946 683
IP18	1.450 620		1.561 545	1.561 545	500/9600	0.110 925	2.946 683

APPENDIX E: DETAILED ANALYSIS FOR TEST 29

Appendix E: WP2.2.Times [sec] Updates Run 29

Run	Ignition [sec]	Ignition I adjust. [μsec]	Main Signal [sec]	Adjusted main signal [sec]	Distance from previous Or ignition [mm]	Time from ignition [sec]
IGN	1.283 448	+22		1.283 470		
IP1	1.283 457	+13	1.316 616	1.316 629	2500/2500	0.033 139
IP2	1.283 456	+14	1.333 587	1.333 601	1500/4000	0.050 131
IP3	1.283 456	+14	1.336 199	1.337 013	500/4500	0.053 543
IP4	1.283 456	+14	1.335 923	1.335 937		0.052 467
IP5	1.283 456		1.337 429	1.337 443		0.053 973
IP6	1.283 452	+18	1.341 770	1.341 788	1000/5500	0.058 318
IP7	1.283 451	+19	1.341 818	1.341 837	300/5800	0.058 367
IP8	1.283 451		1.342 108	1.342 127		0.058 657
IP9	1.283 451		1.342 081	1.342 100		0.058 630
IP11	1.283 452	+18	1.342 169	1.342 188	1300/7100	0.058 718
IP12	1.283 444	+26	1.342 148	1.342 174		0.058 704
IP13	1.283 453	+17	1.342 123	1.342 140		0.058 767
IP10	1.283 452	+18	1.342 447	1.342 465	500/7600	0.058 995
IP14	1.283 448	+22	1.342 340	1.342 362	1000/8600	0.058 892
IP15	1.283 452	+18	1.343 341	1.343 359	500/9100	0.059 871
IP16	1.283 442	+28	1.343 346	1.343 374		0.059 876
IP17	1.283 451	+17	1.343 346	1.343 363		0.059 876
			145			

APPENDIX F: DETAILED ANALYSIS FOR TEST 25

Appendix F: WP2.2.Start Times [sec] Updates Run 25

Run	Ignition [sec]	Ignition I adjust. [μsec]	Main Signal [sec]	Adjusted main signal [sec]	Distance from previous Or ignition [mm]	Final signal [sec]
IGN	1.251 970	+ 0.000 010	1.251 970	1.251 980		2.783 460
IP1	1.251 970			2500/2500		2.783 460
IP2	1.251 970			1500/4000		2.783 460
IP3	1.251 970		1.305 356	1.305 366	500/4500	2.783 460
IP4	1.251 970		1.309 899	1.309 909		2.783 460
IP5	1.251 970		1.275 200	1.275 210		2.783 460
IP6	1.251 970		1.318 600	1.318 610	1000/5500	2.783 460
IP7	1.251 970		1.298 408	1.298 418	300/5800	2.783 460
IP8	1.251 960	+0.000 020				2.783 452
IP9	1.251 960		1.317 600	1.317 620		2.783 452
IP10	1.251 960		1.333 935	1.333 955	1300/7100	2.783 451
IP11	1.251 960		1.339 400	1.339 420	500/7600	
IP12	1.251 960		1.339 000	1.339 020		2.783 450
IP13	1.251 960		1.336 100	1.336 120		

Commercial

IP14	1.251 960	1.358 660	1.358 680	1000/8600		2.783 451
IP15	1.251 960		1.380 410	1.380 430		2.783 451
IP16	1.251 950	+0.000 030	1.380 403	1.380 433	500/9100	2.783 432
IP17	1.251 950		1.380 410	1.380 440		2.783 432
IP18	1.251 950				500/9600	2.783 432
IP19	1.251 950		1.380 871	1.380 901		2.783 432
IP20	1.251 950		1.380 670	1.380 700	1000/10600	2.783 432
IP21	1.251 950		1.380 665	1.380 695		2.783 431
IP22	1.251 950		1.381 623	1.381 653	500/11100	2.783 432
IP23	1.251 950		1.387 000	1.387 030	500/11600	2.783 432
OP0	1.251 605	+0.000 375	1.288 743	1.289 118	2500/2500	2.783 110
OP1	1.251 594	+0.000 386	1.341 715	1.342 101	5600/8100	2.783 100
OP2	1.251 593	+0.000 387	1.365 931	1.366 318	1500/9600	2.783 100
OP3	1.251 591	+0.000 389	1.379 780	1.380 169	2000/11100	2.783 100
KU0	1.251 590	+0.000 390	1.260 220	1.260 610	1500/1500	2.783 100
KU3	1.251 590	+0.000 389	1.267 686	1.268 075	4600/6100	2.783 100
KU5	1.251 592	+0.000 388	1.269 443	1.269 831	1000/7100	2.783 100
KU6	1.251 593	+0.000 387	1.270 625	1.271 012	1500/8600	2.783 110
KU7	1.251 597	+0.000 383	1.271 800	1.272 183	3000/11600	2.783 110